This is to certify that the

dissertation entitled

Elastic Behavior of Noncrystalline Networks

presented by

Wenqing Tang

has been accepted towards fulfillment
of the requirements for

Doctor degree in Physics

M. F. Thorpe
Major professor

Date July 8, 1987

ELASTIC BEHAVIOR
OF
NONCRYSTALLINE NETWORKS

By

Wenqing Tang

A DISSERTATION

Submitted to
Michigan State University
in partial fulfillment of the requirements
for the degree of

DOCTOR OF PHILOSOPHY

Department of Physics and Astronomy

1987

ABSTRACT

ELASTIC BEHAVIOR OF NONCRYSTALLINE NETWORKS

By

Wenqing Tang

It is shown that the random resistor problem can be mapped on to a related network of Hooke's springs of natural length zero stretched on a frame. The conductance of the network is equivalent to the pressure on the frame. This new viewpoint leads to a useful visualization of conductivity in random networks. The mapping can also be used on tight binding Hamiltonians. Chapter 1 presents the general formulation of the mapping, as well as the results for the conductivity and superconductivity of random networks in two dimension. In chapter 2, the method is applied to the Penrose Tiling network or two dimensional quasicrystal. The advantage of the mapping is explored to establish a systematic way to calculate the diffusion constant. The result is compared with the diffusion constants given by other techniques, i.e. the Equation of Motion technique for the scattering spectrum S(q,E) and density of states and a direct evaluation of the diffusion constant by examining Random Walks. Chapter 3 extends the underlying ideas of the mapping to a deeper level and proposes a "tennis racket" model which bridges naturally the conductivity and elasticity percolation problems. A continuous phase diagram is obtained. The results at two extreme cases corresponding to conductivity percolation and pure central force percolation respectively agree with the previous research. The tennis racket model contributes much more enriched information to the macroscopic elasticity of noncrystalline materials.

ACKNOWLEDGEMENTS

First of all I would like to thank my advisor Professor M.F.Thorpe for all of his careful patient guidance over the last three years. His knowledge and insight helped guide me through this wide assortment of problems to produce some coherent results. I am indebted to Drs. W.W.Repko, J.Cowen, R.Stein, P.Duxbury who, as members of my guidance committee, must tolerate my writing for another 140 pages. I would also like to express my gratefulness to Professors S.D.Mahanti, T.A.Kaplan for a lot of useful discussions.

I really appreciate the discussion and coorperation with Dr. R.Day in the area of the elastic network under tension. I also appreciate the communication with Professor D.Sherrington, Dr. T.C.Choy in the research about quasicrystals.

Dr. E.Garboczi, Dr. M.Thomson, Dr.H.He and Mr. W.Xia, J.Gales, Y.Li, H.Yan have been good friends and the sources of much help. Especially the JPLOT developed by J.Gales has been a great tool in my research and the preparation of this thesis. I am grateful to the special help from J.S.Kovacs and J.King.

Finally, I should like to thank Liansheng Cao whose understanding, encouragement and assistance have helped bring this project to completion.

TABLE OF CONTENTS

LIST OF TABLES

LIST OF FIGURES

PREAMBLE

Traditionally, solid state physics has meant crystal physics. Yet, many of the materials we deal with do not have the simplicity and regularity found in crystals. In modern technology, noncrystalline solids play a very important role, for instance, the amorphous semiconductor in solar cells, the ultratransparent optical fibres in telecommunications, and the ubiquitous everyday uses for various kinds of glasses. In recent years, research in noncrystalline solids has been one of the most active fields in condensed matter physics.

It is well known that the mathematical amenities of the solid state theory (Brillouin zones, Bloch states, group-theoretical selection rules, etc.) are associated with the long range translational periodicity in the crystalline solid state. It is an intellectual challenge to achieve physical insights in noncrystalline materials which have no translational symmetry. While some of the traditional approaches remain useful in noncrystalline materials, this challenge has been met mainly by new approaches. (Zallen 1983; Elliott et al 1974)

Percolation theory is one of the new theoretical techniques applied to strongly disordered system. (Zallen 1983; Stauffer 1985; Straley 1983) It deals with the effects of varying a parameter such as the concentration or density in a random system. When increasing (or decreasing) the concentration, a <u>sharp phase transition</u> is found at which long range connectivity of the system suddenly appears (or disappears). The basic concepts in percolation theory can be understood from the following example. Consider the fluid flow in a porous medium which is modeled as a network of interconnected channels. Some of the channels are blocked at random. Those unblocked channels constitute a path through which the fluid can flow. A typical question in percolation is: what fraction of the channels must be blocked in order to prevent the fluid flowing through the whole medium? Or equivalently, one can ask, what is the threshold concentration of the unblocked channels that guarantees a finite probability of the existence of a percolated cluster of unblocked channels which spans the whole system. Since the elements in consideration are the channels (bonds), the problem is called "bond percolation". Its analogy is "site percolation" where instead of channels being blocked, the vertices (sites) of the network are pluged. Whenever a site is pluged, no fluid can flow through the channels adjacent to this site. Both bond and site percolation problems described here are determined by whether or not there exist a geometrically connected path through the system. Therefore, this kind of percolation problem is named connectivity percolation. The concentration p_c at which the dramatic change in the long range connectivity occurs is called the percolation threshold. This kind of percolation transition can be applied to several varieties of transport phenomena occuring in amorphous solids, for instance, the insulator/metal transition in conductor-insulator composite material; the disconnected/connected transition in resistor networks; the normal/superconducting transtion in composite superconductor-metal materials. (Zallen 1983)

One of the most prominent applications of percolation theory in condensed matter physics is the glass transition. It is widely believed that the structure of amorphous solids whose bonding is primarily covalent is well described by some form of covalent random network (Zallen 1983). Examples are $Se_{1-x}As_x$, $Se_{1-x}Ge_x$ and $Se_{1-x-y}As_xGe_y$, etc. Each atom (with coordination n) represents one n-functional unit. Two neighboring atoms are linked by a covalent bond. For example, Se (n=2) atom can form covalent bonds with two other atoms, while Ge has coordination number four. The desired fractions of x and 1-x are achieved through the correct compositions and the melt-quench process. It is easy to relate this fraction x to the concentration probability in an appropriate percolation model. Then a natural question is how do the elastic properties depend on the fraction x? (Thorpe 1983)

The connection between the elastic properties of a network and percolation was first established in a special type of glass transition: the sol → gel transition. (de Gennes 1976; Stauffer 1976) It is convenient to use the elastic properties to describe this transition since it naturally captures the essential feature of the condensation. In a gelation process, the elastic shear modulus vanishes for the sol (a liquid), begins to grow at the sol → gel transition, and continues to increase in the gel (solid) phase. One can see that this transition in the macroscopic elasticity is intimately linked to the percolation process involving the cross-linking between monomers. As the polymerization reaction goes on and more cross-links form, larger and larger molecules appear. Eventually, and abruptly, at a critical stage in the condensation process, an "infinitely extended" molecule appears, a huge molecule whose extent is limited only by the size of the vessel in which the reaction is taking place. Only this gel macromolecule contributes to the elastic shear moduli. It was pointed out by de Gennes that if the interaction between nearest neighbors is modeled by an <u>isotropic</u> elastic force, then the elastic modulus of the gel is exactly equivalent to the conductivity of the resistor network. Therefore the sol → gel transition belongs to the same universality class as connectivity percolation.

A new universality class of percolation was found in an elastic network when the interaction between nearest neighbors was modeled by pure central forces. (Feng & Sen 1984) In this model, the bond between interacting sites is replaced by an ordinary Hooke's law spring. Both numerical simulation and analytical results showed that with purely central forces, the threshold p_{cen} at which the elasticity of the network vanishes is significantly higher than the threshold p_c of the corresponding isotropic force problem. (Feng & Sen 1984; Feng, Thorpe & Garboczi 1985) This transition is called rigidity percolation as opposed to connectivity percolation. In this new class of problem, the elasticity of the network vanishes even when the whole network remains well connected geometrically. This phenomena is explained below. In the pure central force network, when bonds are removed from a pure lattice, some local floppy regions are created. These geometrically connected structures are called floppy since they are not able to transmit elastic forces. Eventually these local floppy regions prevent the rigid regions from percolating and the system loses its elasticity.

Actually, what we have considered as pure isotropic forces (connectivity percolation) and pure central forces (rigidity percolation) are two extreme cases of the Born model:

$$V = \frac{1}{2}\,(\alpha-\beta) \sum_{ij} [(\vec{u}_i-\vec{u}_j)\cdot\hat{r}_{ij}]^2\, g_{ij} + \frac{1}{2}\,\beta \sum_{ij} (\vec{u}_i-\vec{u}_j)^2\, g_{ij}$$

where the first term or $\beta=0$ case is the pure central force and the second or $\beta=\alpha$ case is the pure isotropic force. A crossover is found when both central and isotropic forces are included. (Feng & Sen 1984; Schwartz et al 1985)

However, the Born model has some troubles when one attempts to relate the macroscopic properties of amorphous materials to the microscopic atomic structures. First, the Born model is not rotationally invariant when β is nonzero. (Keating 1966) Second, the internal stress is neglected, which is not justified. It is well known that all real materials have internal stresses. One expects the stress-induced scalar elastic energy to be large and even dominant in many cases. It is unclear how the percolation transition is modified when the internal stresses of the material are involved.

This inspired us to propose and study a new model --- the tennis racket model, which is defined as the central-force network under tension. In Chapter 1, we establish a mapping between the resistor network and the central force network under very large tension (which can be imagined as the system having springs with natural length zero). The validity of this mapping is tested on several well understood systems. One result of this mapping is that it reduces the electrical problem to a geometrical problem and hence provides a useful visualization of the conductivity process. This advantage is explored in Chapter 2 in the calculation of the conductivity of the 2 dimensional quasicrystal or Penrose tiling. (Shechtman et al 1984; Socolar and Steinhardt 1986) Another result of the mapping which may be more important, is that connectivity percolation and rigidity percolation, which have been widely accepted as belonging to two different universality percolation classes, are intimately tied together. In other words, as soon as the internal stress is considered, these two classes of percolation problems occur naturally in a <u>rotational invariant central force spring system</u>. Chapter 3 gives a general discussion of the elastic behavior of such a system. We found that connectivity and rigidity percolations are actually two special cases of the central force network under extremely large tension or zero tension respectively. As the tension is varied, the percolation threshold evolves smoothly between these two limits of p_c and p_{cen}. We believe that the extensive results presented here for the elastic behavior of the noncrystalline network under tension will be useful in understanding many of real systems like glasses (Thorpe 1983, He & Thorpe 1985) and the newly discovered high T_c superconductors. (Khurana 1987)

Chapter 1. Mapping between Random Central Force Networks and Random Resistor Networks

Section 1.1 Introduction

The equilibrium voltage configuration of a random resistor network with an applied external voltage source can be obtained through the minimization of the electric energy stored in the network with respect to the voltage at each node. This leads to the Kirchoff's equations, which can be solved numerically as accurately as desired. This problem is equivalent to many other physical problems.

One example is the spin waves in a Heisenberg ferromagnet at low temperatures. With magnetic atoms on nodes of network, the voltage V_i is analogous to a tilt angle for the magnetic moment i. and the bond conductance maps onto the ferromagnetic exchange integrals. It was shown that the spin stiffness of such systems is the electric conductivity of the corresponding electric network. (Kirkpatrick 1973)

Another example is a gel obtained by polymerization of z-functional monomers. Modeled by an isotropic force constant, the elastic modulus of a gel is analogous to the electrical conductivity of an electrical network. The potential V_i represents one component (say X_i) of the elastic displacement of the $i^{\underline{th}}$ monomer from its rest position on the lattice. (de Gennes 1976)

In this chapter we explore yet another mapping. We will map the random electrical network to a central force network. This mapping is slightly more subtle and leads to some new physical insights.

Our purpose in this chapter is primarily to develop and explore the mapping. The organization of this chapter is as follows. In section 1.2, we develop the mapping and formula. We also show the relationship to the low energy density of states of a tight binding Hamiltonian. In section 1.3, we present the results for dilute resistor networks on square and triangular lattices as an illustration of the centroid algorithm based on the mapping. In section 1.4, we use the new algorithm to study the percolation properties of a 2-dimensional random network. A dual random network is constructed and it is shown how the superconducting/normal network on the dual lattice maps on to the dilute resistor network on the original lattice and vise versa. The relationship of this work to rigidity percolation is discussed in section 1.5.

Section 1.2 General Formulation

1.2.1 The Mapping

To illustrate the mapping, let us consider first a resistor network in which a voltage difference V_0 is applied across the two opposite sides. The current flows in the x direction across the voltage difference V_0. The conductivity G_{xx} is defined by $E = G_{xx}V_0^2$ where E is the electrical energy stored in the resistor network. Let us label the sites by i,j etc. so that a current I_{ij} flows in the ij bond which has a conductance σ_{ij}. Sites that are not connected have $\sigma_{ij} = 0$. Current conservation at each site leads to

$$\sum_j I_{ij} = 0 \tag{1.1a}$$

which using $I_{ij} = \sigma_{ij}(V_i - V_j)$, where V_i is the voltage at site i, leads to

$$\sum_j \sigma_{ij}(V_i - V_j) = 0 \tag{1.2a}$$

or

$$V_i = \frac{\sum_j \sigma_{ij}V_j}{\sum_j \sigma_{ij}} \tag{1.3a}$$

The total energy stored in the network is

$$E = \sum_{\langle i,j \rangle} \sigma_{ij}(V_i - V_j)^2 = G_{xx}V_0^2 \tag{1.4a}$$

where the angular brackets denote that each bond is only counted once in the sum. The conductivity is given by

$$G_{xx} = \sum_{\langle i,j \rangle} \sigma_{ij}(V_i - V_j)^2/V_0^2 \qquad (1.5a)$$

Now let us imagine a central force (Hooke) spring network in which each spring has natural length <u>zero</u>. The whole system is held on a frame to prevent it collapsing to a point. For a large system the shape of the frame is irrelevant, but it is convenient to imagine it to have a square shape. The equilibrium condition for each site i is that the total force acting on it vanishes. We have in the x direction

$$\sum_j K_{ij}(R_{ix} - R_{jx}) = 0 \qquad (1.2b)$$

where $\vec{R}_i$ is the position of the ith atom and K_{ij} is the spring constant. From this we see that

$$R_{ix} = \frac{\sum_j K_{ij} R_{jx}}{\sum_j K_{ij}} \qquad (1.3b)$$

There are equations similar to (1.2b) and (1.3b) in the y direction. The total energy stored in the spring system is

$$E = \frac{1}{2} \sum_{\langle i,j \rangle} K_{ij} \left[(R_{ix} - R_{jx})^2 + (R_{iy} - R_{jy})^2 \right]$$

$$= \frac{1}{2}\left[K_{xx} + K_{yy}\right] L^2 \tag{1.4b}$$

where L is the length of the sample and

$$K_{xx} = \sum_{\langle i,j\rangle} K_{ij}\,(R_{ix} - R_{jx})^2/L^2 \tag{1.5b}$$

and a similar expression for K_{yy}.

We see that the (a) and (b) equations can be made to coincide through the mapping,

$$\begin{aligned} \sigma_{ij} &\to K_{ij} \\ V_i &\to R_{ix} \\ G_{xx} &\to K_{xx} \end{aligned} \tag{1.6}$$

There is an important subtlety in this mapping associated with the boundary conditions. In the resistor problem, the net current flow is in a particular direction; x in the case considered here. This leads to the conductivity G_{xx}. In the spring problem, the frame acts equally in the x and y directions so that K_{xx} and K_{yy} cannot be obtained separately. This is not a problem for high symmetry networks, where the tensors $G_{\alpha\beta}$ and $K_{\alpha\beta}$ are proportional to the unit tensor. We shall refer to such networks as <u>electrically isotropic</u>. We shall only discuss such networks in this chapter. These include square nets, random square nets, triangular nets, random triangular nets and the random networks considered in section 1.4. We are thus led to

$$\mathrm{Tr}^{+}G^{+} = G_{xx} + G_{yy} + K_{xx} + K_{yy}$$

$$= \sum_{\langle i,j \rangle} K_{ij} \, (\vec{R}_i - \vec{R}_j)^2/L^2 \qquad (1.7)$$

The conductance can be calculated from the spring network via eq.(1.7) and the equilibrium condition (1.2b) that may be written in vector form

$$\sum_j K_{ij}(\vec{R}_i - \vec{R}_j) = 0 \qquad (1.8)$$

In 2D, the conductance and conductivity of a square sample are the <u>same</u>. For a sample of hypercubic shape in d dimensions (volume L^d), the current flows between parallel hyperplanes (area L^{d-1}) so that the conductance σ is given by

$$\sigma = G/L^{d-2} \qquad (1.9)$$

where G comes from eq.(1.7). Note that eq.(1.9) holds for electrically isotropic networks. Of course eq.(1.7) must be modified so that the trace is over all d dimensions and L^2

in eqs. (1.4b), (1.5b) and (1.7) must be replaced by L^d so that

$$\mathrm{Tr}\,\overleftrightarrow{G} \rightarrow \sum_{\langle i,j \rangle} K_{ij}\,(\vec{R}_i - \vec{R}_j)^2/L^d \qquad (1.7a)$$

and Eq. (1.4b) can be extended to read

$$E = \frac{1}{2}\ \mathrm{Tr}\,\overleftrightarrow{K}\ L^2$$

$$\rightarrow \frac{1}{2}\ \mathrm{Tr}\,\overleftrightarrow{G}\ L^2 = \frac{d}{2}\,G\,L^2 = \frac{d}{2}\,\sigma\,L^d \qquad (1.4c)$$

The pressure P can be obtained from

$$P = \frac{\partial E}{\partial L^d} \rightarrow \frac{G}{L^{d-2}} = \sigma\ . \qquad (1.10)$$

Thus the <u>conductivity</u> is obtained from (1.7a) while the <u>conductance</u> is equivalent to the the outward pressure needed to prevent the system collapsing to a point. For 2 dimensional systems, this pressure is independent of the size of the system L. For 1 dimensional systems, the pressure increases with size linearly, whereas for d > 2, the pressure decreases as the size gets larger. The total <u>force</u> required to prevent the system collapsing, <u>always</u> increases with size.

It may be convenient in some cases to have the spring network stretched on a circular frame or <u>tennis racket</u>, so that the boundary condition is isotropic.

1.2.2 Tight Binding Hamiltonian

A useful alternative viewpoint is given by the tight binding Hamiltonian

$$H = \frac{1}{2} \sum_{ij} K_{ij} \left[|i\rangle\langle i| - |i\rangle\langle j| \right] \qquad (1.11)$$

where the $|i\rangle$ is a localized s state on the i^{th} site (Alben et al 1972). The overlap integral K_{ij} is the same as the spring constant in Eq. (1.2b). It is convenient to take a (large) unit <u>supercell</u> containing n atoms. This cell is repeated periodically. Each atom is designated by a labeling (ℓ,n) where ℓ designates the cell and n is the atom within the cell. This label pair is conveniently denoted by $i \leftrightarrow (\ell,n)$. We can use Bloch's theorem on the supercell translations $\vec{R}_\ell$ to transform to a new basis

$$|\vec{q},n\rangle = \frac{1}{\sqrt{N_c}} \sum_{\ell} e^{i\vec{q}\cdot\vec{R}_{\ell+n}} \, |\ell + n\rangle \qquad (1.12)$$

The total number of atoms $N = n\, N_c$ where N_c is the number of supercells. The Hamiltonian (1.11) is Block diagonal in this basis and within a $\vec{q}$ block the matrix elements are given by

$$\langle\vec{q},n|H|\vec{q},n'\rangle = \frac{1}{N_c} \sum_{\ell\ell'} K_{ii'}[1 - e^{i\vec{q}\cdot(\vec{R}_i - \vec{R}_{i'})}] \tag{1.13}$$

where atoms i and i' are connected by the hopping matrix element $K_{ii'}$. These two atoms may either be in the same unit cell or in adjacent unit cells.

The Hamiltonian (1.11) deliberately has related diagonal and off diagonal terms so that the band edge is at E = 0. The eigenvector corresponding to zero energy is denoted by $|0\rangle$

$$|0\rangle = \frac{1}{\sqrt{n}} \sum_{n} |\vec{q} = 0,n\rangle \tag{1.14}$$

Labeling the other n-1 eigenvalues at $\vec{q} = 0$ by E_e, we use the matrix analogue of <u>k</u>•<u>p</u> perturbation theory (Harrison 1980). Given

$$\langle\vec{q},n|H|\vec{q},n'\rangle = \frac{1}{N_c} \sum_{i,i'} K_{ii'}\{-i\vec{q}\cdot(\vec{R}_i - \vec{R}_{i'}) + \frac{1}{2}[\vec{q}\cdot(\vec{R}_i - \vec{R}_{i'})]^2\} \tag{1.15}$$

then to second order

$$E_q = \frac{1}{2N} \sum_{i,i'} K_{ii'}[\vec{q}\cdot(\vec{R}_i - \vec{R}_i)]^2 - \sum_{e} \left|\sum_{i,i'} K_{ii'}\frac{\vec{q}\cdot(\vec{R}_i - \vec{R}_{i'})}{N_c\sqrt{n}} \langle\vec{q}=0,n|E_e\rangle\right|^2 / E_e \tag{1.16}$$

There is no term linear in $\vec{q}$ in (1.16) as this vanishes when the sum over all sites is done. If we are interested only in the density of states $\rho(E)$,then distances are irrelevant. We imagine forming an auxilary lattice in which the second term in (1.16) vanishes. This can be achieved if

$$\sum_j K_{ij} (\vec{R}_i - \vec{R}_j) = 0 \qquad (1.17)$$

this is the same condition as (1.8) and defines the same set of new atomic positions $\vec{R}_i$. Thus the sites in the auxilary lattice are coincident with the positions of the sites in the central force network discussed in subsection 1.2.1 . In the auxilary lattice

$$E_q = \frac{1}{2N} \sum_{i,j} K_{ij} [q \cdot (\vec{R}_i - \vec{R}_j)]^2 \qquad (1.18)$$

when i,j go over all sites. The unit supercell is not explicitly appearing in the summations in Eqs. (1.17) and (1.18). Note that (1.17) can be obtained by minimizing the energy in Eq. (1.18) with respect to the $\vec{R}_i$ if the $\vec{R}_i$ are initially regarded as arbitrary.

From (1.17) we may define principal axes where

$$E_q = D_{xx} q_x^2 + D_{yy} q_y{}^2 \qquad (1.19)$$

The area of the ellipse containing states up to an energy E is $\pi E/\sqrt{D_{xx}D_{yy}}$ so that the low energy density of states is

$$\rho(E) = \left(\frac{L}{2\pi}\right)^2 \frac{\pi}{\sqrt{D_{xx}D_{yy}}} \tag{1.20}$$

where L^2 is the area of the sample. This can be written as

$$\rho(E) = \left(\frac{L}{2\pi}\right)^2 \frac{\pi}{\sqrt{\mathrm{Det}\,\overleftrightarrow{D}}} \tag{1.21}$$

where $\overleftrightarrow{D}$ is the diffusion matrix which from (1.18) and (1.19) has matrix elements

$$D_{\alpha\beta} = \frac{1}{2N} \sum_{i,j} K_{ij}(R_{i\alpha} - R_{j\alpha})(R_{i\beta} - R_{j\beta}) \tag{1.22}$$

Note that

$$\mathrm{Tr}\ \overleftrightarrow{D} = \frac{L^2}{N}\ \mathrm{Tr}\,\overleftrightarrow{G} \tag{1.23}$$

where $\mathrm{Tr}\,\overleftrightarrow{G}$ is defined by Eq. (1.7). For electrically isotropic 2d systems we also have

$$\begin{aligned} \sqrt{\mathrm{Det}\,\overleftrightarrow{D}} &= \frac{1}{2}\,\mathrm{Tr}\,\overleftrightarrow{D} \\ &= \frac{L^2}{2N}\ \mathrm{Tr}\,\overleftrightarrow{G} \end{aligned} \tag{1.24}$$

$$= \frac{L^2\sigma}{N}$$

where σ is the conductance. Hence

$$\rho(E) = \frac{N}{4\pi\sigma} \qquad (1.25)$$

This density of states is normalized over all energies to the number of sites N, and the low energy part depends only on the conductance σ. Note that this result is very general and applies to any network that behaves as a continuum in the long wavelength limit. This <u>excludes</u> fractals. The geometry of the network enters only through σ.

These equations are easily generalized to higher dimensions. For Eqs. (1.11) to (1.18) there are no changes. We have to modify Eq. (1.19) to

$$E_q = \sum_\alpha D_{\alpha\alpha} q_\alpha^2 \qquad (1.19a)$$

where α goes over the d principal directions. The density of states given in Eqs. (1.20) and (1.21) becomes

$$\rho(E) = \frac{L^2}{4\pi\Gamma(d/2)\sqrt{\mathrm{Det}\,\overleftrightarrow{D}}} \left(\frac{L^2E}{4\pi}\right)^{d/2-1} \qquad (1.21a)$$

where Γ(d/2) is the Gamma function. Equations (1.22)-(1.23) are unchanged but (1.24)-(1.25) become

$$\sqrt{\mathrm{Det}^{\rightarrow}D^{\rightarrow}} = \frac{1}{d}\,\mathrm{Tr}^{\rightarrow}D^{\rightarrow}$$

$$= \frac{L^2}{dN}\,\mathrm{Tr}^{\rightarrow}G^{\rightarrow} \qquad (1.24a)$$

$$= \frac{L^d\sigma}{N}$$

and hence

$$\rho(E) = \frac{N}{4\pi\sigma}\,\frac{1}{\Gamma(d/2)}\,\left(\frac{E}{4\pi}\right)^{d/2-1} \quad . \qquad (1.25a)$$

Thus as in 2D, the low energy density of states is determined by the conductance σ and the total number of atoms N in the network and $\rho(E)$ is an extensive quantity. An atom is counted as being in the network if it is coupled to the backbone or conducting path. This includes regions that are connected to the backbone but carry no current. They nevertheless contribute to the inertia and so must be counted. Isolated regions that are not coupled to the backbone are ignored.

This method of using the tight binding Hamiltonian (1.11) to derive the centroid condition (1.17) is less satisfactory than mapping onto central force springs of natural length zero. This is because we had to introduce a "supercell" in order to have a $\vec{q}$ vector to work with. The final answer did not explicitly contain reference to this supercell and so we regard the result (1.25) as being quite general and true for any conducting network that is homogeneous on distances greater than some correlation length ξ. The derivation that lead to (1.25) is only valid for $q \ll \xi^{-1}$ and hence for vanishing by small energies as $\xi \rightarrow \infty$. We believe the result is actually much more general as the relevant length ξ is probably <u>not</u> the supercell size but rather the distance that characterizes the structural correlations in the random network. A similar quantity ξ is commonly used in percolation theory. (Kirkpatrick 1973) There is no easy way around this problem in a dynamic approach as given here.

In the static approach in 1.2.1 of this section, everything is rigorous. In order to get the dynamic result (1.25) one has to assume an Einstein relation between the conductance and the diffusivity. (Kirkpatrick 1973) It is here that the problem is glossed over. This area needs further study.

Section 1.3 Illustration of the Mapping and the Centroid Algorithm

1.3.1 Centroid Algorithm

Based on the mapping described in last section, we developed a new algorithm to calculate the electric conductivity of the random resistor networks, which is called as Centroid Algorithm. This name comes from the fact that the condition

$$\sum_j K_{ij} (\vec{R}_i - \vec{R}_j) = 0 \qquad \text{for each } i \qquad (1.8)$$

is just the condition that every site is at the centroid of its nearest neighbors that are present if K_{ij} takes only two values K (with probability p) and 0 (with probability 1-p). We summarize the centroid algorithm as the following:

(i) From the topology of a given resistor network, establish the central force elastic network by replacing a Hooke's spring with natural length zero at the place of each resistor with the spring constant $K_{ij} \sim \sigma_{ij}$.

(ii) Choose an appropriate boundary condition to prevent the elastic network from collapsing. Two boundary conditions usually used are the fixed frame and the periodic boundary condition.

(iii) Relax the elastic network until the energy stored in the springs is minimized. Specifically each site in the network is iteratively moved according to:

$$\vec{R}_i^{(n+1)} = \frac{\sum_j K_{ij} \vec{R}_j^{(n)}}{\sum_j K_{ij}} \qquad (1.8a)$$

For the isotropic case:

$K_{ij} = K$ with probability p

$K_{ij} = 0$ with probability 1-p

(1.8a) is simplified to:

$$\vec{R}_i^{(n+1)} = \frac{\sum_j \vec{R}_j^{(n)}}{z_i} \qquad (1.8b)$$

where z_i is the co-ordination at site i.

(iv) Finally, the conductivity G is proportional to the mean square nearest neighbor distance in the relaxed network:

$$G \sim \sum_{\langle i,j \rangle} \delta_{ij}^2 \; / \; L^2 \qquad (1.26)$$

where $\delta_{ij} = | \vec{R}_i - \vec{R}_j |$ is a nearest neighbor distance.

1.3.2 Simulation Results on Square and Triangular Net

Before we apply this method to any new structure, we use it on two well studied 2-dimensional systems: square net and triangular net. Let us consider the network shown in Figure 1.1a, where all the nearest neighbor bonds have resistance σ_0^{-1} and a fraction 1-p have been randomly removed. In the percolation problems one really wants to study the system in the thermodynamic limit ($N \to \infty$). Periodic boundary conditions are better than any other kind as every atom is properly coordinated. We therefore periodically repeat the "supercell" in Figure 1.1a. Bonds are removed randomly in the reference supercell and also in all others. Rather than put the network on a frame when we go to the central spring model, we hold the supercell repeat vectors constant. This is equivalent to an external pressure and more convenient in practice. The network is relaxed iteratively, site by site, until the energy stored in the springs is minimized. Figure 1.1b shows the relaxed network of Figure 1.1a. It is observed that isolated islands do not contribute to the conductivity and so relax to points and the side groups on the backbone that do not carry current also relax to points. Thus the conducting backbone is clearly and simply exposed by this algorithm. Those bonds that carry most current are stretched the most and so make the largest contribution to G.

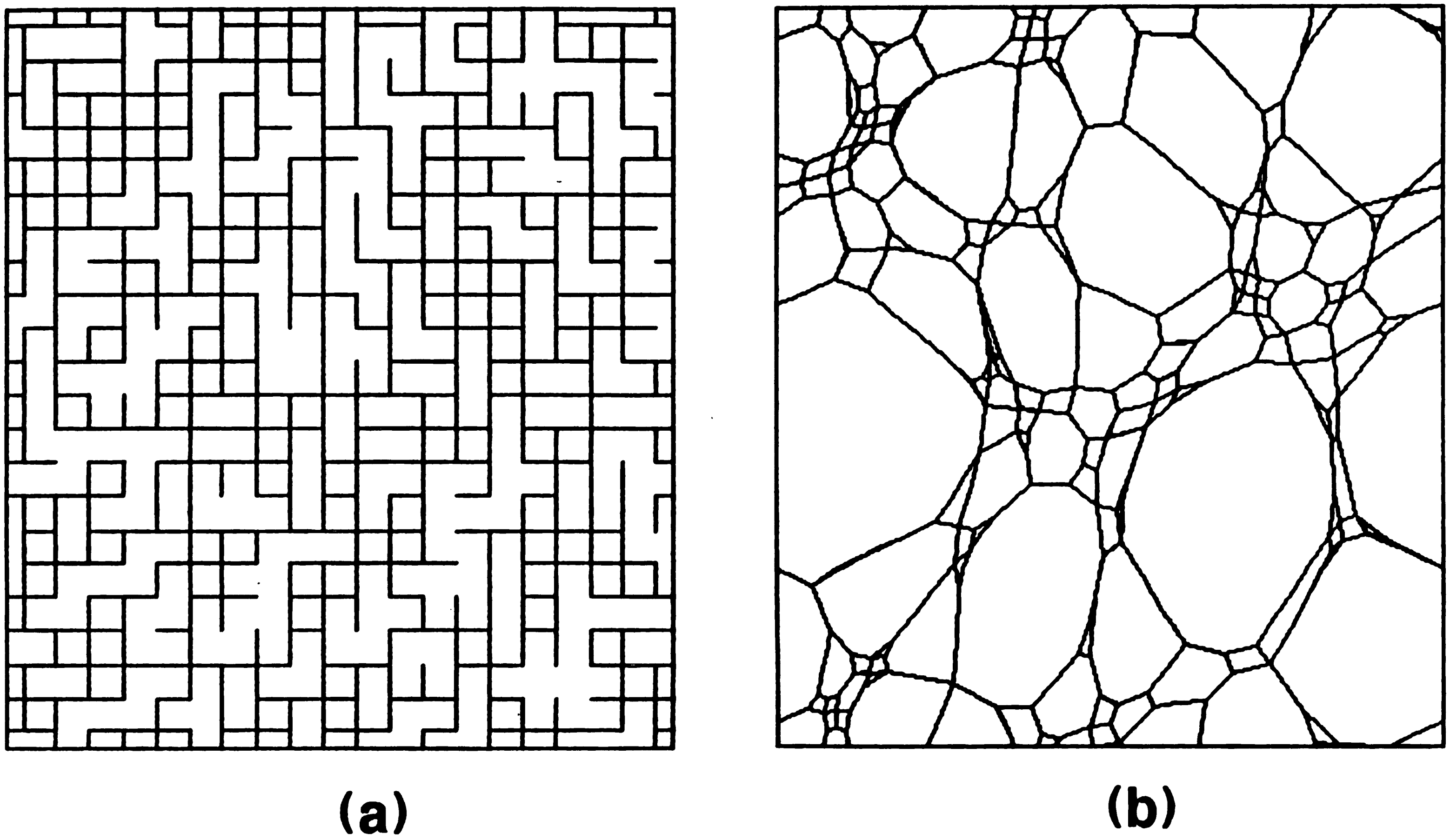

Figure 1.1 A square net with 70% of bonds present (a) before and (b) after relaxation with the centroid condition.

In Figure 1.2 we show some typical results for various values of p. Note that many of the long straight connections in Figure 1.2 are actually made up of many bonds and collapsed side groups. Below p_c, the whole network is broken and collapsed to many independent points, which corresponds to the vanishing of the conductivity. The networks for p = 0.70 in Figure 1.2 and Figure 1.1a are examples of different random configurations.

In Figure 1.3 we compared our simulation results for the conductance for site percolation on the square net with the result of Waston and Leath (1974). It can be seen that our results lie close to the effective medium theory which agrees well with a direct solution of Kirchoff's laws except very close to p_c. The tail that extends slightly below $p_c = 0.59$ in our simulations is due to finite size effects.

As our method is quite general, it works equally well for bond or site depleted networks. The simulation results on a square net and on a triangular net, for both site and bond percolation problems, are shown in Figures 1.4 and 1.5 respectively. The thresholds p_c agree well with previous work. Appendix A collects together the known results for the effect of a single defect into a single compact form that can be used in any lattice in the static limit. The result is used to calculate the effect of single defect, either bond or site, on the conductivity of various lattices, as well as the corresponding p_c.

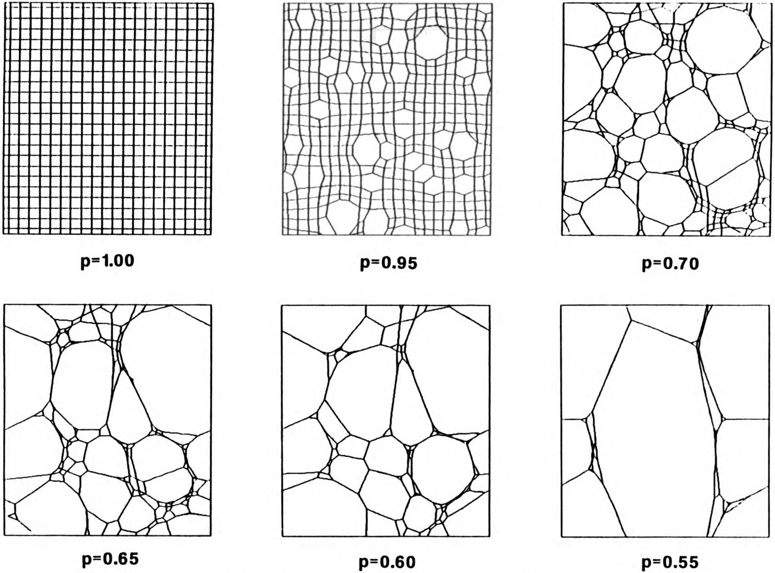

p=1.00

p=0.95

p=0.70

p=0.65

p=0.60

p=0.55

Figure 1.2 Square nets with a fraction p of bonds present after relaxation.

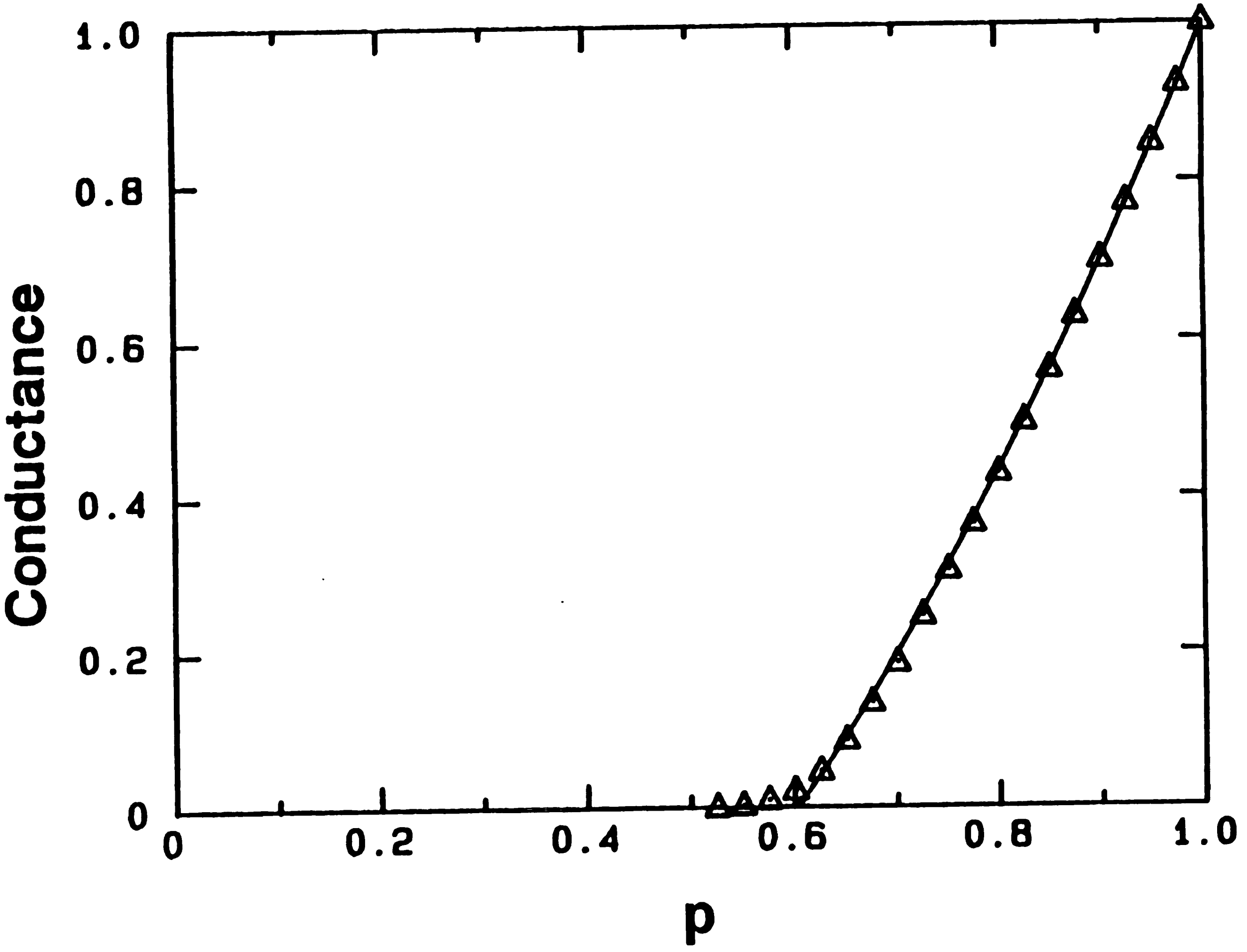

Figure 1.3 Conductance of a square net with fraction p of the sites present compared with the effective medium result of Watson and Leath.

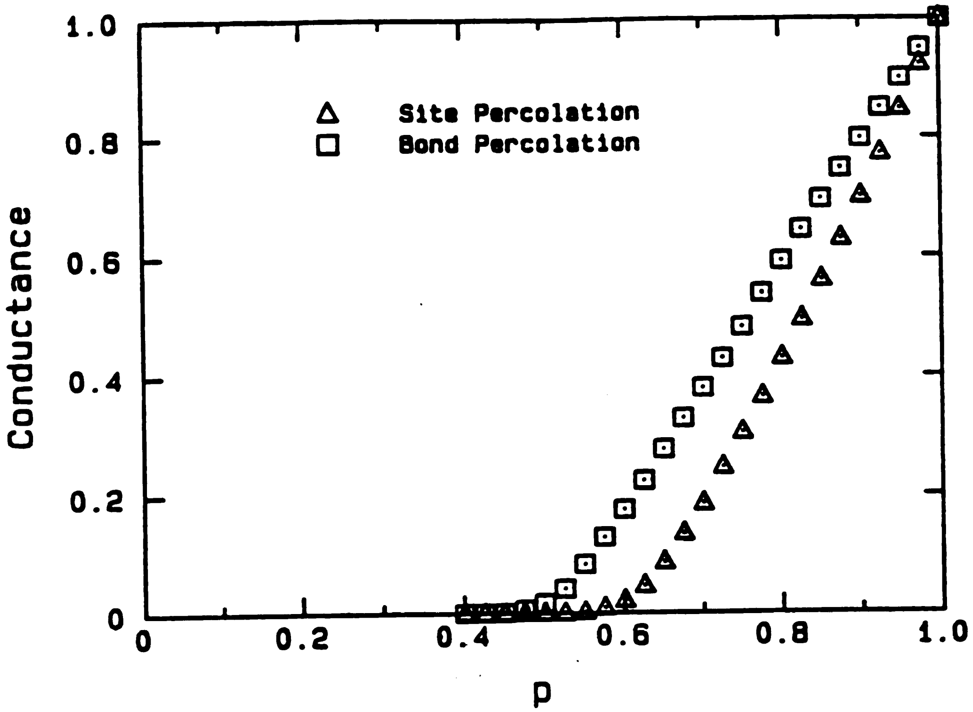

Figure 1.4 Conductance of square net for site and bond percolations.

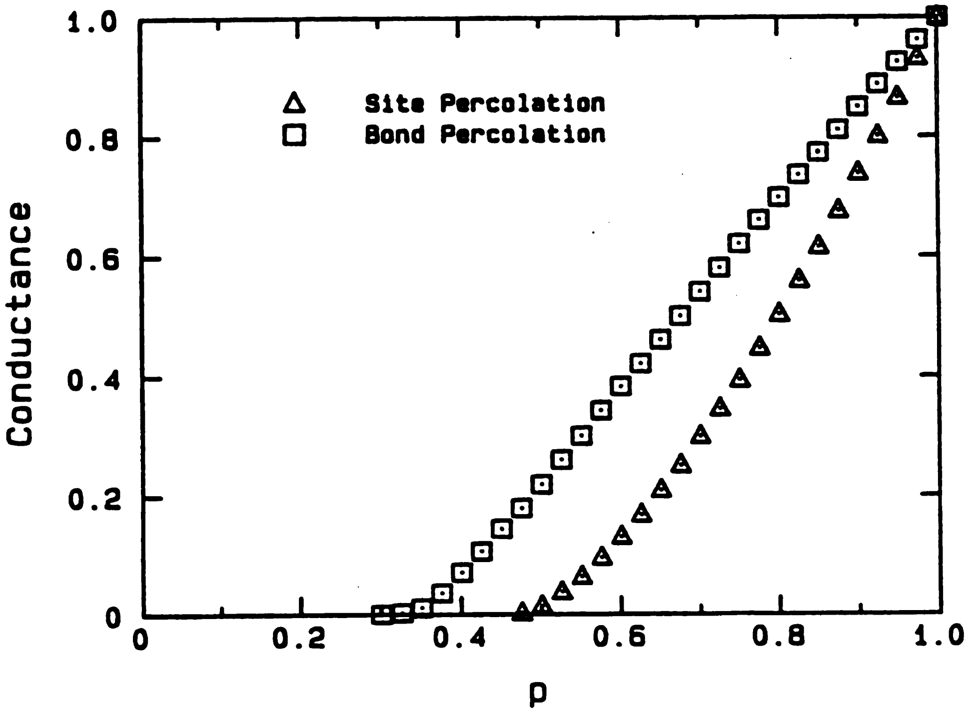

Figure 1.5 Conductance of triangular net for site & bond percolation.

Before leaving this section, we consider a general two dimensional network with nearest neighbor conductors of magnitude σ_0. The relaxed network and tight binding model [using Eqs. (1.17) and (1.18)] with the nearest neighbor $K_{ij} \to \sigma_0$, leads to

$$E_q = \frac{q^2}{4N} \sigma_0 \sum_{i,j} \delta_{ij}^2 \quad . \tag{1.27}$$

From this the density of states is

$$\rho(E) = NL^2/(\pi\sigma_0 \sum_{i,j} \delta_{ij}^2) \tag{1.28}$$

and hence from (1.25), the conductance σ is given by

$$\sigma = \sigma_0 \frac{\sum_{i,j} \delta_{ij}^2}{4L^2} \tag{1.29}$$

This is a convenient form. For the square net with N atoms and nearest neighbor distance a, we have $L^2 = Na^2$ so that

$$\sigma = \sigma_0 \tag{1.30}$$

Similarly for the triangular net

$$\sigma = \sqrt{3}\, \sigma_0 \tag{1.31}$$

and for the honeycomb lattice

$$\sigma = \sigma_0 / \sqrt{3} \quad . \qquad (1.32)$$

Section 1.4 Random Networks

1.4.1 Conductivity of 3-fold Co-ordinated Random Network and its Dual Network

We consider a random network where every site is three fold coordinated as shown in Figure 1.6a. This 800-site network was constructed by successively disordering a honeycomb lattice while maintaining the coordination. (He 1985) The lattice was then relaxed to make lengths as equal as possible. There is a small (~5%) variation in the bond lengths. We give all the bond conductor equal magnitude σ_0. We could have made the resistance proportional to the bond length but this seems unnecessarily complicated.

In order to calculate the conductivity, every atom is moved to the centroid of its three neighbors. The relaxed network is shown in Figure 1.7a. The changes are surprisingly large. The large polygons have grown and the small polygons have shrunk. There is also much more variability in the bond lengths than in Figure 1.6a.

Because the supercell of the sample shown in Figures 1.6a and 1.7a is not a square some additional care must be taken. The supercell shown has repeat distances L_x and L_y, where $L_x/L_y = 2/\sqrt{3} = 1.16$. These are held fixed during the relaxation. Minor changes in the previous formalism can easily be made for such a network. It can be shown that

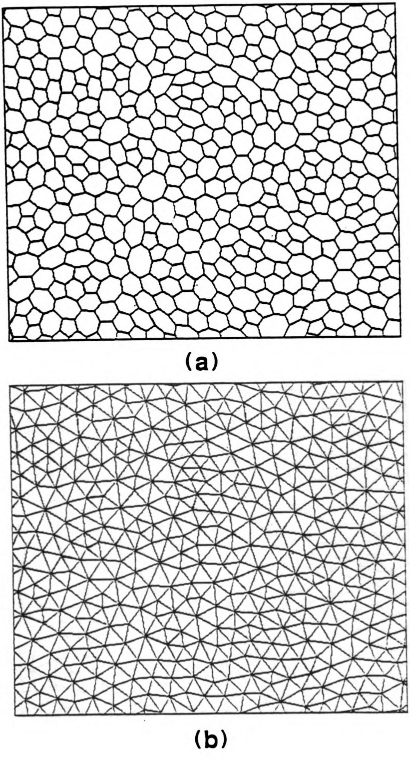

Figure 1.6 (a) A three coordinated random network (b) Dual net of (a).

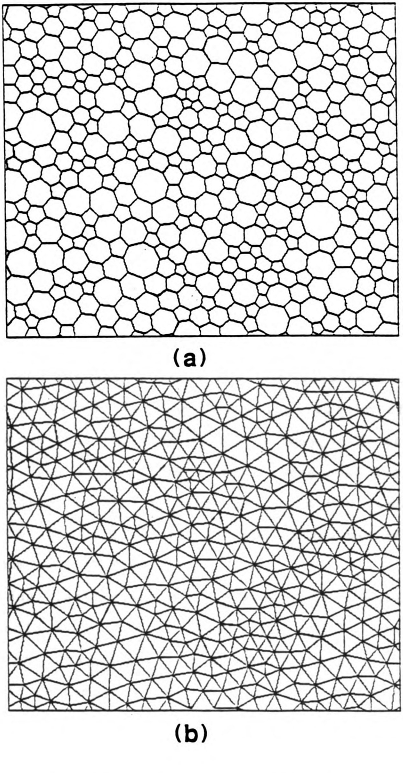

(a)

(b)

Figure 1.7 Relaxed configurations of Figure 1.6.

Eq. (1.29) holds for any electrically isotropic network, independent of the shape, if L^2 is replaced by the area A.

$$\sigma = \sigma_0 \frac{\sum_{i,j} \delta_{ij}^2}{4A} \qquad (1.29a)$$

We use the relaxed network of Figure 1.7a, to compute $\sigma = 0.555\ \sigma_0$. This should be compared to $\sigma = 0.577\ \sigma_0$ for the honeycomb lattice Eq. (1.32).

We also constructed the dual lattice of the random network as shown in Figure 1.6b. The dual transformation is simply assigning a dual vertex at the center of each polygon, then connecting those dual vertices that belong to adjacent polygons. An elementary application of Euler's theorem shows that the mean size of a polygon in the network of Figure 1.6a is six. Therefore in the dual lattice, the mean co-ordination is six, although it is not constant but varies from site to site; the minimum co-ordination is 5 and the maximum is 9 in Figure 1.6b.

The dual lattice shown in Figure 1.6b is relaxed using the centroid algorithm to obtain the relaxed lattice of Figure 1.5b. Using Eq. (1.29a) we find that $\sigma = 1.81\ \sigma_0$. This should be compared to $\sigma = 1.73\ \sigma_0$ for the triangular net in Eq. (1.31).

1.4.2 Duality Relationship for 2D Resistor Networks

It was known that there is a relationship between the conductivity of a 2D lattice with conductances chosen at random and the conductivity of a related distribution of conductances on the dual lattice. (Keller 1964)

Figure 1.8 can be used to explain the dual problem, where solid lines denotes a portion of direct random network and dashed lines shows the corresponding dual lattice. Let the potential at the vertex i on direct lattice be V_i and the conductance of the bond between i and its neighbor j be σ_{ij}. We can write down two conditions involving $V_{ij} = V_i - V_j$, which correspond to the continuum conditions $\nabla\times\nabla V = 0$ and $\nabla\bullet\vec{J} = 0$:

$$\sum V_{ij} = 0 \qquad \text{summed along any single loop} \qquad (1.33a)$$

$$\sum \sigma_{ij} V_{ij} = 0 \qquad \text{summed over all bonds involving site i} \qquad (1.33b)$$

Now we wish to introduce a function W_i similar to V_i, defined on the dual lattice. We label the dual lattice sites by i', j' etc. under the convention that bond (i',j') crosses bond (i,j). Then we define:

$$W_{i'j'} = \sigma_{ij} V_{ij} \qquad (1.34)$$

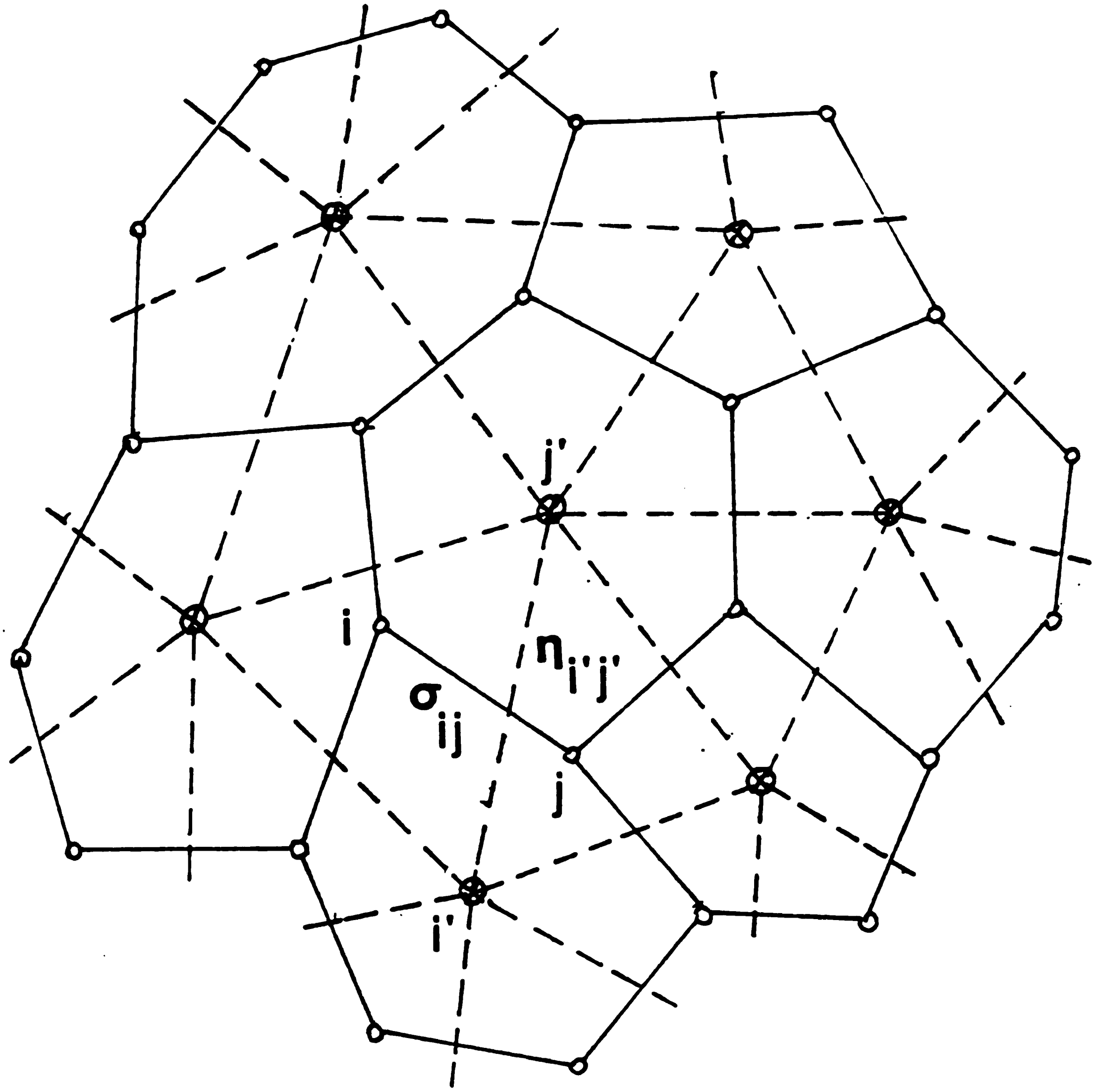

Figure 1.8 Illustration of the dual problem on random network.

That means the W difference between regions seperated by a lattice bond is the current flowing along that bond. It is easy to see that W around any closed loop on the dual lattice sums to zero, because it is equivalent to the condition that no net current flows into any vertex of the direct lattice. Actually condition (1.33b) gives:

$$\sum W_{i'j'} = 0 \qquad (1.35a)$$

To get an equation on dual lattice equivalent to (1.33b), we define the conductance of each dual bond $\eta_{i'j'}$ as the reciprocal of the conductance of the direct bond it crosses, i.e.

$$\eta_{i'j'}\, \sigma_{ij} = 1 \qquad (1.36)$$

Substituting (1.34), (1.36) into (1.33a) we have:

$$\sum V_{ij} = \sum \eta_{i'j'} W_{i'j'} = 0 \qquad (1.35b)$$

Now it is clear that W is the solution to Kirchoff's equation for this dual problem.

It was proved (Mendelson 1975) that the conductivity of direct lattice $\sigma_{direct}(q,a;\, p,b)$ of a concentration q of conductances a and concentration p of conductances b are related to that for dual lattice by:

$$\sigma_{direct}(q,a;\ p,b) = [\ \sigma_{dual}(p,b^{-1};\ q,a^{-1})\ ]^{-1} \qquad (1.37)$$

where $q=1-p$. This relation holds for any planar graph.

1.4.3 Simulation of Insulator/normal and Superconductor/normal Percolation

If we substitute

$a = 0$ (insulator)

$b = 1$ (normal)

into (1.37), we get:

$$\sigma_{direct}(q,0;\ p,1) = [\ \sigma_{dual}(p,1;\ q,\infty)\ ]^{-1} \qquad (1.38)$$

Note that the distribution of insulator in direct lattice is related to that of the superconductor in the dual lattice. This relation tells us that the conductivity in insulator/normal percolation is equal to the resistivity in superconductor/normal percolation on its dual lattice.

We proceed four sets of computer simulations:

(1) Insulator/normal percolation on random network. (Figure 1.6a)

(2) Superconductor/normal percolation on dual network. (Figure 1.6b)

(3) Superconductor/normal percolation on random net. (Figure 1.6a)

(4) Insulator/normal percolation on dual network. (Figure 1.6b)

We expect (1) and (2), (3) and (4) would satisfy the duality relation (38). Quantities referring to the direct lattice (Figure 1.6a) are denoted with subscripts 1 and quantities referring to the dual network (Figure 1.6b) are denoted by subscript 2.

In the insulator/normal percolation problem (1) and (4), we randomly remove bonds from these networks with probability 1-p. The depleted networks are relaxed using centroid algorithm and the conductances are computed by the method we have discussed in this chapter. The results for σ_1, against p_1, and σ_2 against p_2 are shown in Figures 1.9 and 1.10. These results have been obtained be averaging over 15 random depletions and σ_1 and σ_2 are set equal to one for the undepleted systems for convenience. As expected for such dual lattices, the critical points are related by $p_{1c} = 1-p_{2c}$. Note that for the honeycomb lattice (also coordination 3) the bond percolation concentration $p_c = 0.65$. From our simulations this $p_c \simeq p_{1c}$ as might be expected. In Figures 1.9 and 1.10, the solid lines are the effective medium theory results (for details see Appensix A)

$$\sigma_1 = 3p_1-2 \tag{1.39}$$

$$\sigma_2 = (3p_2-1)/2 \tag{1.40}$$

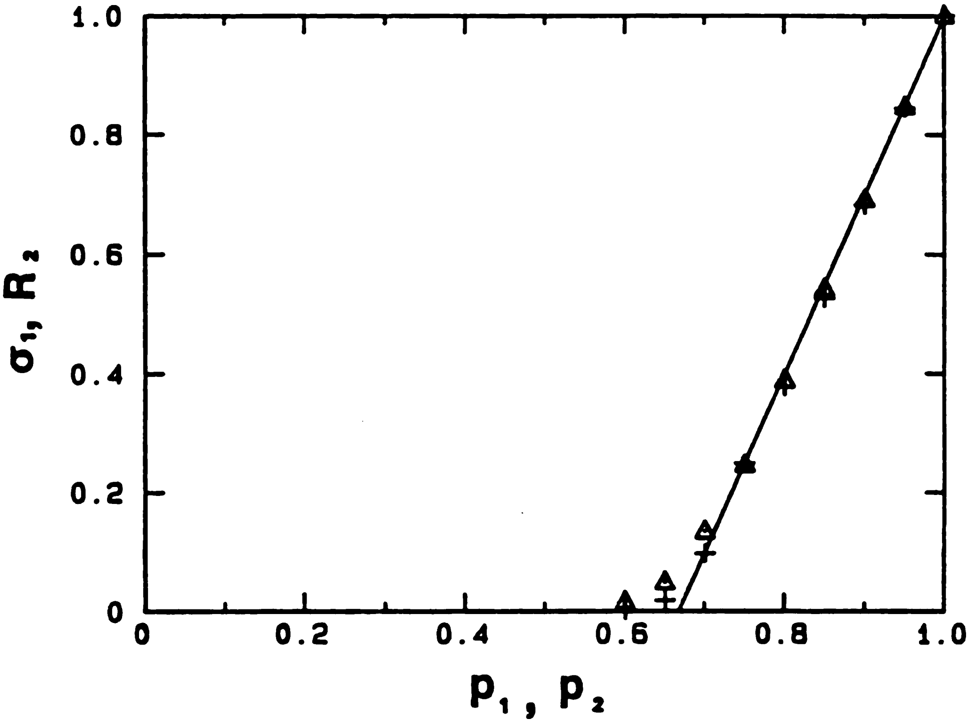

Figure 1.9 Conductance σ_1 of the network shown in Figure 1.6a, where p_1 is the fraction of normal bonds and $1-p_1$ insulating bonds. Also shown is resistance R_2 of the dual net shown in Figure 1.6b, where p_2 is the fraction of normal bonds and $1-p_2$ superconducting bonds. The solid line is the effective medium theory result.

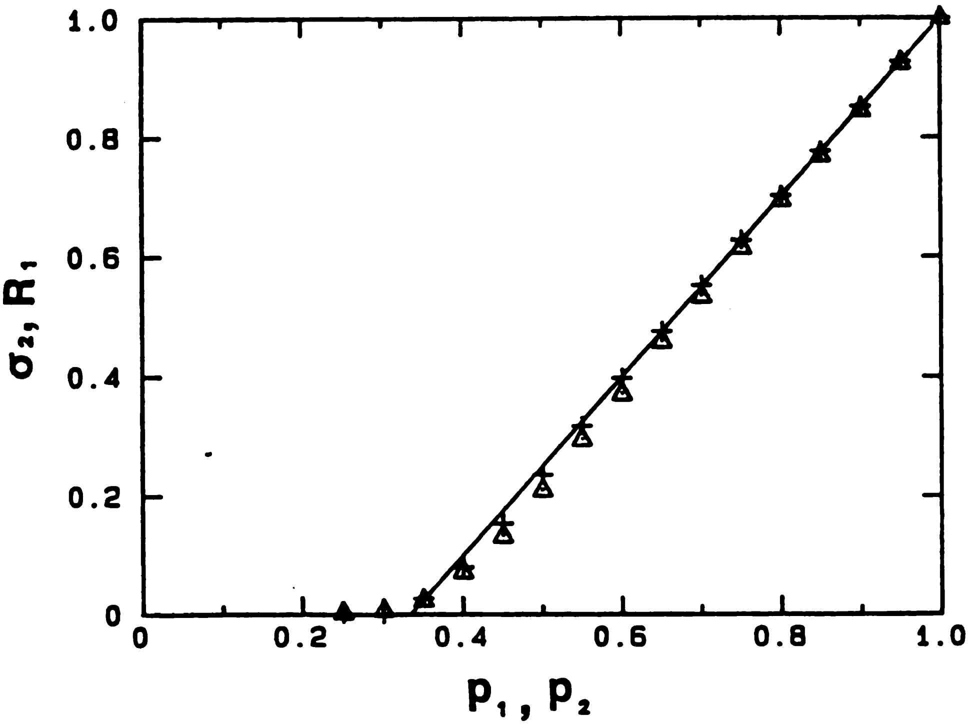

Figure 1.10 Same as Fig.1.9 except σ_2 and R_1 are substituted for σ_1 and R_2.

which are there as useful guides to the eye.

In the superconductor/normal percolation problems (2) and (3), we randomly change a fraction 1-p bonds from normal to superconducting. The resistance of the normal systems is normalized to 1. The resistivity for these networks, averaged over 15 samples, are also shown in Figures 1.9 and 1.10 and are seen to have the behavior expected of dual networks. In order to facilitate numerical simulations we have used a ratio of conductivities of 1000:1 between superconducting and normal bonds. The error introduced by this is mainly near p_c when there is a small incremental enhancement in the finite size tail. It would not be hard to take a larger conductivity ratio. Note that in the relaxed network, the superconducting bonds are fused together to a point so that consequently the normal bonds are elongated as the sample must remain fully connected and is not allowed to collapse. It can be seen that the dilute resistor problem on a network maps onto the superconducting/normal network on the dual network as expected.

Section 1.5 Conclusions

We have introduced a new mapping for the random resistor problem. Its utility is that it reduces the electrical problem to a geometric problem and hence provides a useful visualization of the conduction process.

We have applied these results to a few well studied problems. We have also studied depleted random networks and their dual networks for the first time. The results for the depleted three-coordinated random network are very close to those for the depleted honeycomb lattice and the results for the dual networks with mean coordination 6 are very similar to the depleted triangular lattice. This is to be expected since the co-ordination is the single most important parameter characterizing a percolating network. Also, the duality relationship is checked through the simulation of insulator/normal and superconductor/normal percolation.

The depletion of central force networks has recently been studied by many authors. These networks are such that every spring has its natural length in the absence of external stresses. This is often referred to as <u>rigidity percolation</u>. The elasticity vanishes at $p_{cen} > p_c$ because connected paths are inelastically ineffective. This is <u>not</u> the case in the work here as all springs in the conducting backbone are stretched by the frame. Hence the conductivity and elasticity are intimately tied together as we have shown.

Chapter 2. Low Energy Behavior of Infinitely Large 2D PENROSE Tiling

Section 2.1 Introduction

Unlike crystalline and glassy structures, which have one and an infinite number of unit cells respectively, the quasicrystal structure can be generated from two or more (but finite) number of unit cells.

One of the advantages of the "Centroid Algorithm" developed in Chapter 1 is the geometrical visualization of conductivity problem on random networks. It is noticed that on crystalline lattice the realization of the centroid condition is trivial since there is only one unit cell. On the other hand, for glassy structure, since there are an infinite number of units, we can only realize the centroid condition by numerical simulation as shown in Chapter 1. As a phase between these two, a quasicrystal has more than two (but finite) unit cells. The question then arose as to the possibility of solving the centroid condition on Penrose Tiling exactly, i.e. not to depend on the numerical simulation.

The so called Penrose Tiling is actually a two dimensional quasicrystal with "thin" and "fat" rhombi [with angles ($\pi/5$, $4\pi/5$) and ($2\pi/5$, $3\pi/5$) respectively] as two unit cells. The tiling invented by British mathematical physicist Roger Penrose is important here because (1) it gives us a non-trivial structure with purely Bragg diffraction and non-crystalline symmetry; (2) decorations of Penrose tilings are good structural models for the experimental realization.

In this Chapter, we report our numerical simulation on Penrose tiling at first in section 2.2. Then in section 2.3 we explore the self-similar properties and establish a systematic method to analyze the centroid configuration from which the conductivity is extracted. Section 2.4 presents the spin stiffness given by the density of states (DOS) and intensity spectrum S(q,E) by using the Equation of Motion technique. Section 2.5 presents the diffusion constant extracted from Random Walk simulation. Section 2.6 gives a comparison of these three techniques and conclusions.

Section 2.2 Numerical Simulation on Penrose Tiling

There are several methods to generate the Penrose Tiling: (1) the matching and deflation rules, (2) grid projection, (3) direct projections, and (4) generalized dual method. (Levine and Steinhardt 1986) We applied the first method in our computer modeling. The main idea of our algorithm is illustrated in Figure 2.1 . We start from one of the two basic unit cells: rhombi with acute angles 36° and 72°, called "fat" and "thin" rhombus respectively. During the process of deflation, each fat rhombus is deflated into three fat and two thin rhombi, and each thin rhombus is deflated into two fat and two thin. The arrows are used to explain the matching rules. Solid arrows are associated with seed rhombi which give a unique direction of deflation. Correspondingly, the dashed arrows are added to current rhombi to denote the direction of next generation of deflation. The matching rule embedded in these arrows guarantees that there will be no holes of mismatch appearing during deflation. Figure 2.2 shows a fragment of Penrose Tiling generated by this algorithm.

The centroid condition illustrated in Chapter 1 is used to relax the Penrose Tiling through numerical simulation. We took the circular piece as shown in Figure 2.3a, which contains 788 interior sites and 100 sites on the boundary. Recall that the bonds between nearest neighbors are imaginary central force springs with natural length zero,

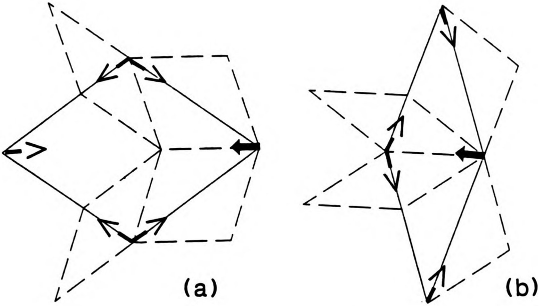

Figure 2.1 Deflation and matching rules in the generation of 2-d Penrose tiling with seed (a) Fat rhombus (b) Thin rhombus.

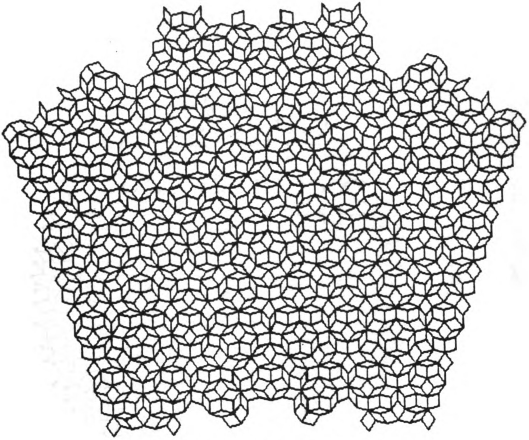

Figure 2.2 A portion of Penrose tiling lattice.

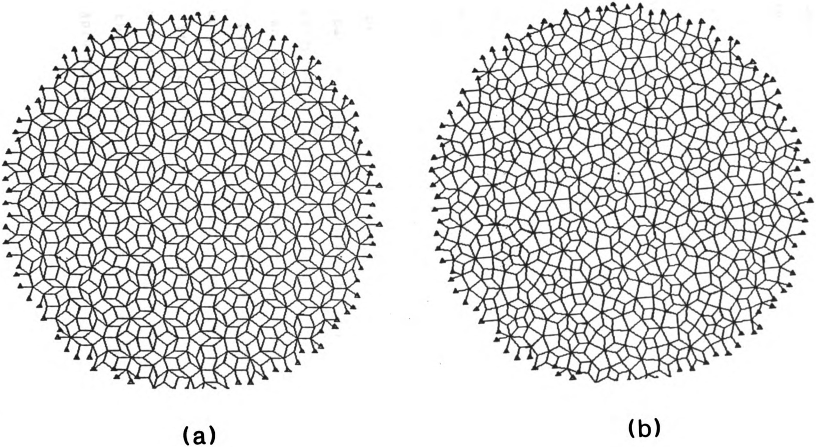

Figure 2.3 Penrose tiling with fixed circular boundary (a) before and (b) after the relaxation by centroid condition.

the whole sample must be put on a frame to prevent it from collapsing to a point. This is actually realized by fixing those boundary sites during the relaxation. Each interior site is moved to the center of its nearest neighbors iteratively. Figure 2.3b is the relaxed Penrose tiling.

By using the formula given in Chapter 1, we obtain the conductivity on the Penrose Tiling,

$$\sigma = \sigma_0 \frac{\sum_{i,j} \delta_{ij}^2}{zNa^2} = 0.936\ \sigma_0 \qquad (2.1)$$

where a is the unit length in the unrelaxed Penrose Tiling and z is the average coordination number which is four for Penrose tiling. It is known that σ is equivalent to the diffusion constant D through Kirkpatrick relation G=PD with the probability of a site belong to the backbone P=1 (Kirkpatrick 1973), noting that the conductance is equal to the conductivity σ in 2-dimension.

An interesting phenomenon is observed that there are some points kept stationary during the relaxation (in range of our precision). The significance of this observation is that if these vertices are really stationary, then we must be able to find out some basic cells and from which to realize the controid condition analytically. This possibility is explored in next section.

Section 2.3 Centroid Configuration Analysis

2.3.1 Fixed Vertices Hypothesis

It is not too surprising to notice that those points which seem stationary numerically during relaxation happen to be those vertices with the local five fold symmetry. In other words, in the unrelaxed Penrose structure, these points are automatically located at the centroid of their nearest neighbors. What inspired us is that if we connect these points in an appropriate way, we get a pattern with the Penrose Tiling topology as shown in Figure 2.4, where on the relaxed Penrose Tiling, we superimposed this pattern by heavy lines. We know that in the original unrelaxed Penrose tiling, this pattern is exactly the same as the original one but scaled by a factor τ^3,where $\tau = (1+\sqrt{5})/2$ is the golden ratio. However, on the relaxed Penrose Tiling where each site has been moved to the centroid of its nearest neighbors, we only can say this superlattice has the Penrose Tiling topology. This is a necessary but not sufficient condition for the existence of basic unit cells. The sufficient condition is one of the following three arguments which are equivalent each other:

(1) The vertices with local five fold symmetry are stationary points in the centroid relaxation.

(2) The superlattice on the unrelaxed Penrose Tiling is identical with that of the relaxed one.

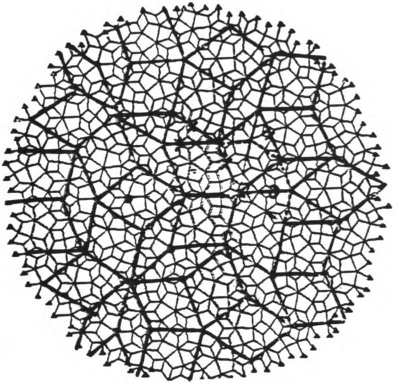

Figure 2.4 Most stationary vertices during relaxation connected appropriately to form a super Penrose tiling.

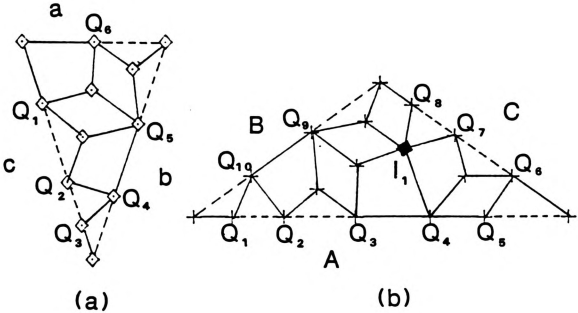

Figure 2.5 Basic cells (a) unit-1 and (b) unit-2.

(3) There are only two basic unit cells in the centroid configuration as shown in Figure 2.4. Figure 2.5 presents the topology of these two cells. These cells must match each other preserving the centroid condition on the boundary between them.

These equivalent arguments are called as "Fixed Vertices" hypothesis.

Our purpose was to find out the exact centroid configuration of the infinitely large Penrose Tiling and from which to extract the average bond length (which is related to the conductivity or diffusion constant through the mapping introduced in Chapter 1). Aiming at this, we took the third argument as our working hypothesis, i.e., we started by studying the two unit cells suggested by numerical simulation. The validity of the hypothesis will be self-evident from the results.

2.3.2 Method of Centroid Configuration Analysis

We consider the unit cell of the superlattice with isosceles triangle shapes and internal structures as shown in Figure 2.5. Notice that unit-1 in Figure 2.5a has the same topology as part of unit-2 in Figure 2.5b. We assume the shape of these two units are [72°, 72°, 36°] and [36°, 108°, 36°] respectively and the ratio of the sides is $1:\tau$. We take unit-2 as an example to illustrate the procedure of centroid configuration analysis.

(i) Degrees of Freedom and Variables

To analyze the centroid condition at each vertex, we assign the variables shown in Figure 2.5b. There are four kinds of vertices:

F's: The three fixed vertices of the triangle, with zero degree of freedom.

Q's: The vertices on the boundaries. They are only allowed to move along the boundaries of the triangle so that with one degree of freedom each.

I's: The interior vertices, with two degrees of freedom each.

C's: The interior vertices which could be expressed in terms of the F's, Q's, I's through the centroid condition.

Now we introduce variables to describe these degrees of freedom. We use l_i's to express the position of Q_i relative to a vertex along the boundary and use x_i, y_i as the horizontal and verticle coorditions of I_i. In summary, we list the functional coordinates of all sites in unit-2 as the following:

$$F_1=(0,0) \qquad F_2=(\cos 36°,\ \sin 36°) \qquad F_3=(\tau,0) \qquad (2.2a)$$

$$Q_i=(l_i,0) \qquad \text{where} \qquad i=1,2,\cdots,5$$

$$Q_i=[\tfrac{\tau}{2}+l_i\cos 36°,\ (1-l_i)\sin 36°] \qquad \text{where} \qquad i=6,7,8$$

$$Q_i=(l_i\cos 36°,\ l_i\sin 36°) \qquad \text{where} \qquad i=9,10 \tag{2.2b}$$

$$I_1=(x_1,\ y_1) \tag{2.2c}$$

$$C_1=(Q_2+Q_3+Q_9)/3$$

$$C_2=(I_1+Q_3+Q_9)/3$$

$$C_3=(I_1+F_2+Q_9)/3$$

$$C_4=(Q_4+Q_6+Q_7)/3 \tag{2.2d}$$

(ii) Symmetry and Centroid Conditions

Let us consider the site interior of the unit cell at first. Remembering that for C's the centroid conditions arebuilt in their definition, we only have constraints from the centroid condition for I's sites, i.e.

$$\sum_j (\vec{I}_i-\vec{R}_j) = 0 \tag{2.3}$$

for each i, where j are nearest neighbors of i.

It is a little bit more complicated for those sites on the boundary. Let us go back to the global structure shown in Figure 2.4. We can see that all of the three sides of unit-2 are the reflecting symmetry planes. One comes from the interior symmetry of the cell, the other two come from the tiling. This observation enable us to be able to write down the centroid conditions for those sites on the boundaries by assigning an appropriate weight to each bond. The constraint at site i which is on the boundary is:

$$\hat{Y}_k \cdot \sum_j (\vec{Q}_i - \vec{R}_j) w_{ij} = 0 \qquad (2.4)$$

where j's are nearest neighbors of i, $\hat{Y}_k$ is the unit direction of the side to which i belong to. Particularly for unit-2, we have:

$$\hat{Y}_1 = (1, 0)$$

$$\hat{Y}_2 = (\cos 36°, \sin 36°)$$

$$\hat{Y}_3 = (-\cos 36°, \sin 36°) \qquad (2.5)$$

and w_{ij} is the weight of bond between i and j:

$$w_{ij} = 1 \quad \text{if j is on the same boundary side as i,}$$

$$w_{ij} = 2 \quad \text{otherwise.} \qquad (2.6)$$

(iii) Equations and Solutions

We input these variables and conditions into a computer program by algebra language SCHOONSHIP to derive the set of linear equations for variables l_i and x_i, y_i in terms of the golden ration τ. We express our results in terms of the matrix relation:

$$A\ X = B \tag{2.7}$$

where for unit-2:

$$X^T = (l_1,\ l_2,\ \cdots,\ l_{10},\ x_1,\ y_1)$$

and A=

$$\begin{array}{cccccccccccc}
1 & 2 & 3 & 4 & 5 & 6 & 7 & 8 & 9 & 10 & 11 & 12 \\
\hline
-3 & & & & & & & & & \tau & & \\
 & \frac{-10}{3} & \frac{2}{3} & & & & & & \frac{\tau}{3} & \tau & & \\
 & \frac{2}{3} & \frac{-11}{3} & 1 & & & & & \frac{2\tau}{3} & & \frac{2}{3} & \\
 & & 1 & \frac{-16}{3} & 1 & \frac{\tau}{3} & \frac{\tau}{3} & & & & 2 & \\
 & & & 1 & 3 & \tau & & & & & & \\
 & & & \frac{-\tau}{3} & -\tau & \frac{13}{3} & \frac{-2}{3} & & & & & \\
 & & & \frac{-\tau}{3} & & \frac{-2}{3} & \frac{10}{3} & & & & -\tau & 2S36 \\
 & & & & & & & 3 & & & -\tau & 2S36 \\
 & \frac{\tau}{3} & \frac{2\tau}{3} & & & & & & -5 & 1 & \frac{2\tau}{3} & \frac{4}{3}S36 \\
\tau & \tau & & & & & & & 1 & -5 & & \\
 & & \frac{-1}{3} & -1 & & & \frac{-\tau}{2} & \frac{\tau}{2} & \frac{\tau}{3} & & \frac{13}{3} & \\
 & & & & & & S36 & S36 & \frac{-2}{3}S36 & & & \frac{13}{3} \\
\hline
\end{array}$$

and

$$B^T =$$

$$\left(0 \quad 0 \quad 0 \quad \frac{-2\tau}{3} \quad -\tau \quad \frac{7-4\tau}{3} \quad \frac{4(1-\tau)}{3} \quad (1-\tau) \quad \frac{-2}{3} \quad 0 \quad \frac{7\tau}{6} \quad \frac{7}{3}S36\right)$$

where $S36 = \sin 36° = \surd(3-\tau) / 2$.

By substituting the solution of this equation back to eq.(2.2), we can calculate the coordinates and the bond lengths, which are listed in Table 1(b).

2.3.3 Discussion about the Fixed Vertices Hypothesis

We have been concentrated on unit-2 and deliberately did not take unit-1 simultaneously. Now we will consider the inteference between unit-1 and unit-2.

At first, let us study the symmetry associated with unit-1. In Figure 2.5, we denote the three sides of unit-1 and unit-2 by a, b, c and A, B, C respectively. Careful examination of Figure 2.5 tells us that the side b of unit-1 is always adjacent with the side B of unit-2, while the side c of unit-1 is adjacent to c of unit-1 or C of unit-2 alternatively. This implies that unit-1 does not have exact enviroment as unit-2 so that it is not suitable to apply the same procedure described as above to solve unit-1, because not all three sides are reflecting symmetry planes any more. However, as we mensioned before, the unit-1 has the same topology as the shaded area of unit-2. Taking this fact into

Table 1 Solution of the Centroid Condition on the Unit Cells

(a) Unit-1

i	X_i	Variable
1	0.30833454	l_1
2	0.61296709	l_2
3	0.83629833	l_3
4	0.30351959	l_4
5	0.62649066	l_5
6	0.31246202	l_6

(b) Unit-2

i	X_i	Variable
1	0.16471666	l_1
2	0.38990027	l_2
3	0.69890436	l_3
4	1.01875734	l_4
5	1.25438254	l_5
6	0.69612647	l_6
7	0.39224764	l_7
8	0.16665261	l_8
9	0.62961840	l_9
10	0.30540149	l_{10}
11	0.90719375	x_1
12	0.29762443	y_1

Table 1 (cont'd.)

(c) Unit-3

i	X_i	variable
1	0.16379400	l_1
2	0.38788255	l_2
3	0.69605994	l_3
4	1.01615460	l_4
5	1.25276893	l_5
6	0.30525666	l_6
7	0.61072082	l_7
8	0.83913176	l_8
9	1.00978410	l_9
10	1.30786311	l_{10}
11	0.16403498	l_{11}
12	0.38771008	l_{12}
13	0.69235305	l_{13}
14	0.36726194	x_1
15	0.50803990	y_1
16	0.76697177	x_2
17	0.56379454	y_2

Table 1 (cont'd.)

(d) Unit-4

i	X_i	variable
1	0.16331457	l_1
2	0.38681679	l_2
3	0.69444045	l_3
4	1.01465665	l_4
5	1.25235023	l_5
6	0.30988959	l_6
7	0.60737915	l_7
8	0.77804903	l_8
9	1.00660513	l_9
10	1.31239882	l_{10}
11	2.25230592	l_{11}
12	2.01537787	l_{12}
13	1.69463300	l_{13}
14	1.38461450	l_{14}
15	1.15490521	l_{15}
16	0.98241525	l_{16}
17	0.62387806	l_{17}
18	0.30280186	l_{18}
19	0.69621370	x_1
20	0.23284415	y_1
21	0.83641407	x_2
22	0.09678353	y_2
23	1.04217145	x_3
24	0.15649422	y_3

Table 1 (cont'd.)

i	X_i	variable
25	1.11907083	x_4
26	0.36923084	y_4
27	1.21627382	x_5
28	0.65876242	y_5
29	1.50498894	x_6
30	0.36993531	y_6
31	1.90282232	x_7
32	0.29948289	y_7

account, it will not be meaningless to solve unit-1 independently under the assumed constraints that all three sides are reflecting symmetry planes and see what happen. Table 1(a) lists the results about unit-1.

Now let us come back to the global structure (Figure 2.4) to investigate the tiling of the whole space by these centroid unit cells. We have the following observations:

(1) Two sides of unit-2 are not only self reflecting but also should match with two sides of unit-1 respectively.

(2) Two sides of unit-2, B and C, are not self reflecting simultaneously, i.e. if the B or C side is reflecting, the other one must be adjacent with unit-1.

(3) Only the side c of unit-1 is self reflecting. The other side b is always adjacent to B of unit-2.

We express these observations in terms of the Adjacent Probability Matrix AP:

$$AP = \begin{array}{c|cccccc} & a & b & c & A & B & C \\ \hline a & 1 & 0 & 0 & 0 & 0 & 0 \\ b & 0 & 0 & 0 & 0 & p_{bB} & 0 \\ c & 0 & 0 & p_{cc} & 0 & 0 & p_{cC} \\ A & 0 & 0 & 0 & 1 & 0 & 0 \\ B & 0 & p_{Bb} & 0 & 0 & p_{BB} & 0 \\ C & 0 & 0 & p_{Cc} & 0 & 0 & p_{CC} \end{array} \qquad (2.8)$$

where $p_{\alpha\beta}$ is a number less than one denoting the porbability of corresponding adjacency of cell α and β.

Figure 2.6 shows all four possible adjacent situation of unit-1 and unit-2. The double shaded triangles are the host unit-1 and unit-2. The triangles around the host are the possible adjacent cells. Considering in combination the host cell and enviroment we find that the shaded area in each case forms two configurations as shown in Figure 2.7, which are called unit-3 and unit-4 respectively.

We apply the same procedure used before on these bigger cells. The results are listed in Table 1(c) and Table 1(d) respectively for unit-3 and unit-4.

Now we are at a point to check the validity of the "Fixed Vertices" hypothesis. If it is correct, then we would expect:

(1) In Figure 2.6, those points marked by "Δ" in middle of one side should divide the corresponding side into two parts with length ratio 1:τ.

(2) The two independently solved configurations unit-3 and unit-4 should have sides matchness as shown in Figure 2.8.

In Table 2, we showed the degree of incoincidence of the boundaries of the adjacent unit cells which are supposed to matched each other, as shown in Figure 2.8.

In Table 3(a), we listed all the bond lengths solved independently from the four unit cells, with the bond sequence number as shown in Figure 2.9a. The higher order unit cell includes the topology in the lower order one, as unit-4 includes unit-3, etc. We listed the corresponding bonds in the same row for reader's convinence. The number between is the relative deviation of the two bonds adjacent in the table.

In Figure 2.9b, we can see that the larger unit could be chopped into smaller parts with the same topology of the lower order unit cells. We compared these smaller parts in Table 2(b) and (c).

Unfortunately, none of our proposed checks has been verified exactly although the deviation is small. We are forced to admit that these points suggested by numerical simulation to be "stationary" are not exactly fixed.

2.3.4 Conductivity of Infinite Large Penrose Tiling

Although we showed the "Fixed Vertices" hypothesis not valid exactly, we are still rewarded by this research. We calculated the bond lengths in each unit cell. Through the mapping described in Chapter 1, we know that the average bond length gives the conductivity.

To calculate this quantity, each bond in the unit cell is associated with a weight. Depending on where the bond is located in the cell, there are five weights as listed below: (also see Figure 2.9a)

$P_1 = \tau$ (A - inside)

$P_2 = 1$ (B - inside)

$P_3 = 1/2$ (B - boundary)

$P_4 = \tau/2$ (A - boundary)

$$P_5 = 1/2 + \tau/2 = \tau^2/2 \quad (\text{ A-B boundary }) \qquad (2.9)$$

where A is the shaded and B is unshaded area in Figure 2.9a.

The formula we used to calculate the average bond length is:

$$\langle \delta^2 \rangle = \sum_i P(i)\, D_i^2 \,/\, \sum_i P(i) \qquad (2.10)$$

where i is summed over all the bonds in the cell and P(i) has the weight listed in (2.9) depends on where i-th bond is.

We finish this section by listing the results about the conductivity as the following,:

$$\begin{aligned} G\ (\text{unit-2}) &= 0.9362 \\ G\ (\text{unit-3}) &= 0.9333 \\ G\ (\text{unit-4}) &= 0.9316 \qquad (2.11) \end{aligned}$$

Result for unit-1 is not included since unit-1 cannot be futher chopped into two parts which is necessary to tile the whole space. We can see that the results are convergent in going to bigger and bigger unit cells. This can be understood through the fact that when tiling the infinite space by two bigger cells, the error due to the unmatchness between cells, i.e. the unsatisfactory of the centroid condition on board between cells is reduced progressively. In principle, to get a result as precise as required, one can always build up bigger and bigger unit cell systematically, and solve the centroid configuration as we have shown in this section.

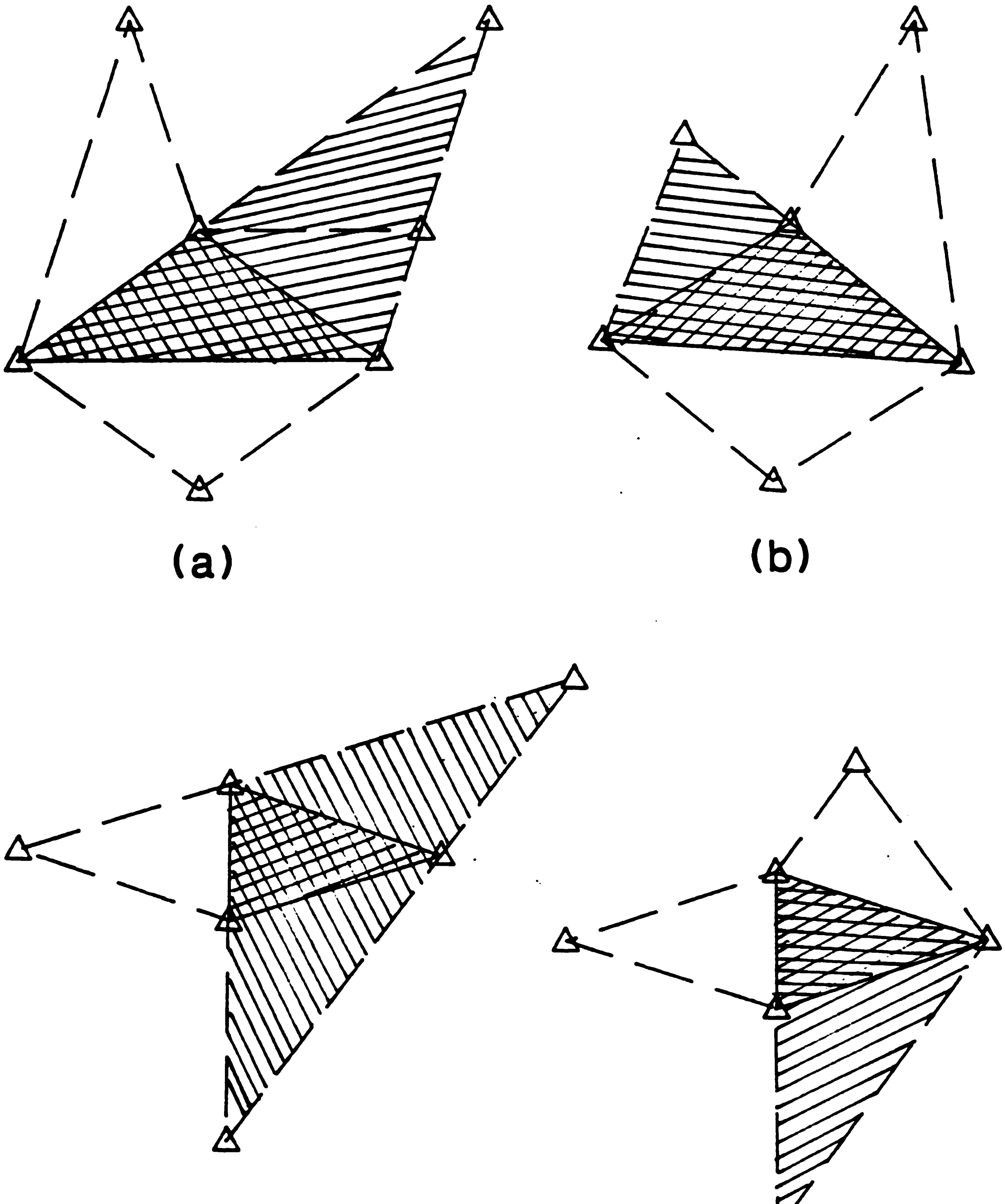

Figure 2.6 Enviromental configuration of unit-1 and unit-2 in Penrose tiling.

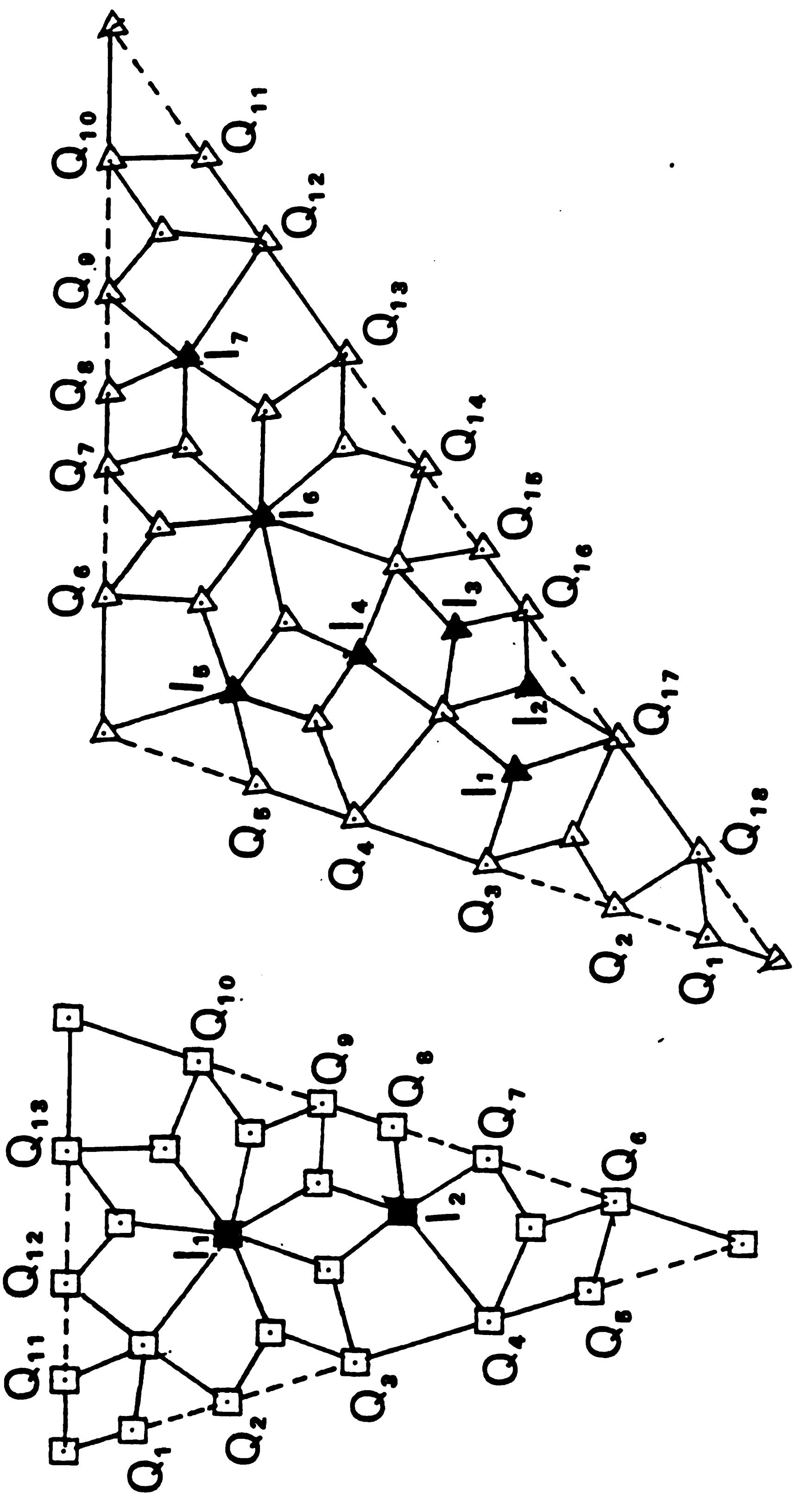

Figure 2.7 Basic cells (a) unit-3 and (b) unit-4.

Table 2 Degree of Incoincidence of the Cells Boundary

(a) Comparison of Unit-1 and Unit-2

site	Unit-1*	Unit-2*	|Δ| (%)
a	0.6264907	0.6296184	0.3128
b	0.3035196	0.3054015	0.1882
c	0.1637017	0.1666526	0.2951
d	0.3870329	0.3922476	0.5215
e	0.6916655	0.6961265	0.4461

(b) Comparison of Unit-3 and Unit-4

site	Unit-3*	Unit-4*	|Δ| (%)
A	1.3078631	1.3081445	0.0281
B	1.0097841	1.0106549	0.0871
C	0.8391318	0.8399849	0.0853
D	0.6107208	0.6114288	0.0708
E	0.3052567	0.3056351	0.0378
F	1.2527689	1.2523502	0.0419
G	1.0161546	1.0146567	0.1498
H	0.6969599	0.6944405	0.1619
I	0.3878826	0.3868168	0.1066
J	0.1637940	0.1633146	0.0479

* Number in the column is the distance from the site to the corresponding vertex in the unit cell.

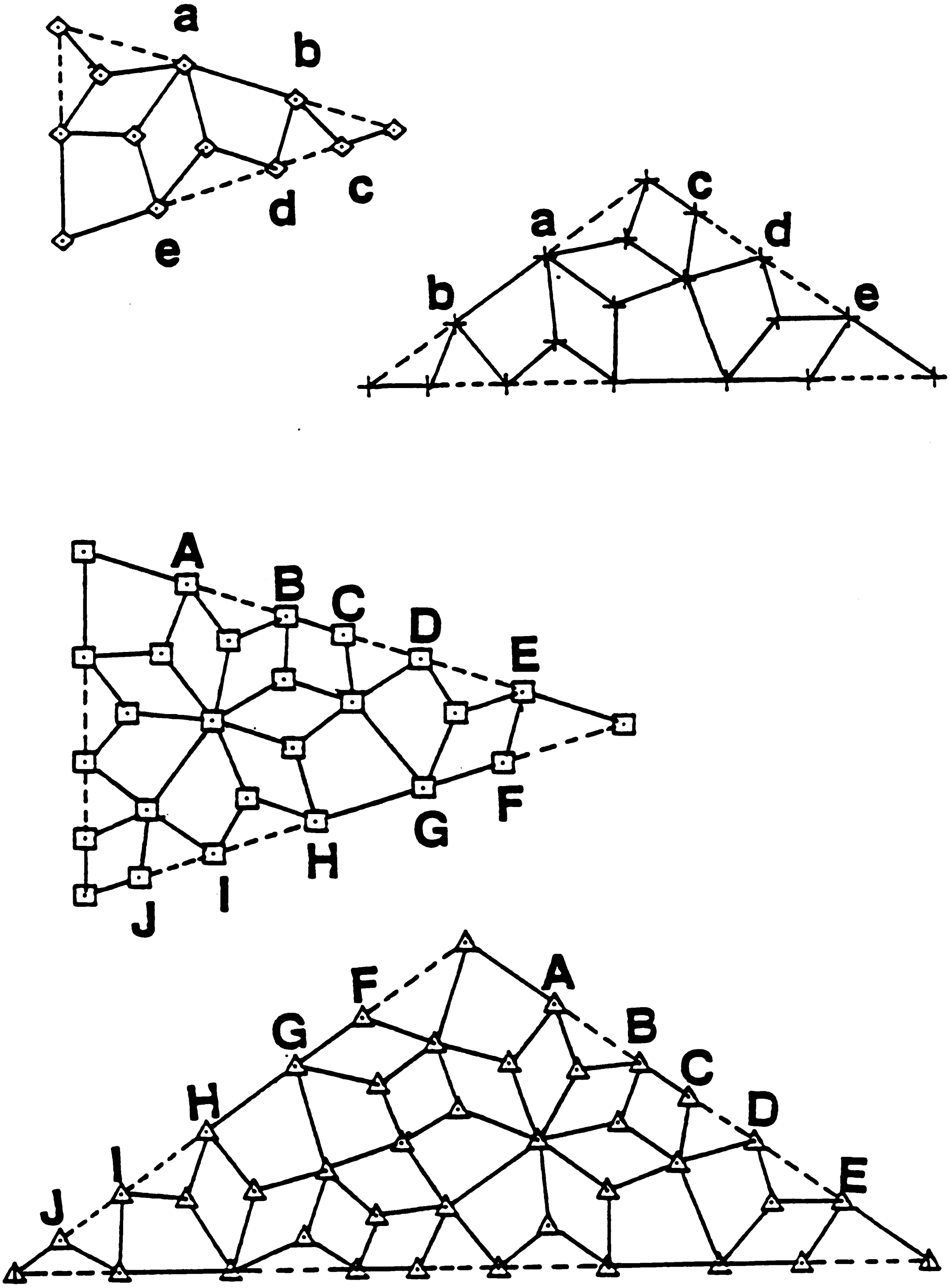

Figure 2.8 Illustration of the boundary fitting requirements between unit-1 & unit-2 and unit-3 & unit-4.

Table 3 Comparison of Bond Lengths Belong to Different Unit Cells

(a)

Bond No.	Unit 1		Unit 2		Unit 3		Unit 4
1	.30833454	3.736	.31985298	.076	.32009466	.203	.32074487
2	.16370167	.620	.16471666	.560	.16379400	5.309	.17248996
3	.32297107	.386	.32421691	.384	.32297207	.814	.32560216
4	.24291151	.916	.24513564	.214	.24461007	.052	.24473820
5	.22198558	.302	.22265608	.172	.22303828	.084	.22322501
6	.20417033	1.367	.20696165	.113	.20672803	.245	.20723438
7	.18730620	.757	.18872409	.300	.18815849	.541	.18917664
8	.24644936	.557	.24782309	.089	.24760227	.040	.24770207
9	.22769456	.748	.22939720	.385	.22851323	.432	.22950013
10	.19628466	.620	.19750167	.385	.19674089	1.053	.19881272
11	.31246202	1.732	.31784704	.565	.31964445	.091	.31993554
12	.21634506	.378	.21552818	.027	.21558575	.170	.21595227
13	.20328655	.747	.20480491	.730	.20629913	.060	.20642365
14	.23812550	.272	.23747681	.484	.23632762	.153	.23668902
15	.18361256	.812	.18212236	1.162	.18423796	.127	.18447194
16			.23562520	.420	.23661438	.133	.23692805
17			.30387353	.455	.30525666	.124	.30563516
18			.16665261	2.400	.17065234	.010	.17066988
19			.23562581	.430	.23663847	.130	.23694645
20			.19566756	.813	.19725803	.119	.19749211
21			.22711872	.503	.22826175	.125	.22854624
22			.18446341	.517	.18541743	.109	.18561947
23			.19976031	.462	.20068242	.122	.20092813

Table 3(a) (cont'd.)

Bond No.	Unit 1	Unit 2		Unit 3		Unit 4
24		.21396773	.444	.21491871	.127	.21519078
25				.16403498	2.121	.16751491
26				.19633892	1.998	.20026236
27				.22779152	.821	.22592235
28				.18722631	.342	.18786608
29				.24576845	.505	.24452781
30				.24268942	.214	.24216976
31				.20384074	.373	.20308063
32				.22094070	.889	.21897710
33				.23792241	.134	.23824238
34				.20136444	.147	.20106871
35				.21580831	.168	.21544558
36				.31017087	.091	.30988959
37				.30764695	.323	.30665475
38				.17939189	.031	.17944667
39						.32107620
40						.23769358
41						.32021620
42						.16331457
43						.19582051
44						.22759118
45						.18724714
46						.24563965
47						.24382133
48						.23353502

Table 3(a) (cont'd.)

Bond No.	Unit 1	Unit 2	Unit 3	Unit 4
49				.17516676
50				.20468290
51				.21458433
52				.22092206
53				.20597108
54				.31686367
55				.19313323
56				.23006690
57				.18480567
58				.23763567
59				.20179370
60				.20308063

Table 3 (cont'd.)

(b)

Unit 1	Unit 2	Unit 3a	Unit 3b	Unit 4a	Unit 4b	Unit 4c
.30833454^{1}	.31985298^{1}	.32009466^{1}	.30764695^{37}	.32074487^{1}	.32021620^{41}	.30665475^{37}
.16370167^{2}	.16471666^{2}	.16379400^{2}	.16403498^{25}	.17248996^{2}	.16331457^{42}	.16751491^{25}
.32297107^{3}	.32421691^{3}	.32297207^{3}	.32297207^{3}	.32560216^{3}	.32107620^{39}	.32560216^{3}
.24291151^{4}	.24513564^{4}	.24461007^{4}	.24268942^{30}	.24473820^{4}	.24382133^{47}	.24216976^{30}
.22198558^{5}	.22265608^{5}	.22303828^{5}	.22094070^{32}	.22322501^{5}	.22092206^{52}	.21897710^{32}
.20417033^{6}	.20696165^{6}	.20672803^{6}	.20384074^{31}	.20723438^{6}	.20597108^{53}	.20308063^{31}
.18730620^{7}	.18872409^{7}	.18815849^{7}	.18722631^{28}	.18917664^{7}	.18724714^{45}	.18786608^{28}
.24644936^{8}	.24782309^{8}	.24760227^{8}	.24576845^{29}	.24770207^{8}	.24563965^{46}	.24452781^{29}
.22769456^{9}	.22939720^{9}	.22851323^{9}	.22779152^{27}	.22950013^{9}	.22759118^{44}	.22592235^{27}
.19628466^{10}	.19750167^{10}	.19674089^{10}	.19633892^{26}	.19881272^{10}	.19582051^{43}	.20026236^{26}
.31246202^{11}	.31784704^{11}	.31964445^{11}	.31017087^{36}	.31993554^{11}	.31686367^{54}	.30988959^{36}
.21634506^{12}	.21552818^{12}	.21558575^{12}	.21580831^{35}	.21595227^{12}	.21458433^{51}	.21544558^{35}
.20328655^{13}	.20480491^{13}	.20629913^{13}	.20136444^{34}	.20642365^{13}	.20468290^{50}	.20106871^{34}
.23812550^{14}	.23747681^{14}	.23632762^{14}	.23792241^{33}	.23668902^{14}	.23353502^{48}	.23824238^{33}
.18361256^{15}	.18212236^{15}	.18423796^{15}	.17939189^{38}	.18447194^{15}	.17516676^{49}	.17944667^{38}

Table 3 (cont'd.)

(c)

Unit 2	Unit 3	Unit 4a	Unit 4b
.31985298^{1}	.32009466^{1}	.32074487^{1}	.32021620^{41}
.16471666^{2}	.16379400^{2}	.17248996^{2}	.16331457^{42}
.32421691^{3}	.32297207^{3}	.32560216^{3}	.32107620^{39}
.24513564^{4}	.24461007^{4}	.24473820^{4}	.24382133^{47}
.22265608^{5}	.22303828^{5}	.22322501^{5}	.22092206^{52}
.20696165^{6}	.20672803^{6}	.20723438^{6}	.20597108^{53}
.18872409^{7}	.18815849^{7}	.18917664^{7}	.18724714^{45}
.24782309^{8}	.24760227^{8}	.24770207^{8}	.24563965^{46}
.22939720^{9}	.22851323^{9}	.22950013^{9}	.22759118^{44}
.19750167^{10}	.19674089^{10}	.19881272^{10}	.19582051^{43}
.31784704^{11}	.31964445^{11}	.31993554^{11}	.31686367^{54}
.21552818^{12}	.21558575^{12}	.21595227^{12}	.21458433^{51}
.20480491^{13}	.20629913^{13}	.20642365^{13}	.20468290^{50}
.23747681^{14}	.23632762^{14}	.23668902^{14}	.23353502^{48}
.18212236^{15}	.18423796^{15}	.18447194^{15}	.17516676^{49}
.23562520^{16}	.23661438^{16}	.23692805^{16}	.23769358^{40}
.30387353^{17}	.30525666^{17}	.30563516^{17}	.30665475^{37}
.16665261^{18}	.17065234^{18}	.17066988^{18}	.16751491^{25}
.23562581^{19}	.23663847^{19}	.23694645^{19}	.23763567^{58}
.19566756^{20}	.19725803^{20}	.19749211^{20}	.19313323^{55}
.22711872^{21}	.22826175^{21}	.22854624^{21}	.23006690^{56}
.18446341^{22}	.18541743^{22}	.18561947^{22}	.18480567^{57}
.19976031^{23}	.20068242^{23}	.20092813^{23}	.20179370^{59}
.21396773^{24}	.21491871^{24}	.21519078^{24}	.20308063^{60}

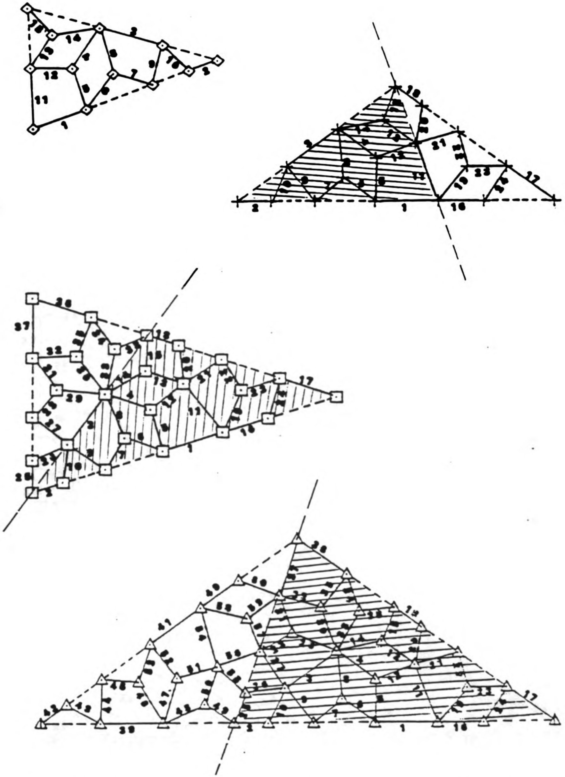

Figure 2.9a Illustration of the assignment of weights to bonds in different region of unit.

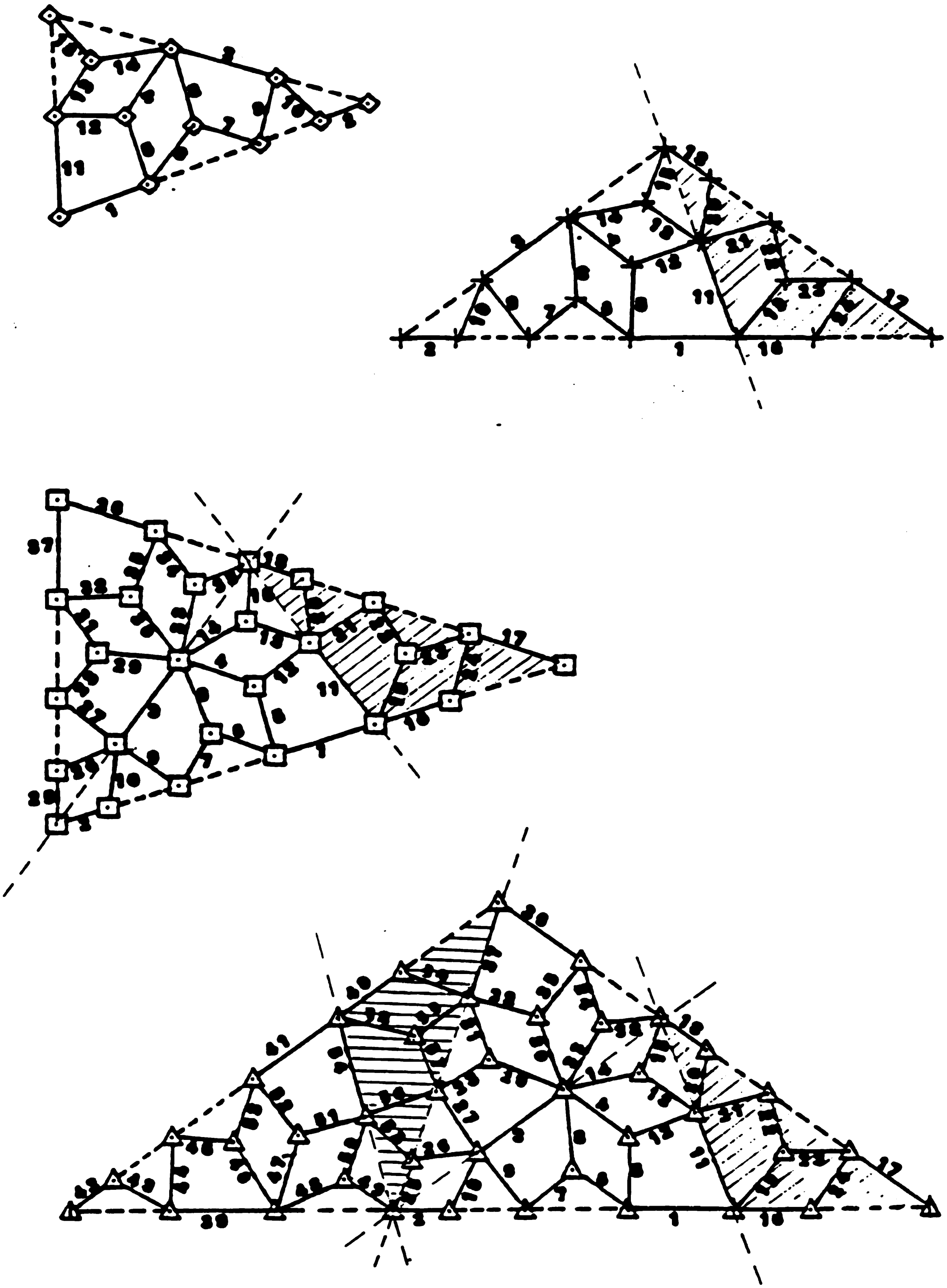

Figure 2.9b Illustration of the similar topology between adjacent generations of units.

Section 2.4 Equation of Motion Approach

In this section, we apply the well established Equation of Motion method on Penrose Tiling to calculate the DOS and S(q,E) on purpose to compare with the Centroid method result.

2.4.1 Equation of Motion Method

Let us consider a spin system on a Penrose Tiling lattice. On each lattice point there is a spin and the interaction between spins is of the Heisenberg form:

$$H = -\sum_{\langle i,j\rangle} J_{ij}\, \vec{S}_i \cdot \vec{S}_j \qquad (2.12)$$

where the sum is over pairs of nearest-neighbor sites and J_{ij} is the exchange constants between site i and j.

We make the linear spin approximation via the lowest-order Holstein-Primakoff transformation

$$\begin{aligned} S_i^+ &\rightarrow (2S)^{1/2}\, a_i \\ S_i^- &\rightarrow (2S)^{1/2}\, a_i^+ \\ {S^z}_i &\rightarrow S - a_i^+\, a_i \end{aligned} \qquad (2.13)$$

where S is the value of the spin (the same for all atoms) and a_i and a_i^+ are Bose destruction and creation operators. From (2.12) and (2.13) we obtain the quadratic, linear spin-wave Hamiltonian:

$$H = \sum_{(i,j)} S J_{ij} (a_i^+ a_i - a_i^+ a_j) \qquad (2.14)$$

where pairs occur twice in the summation.

In principle, the quadratic Hamiltonian (2.14) can be transformed to a set of normal modes q with energies E_q. What we are interested is to obtain the distribution of the E_q's (density of states) and also the scattering intensity S(q,E).

We define a set of quantities $g_{iq}(t)$:

$$g_{iq}(t) = \langle a_i(t) \sum_j a_j^+(0) e^{i\vec{q}\cdot\vec{R}_j} \rangle \qquad (2.15)$$

where $\vec{R}_j$ is the position of site j and ⟨ ⟩ indicates the ground state expectation value. Note that the sum is over all sites. The g_{iq}'s obey the following <u>Equation-of-Motion</u>:

$$i\, h \frac{dg_{iq}}{dt} = \sum_j S J_{ij} (g_{iq} - g_{jq}) \qquad (2.16)$$

with the initial condition

$$g_{iq}\ (t=0) = e^{i\vec{q}\cdot\vec{R}i} \qquad (2.17)$$

The normalized form for the scattering intensity is defined as (Alben et al 1977):

$$S(q,E)$$

$$= \frac{1}{2\pi Nh} \int_{-\infty}^{+\infty} e^{iEt/h} < (\sum_i a_i(t)\ e^{-i\vec{q}\cdot\vec{R}_i})(\sum_j a_j^+(0) e^{i\vec{q}\cdot\vec{R}_j}\ )> dt$$

$$= \lim_{\lambda\to 0^+} \lim_{T\to\infty} \frac{1}{\pi Nh} \text{ Re } \int_0^T \sum_i e^{-i\vec{q}\cdot\vec{R}i}\ g_{iq}(t)\ e^{iEt/h}\ e^{-\lambda t^2}\ dt \qquad (2.18)$$

where N is the number of spins and E is the energy. The normalization is such that the energy integral of S is unity. The essential point of the Equation-of-Motion procedure is that if we are interested only in broadened spectra, we can do the transform in eq.(2.18) with a nonzero value for the damping constant λ and a finite value for the time interval T.

Specifically, we proceed the following procedures:

(1) Initially assigning N values of $g_{iq}(t=0)$ by eq.(2.17) for a given $\vec{q}$.

(2) Integrating the N simultaneous differential equation (2.16) forward in time to obtain N g_{iq} over a time interval from 0 to T.

(3) Choose the damping constant λ to give an approximately Gaussian broadening function and compute S(q,E) by doing the integral in (2.18).

The Density of States can be obtained by using the exactly same procedures as above just replacing $e^{i\vec{q}\cdot\vec{R}i}$ by an random phase factor $e^{i\alpha_i}$, where the α_i's are random angle specified for each site. The average over many sets of α_i's gives exactly the density-of-states spectrum.

2.4.2 Calculation of Density of States

Our purpose to calculate DOS is to extract the conductance of the resistor network with the corresponding topology. We have shown in Chapter 1 that for a tight-binding Hamiltonian

$$H = \frac{1}{2}\sum_{\langle i,j\rangle} J_{ij} \left[\, |i\rangle\langle i| - |i\rangle\langle j| \,\right] \qquad (1.11)$$

its density of state at long wavelength limit can be expressed in terms of the conductance

$$\rho\ (E\to 0) = \frac{N}{4\pi\sigma} \qquad (1.25)$$

In Figure 2.10 we show the result of equation of motion calculation of density of state for a 888-site circular Penrose Tiling. We applied the fixed boundary condition. We found out the initial DOS is:

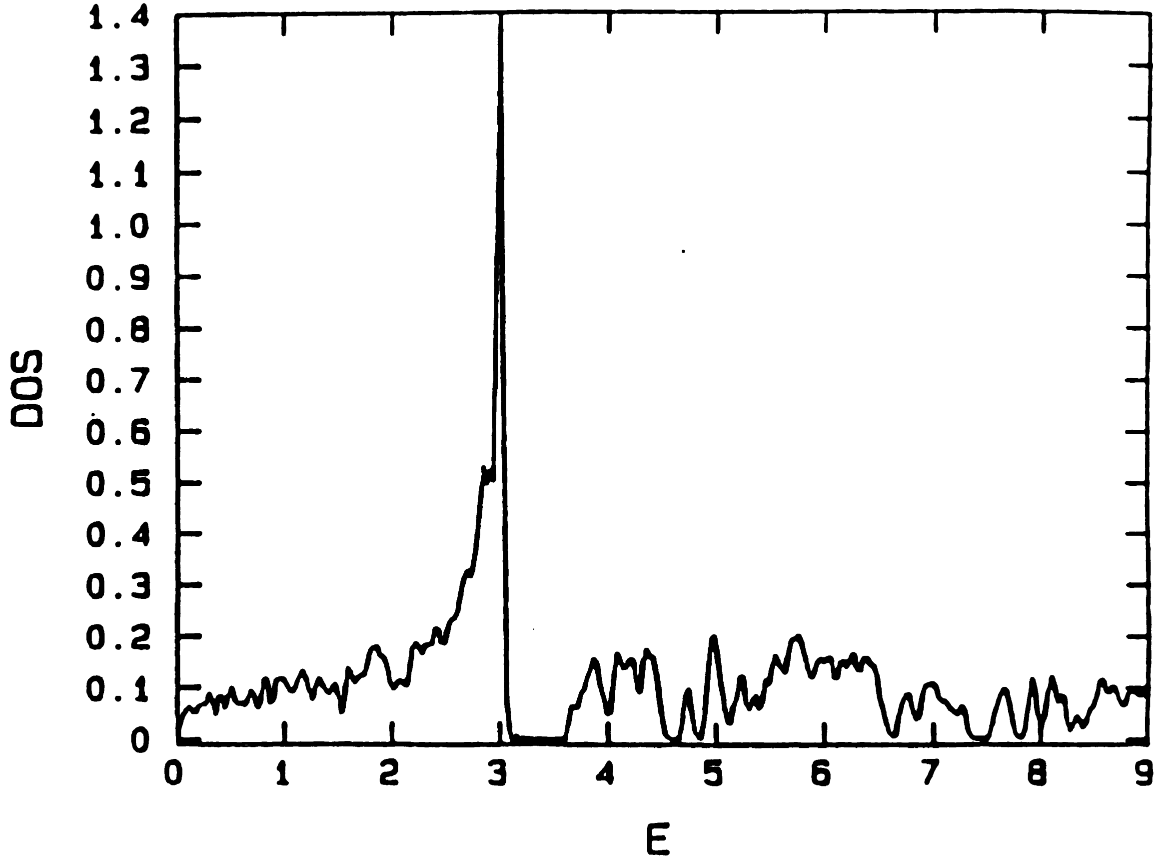

Figure 2.10 Density of states of Penrose tiling by the Equation of Motion.

$$\rho\ (E\to 0) = 0.085 \pm 0.002$$

from which we have

$$\sigma/\sigma_0 = 0.93 \pm 0.02$$

which is consistent with the result in section 2.3.

2.4.3 Calculation of the Intensity Spectrum S(q,E)

It is known that in an ordered crystal, $S(q,E)$ would show sharp peaks at energies corresponding to selected excitation with the proper momentum. While in the disordered alloy, all modes usually contribute for any q. However, for different q's, different modes contribute most strongly. The spectra are usually best thought of as the density of states with different regions of energy weighted differently as q varies.

Because of the total spin rotation symmetry of the Hamiltonian for the disordered alloy $S(q,E)$ for $q\to 0$ has a rather special behavior, even in the absence of the translational symmetry. It is easy to show that for $q=0$, $S(q,E)$ is given by a δ function of unit weight at $E=0$. For q slightly different from zero, there is always a regime of very small q such that $S(q,E)$ is sharply peaked at an energy $\bar{E}(q)$ given by

$$\bar{E}(q) = D\,q^2 \qquad (2.19)$$

where D is the spin stiffness. The width of the peak varies as q^4.

In Figure 2.11 we show a series of spectrum $S(\vec{q},E)$ for different value of $\vec{q}$ in x direction. Since we used a sample of finite size, we observed multiple discrete peaks. To analysize the contribution of a particular mode at energy E, we replotted the spectrum S(q,E) vs. q for a value of E at which there is a peak in the S(q,E). The result is shown in Figure 2.12. From which, we find out the position of q corresponding to the peak through fitting and established the relation between this mode E and the q-value which makes this mode contribute most to the spectra. Figure 2.13 plots this correspondence, i.e. $\bar{E}$ vs. $(qa)^2$. Its slope gives the spin stiffness constant $D=0.94\pm0.01$.

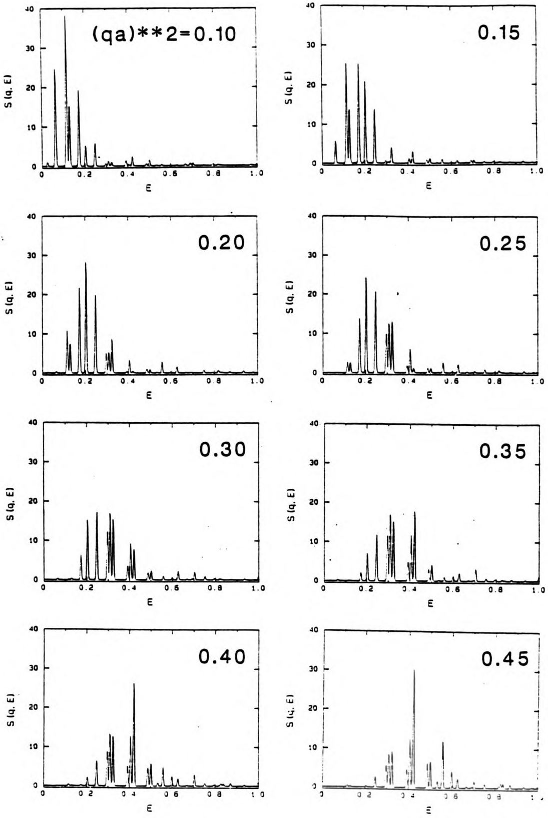

Figure 2.11 Low energy neutron scattering spectrum S(q,E) vs. E.

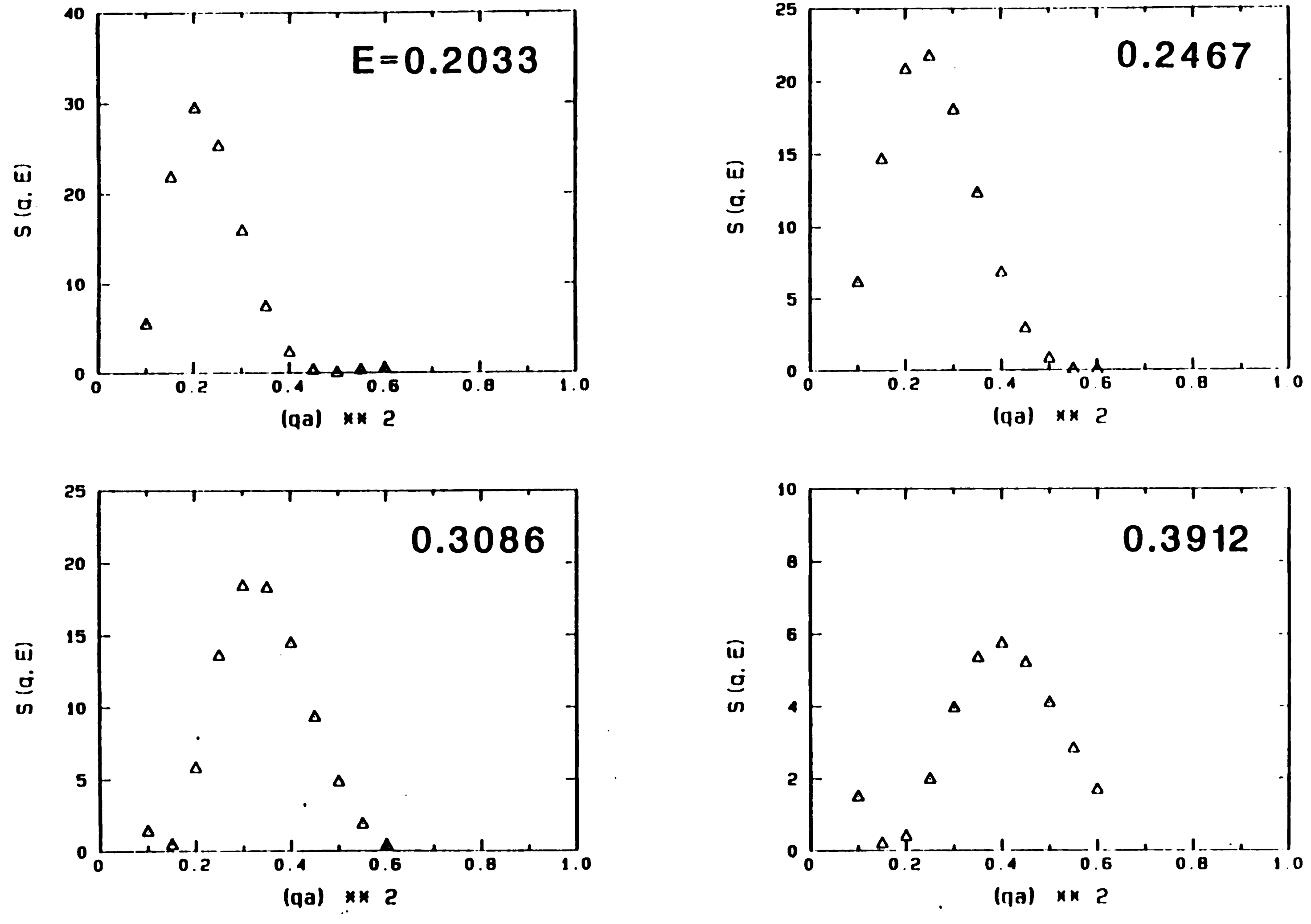

Figure 2.12 Low energy neutron scattering spectrum S(q,E) vs. q.

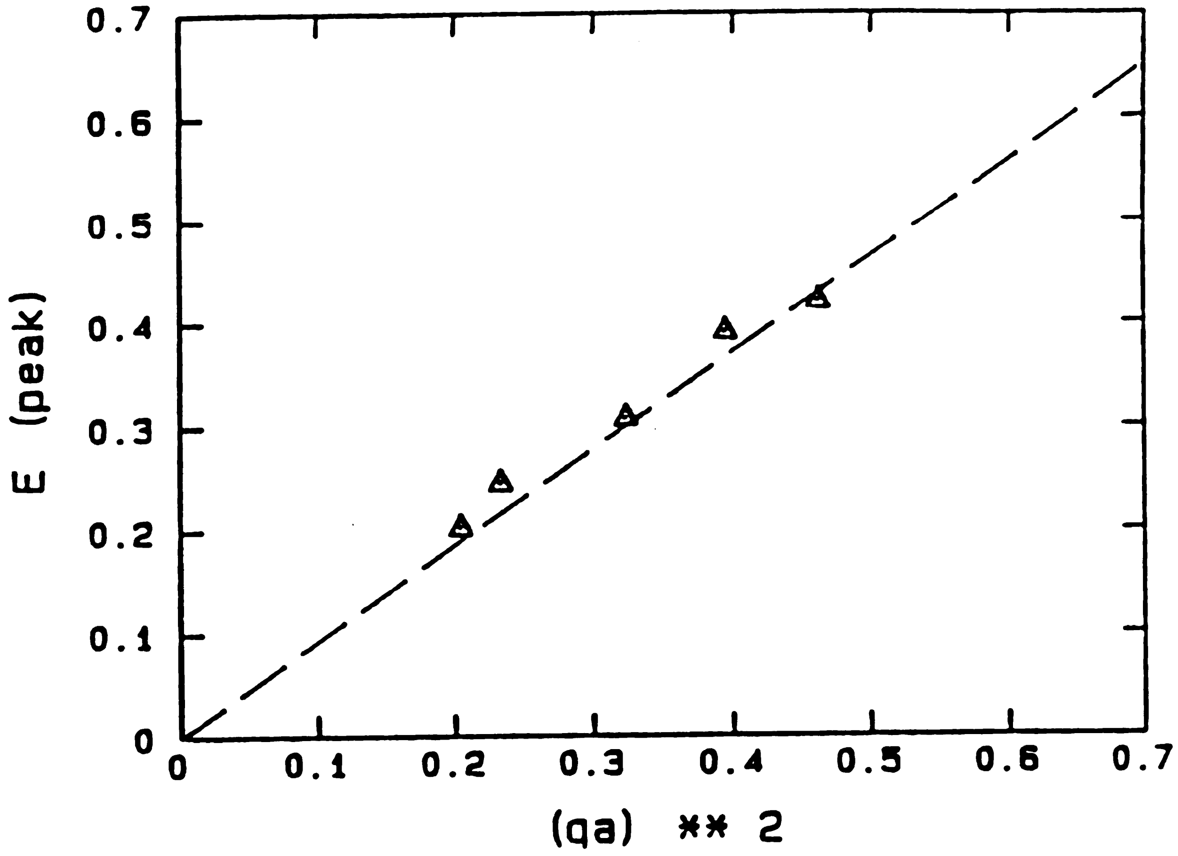

Figure 2.13 E_{peak} vs. $(qa)^2$ in spectrum S(q,E), to extract the slope D.

Section 2.5 Random Walk Approach

It is well known that the differential equation of the probability distribution in the Random Walk problem is exactly the diffusion equation in an appropriate limit. In this section we attempted to simulate the random walk on the Penrose Tiling and try to extract directly the diffusion constant.

In random walk problem, a particle undergoes a sequence of displacements $\vec{r}_1$, $\vec{r}_2$, ..., $\vec{r}_i$, ..., the magnitude and direction of each displacement being independent of all the proceeding ones. More specifically, in the background of the Penrose tiling, the particle can move to any of its nearest neighbors in one time step. Because we are working on a finite size sample, we have to decide what will happen to the particle at the time it reaches the boundary. Two special boundary conditions are: absorbing and reflecting boundary, as illustrated as follows.

Reflecting Boundary

Let us imagine the boundary of the region under consideration is a perfect reflecting wall. In the isotropic two dimensional case, it is a reflecting circle at $r=r_0$, which simply has the effect that whenever the partical arrives at r_0, it has a probability unity of coming back to the interior region when it takes next step. This condition can be expressed mathematically as:

$$\left.\frac{\partial P(r,t)}{\partial r}\right|_{r=r_0} = 0 \qquad (2.20)$$

where $P(r,t|r_0)$ is the probability that the partical will arrive at $r \leq r_0$ after t steps.

Absorbing Boundary

Now we interpose a perfect absorbing wall on the boundary. The presence of this absorbing wall at $r=r_0$ means that whenever the particle arrives at r_0, it at once becomes incapable of suffering further displacement. This boundary condition is written as:

$$P(r=r_0,t;\ r_0) = 0 \qquad (2.21)$$

where $P(r,t;r_0)$ is defined as the probability of a partical at r at time t. One interesting question which is characteristic of the present problem concerns the average rate at which the particle will deposit itself on the absorbing screen.

In our computer simulation on the Penrose tiling, we will use the absorbing boundary condition. The statistical quantity we actually observe is the deposit rate, i.e. the reciprocal of the average time $\langle t \rangle$ for a particle to reach the absorbing boundary. In Appendix B, we derive the relation between the diffusion constant D, the sample radius r_0 and the deposit rate $1/\langle t \rangle$. In 2-dimension, with circular sample, and initial distribution of the form

$$P\ (r,0) = \delta\ (r) \tag{2.22}$$

we have

$$D = \frac{r_0^2}{\langle t \rangle} \tag{2.23}$$

We will use this relation to extract D from the simulation data.

We work on the circular piece of the Penrose tiling of 888 atoms which has been used in the Equation of Motion calculation. Initially, the particle is confined in the small region around the center of the sample. We measure the time (number of steps) t between from the particle starts to move until it is captured by the detectors on the boundary. During this period, at each time step, the particle can jump from its current position to any one of its nearest neighbors with equal probability $1/z_i$, where z_i is the coordination number at site i. Our result averaged over 40000 runnings gives $D = 0.91 \pm 0.01$.

Section 2.6 Conclusion

In this chapter we applied three techniques to study the low energy behavior of 2D Penrose tiling. Our results for the diffusion constant D, which is equivalent to the conductivity, of an infinitely large Penrose tiling are summarized in Table 4. All three techniques give the consistent results, although with different ranges of error.

Centroid Algorithm takes the advantage of the combination of self-similarity property of the Penrose tiling and the geometrical character of the conductivity problem through the mapping. A systematic routine is established to obtain the result which can meet any precision requirement. By solving the centroid configuration of a unit cell with a finite number of atoms, one can obtain the centroid configuration of the infinitely large Penrose tiling. In other words, the conductivity or the diffusion constant of the infinitely large Penrose tiling can be obtained from unit cell with finite number sites. It should be emphasized that it is the intrinsic self-similar property of the quasicrystal which makes this possible and necessary. In a crystal there is a unique basic cell such that one does not need the series unit-cells, while in glassy structure there is no unit cell in any order. It provides a method to study physical properties, especially those depending strongly on the geometrical structure, by exploring the intrinsic structure of the quasicrystal.

Table 4 Summary of the Diffusion Constant on 2D Penrose Tiling

CENTROID METHOD

numerical simulation		0.936	
centroid unit cell	$0.9366^{(2)}$	$0.9333^{(3)}$	$0.9316^{(4)}$

EQUATION OF MOTION

S(q,E)	0.94 ± 0.02
DOS $\rho(E\to 0)$	0.93 ± 0.01

RANDOM WALK

0.91 ± 0.01

The other two techniques, the Equation of Motion approach and the direct Random Walk approach, have been used widely in dealing with the random system. Because of their numerical simulation characteristics, the results are affected more or less by the sample size. Moreover, since for quasicrystals it is unsuitable to use the periodic boundary condition as one usually does for random system, one always encounters a finite sample and its boundary sites are not properly co-ordinated.

Chapter 3. Percolation on Stretched Elastic Networks

Section 3.1 Introduction

In Chapter 2, the visualization of the conductivity problem based on the mapping introduced in Chapter 1 was explored on a new structure --- quasicrystal, which distinctly lies in between conventional crystal and glassy structure. In this chapter, we will explore the implication of the mapping on a deeper physical level. We will propose and study a generalized "tennis racket" model.

It is widely accepted that conductivity percolation and rigidity percolation belong to two different universality classes. (Feng & Sen 1984) The percolation threshold p_{cen} of a central force network, at which the elasticity vanishes, is much higher than p_c at which a resistor network loses its conductivity. These two systems also have quite different scaling exponents in the critical region, near p_{cen} and p_c respectively. Mean field theory, as well as numerical simulation results strongly support this classification. What is interesting is that our mapping seems to suggest the existence of a bridge between these two classes. Our working frame, the mapped tennis racket, composed with Hooke's law springs (natural length zero), is certainly a central force network. The problem it solves is identical to the conductivity problem. This can be understood by noticing the fact that the percolation in either resistor network or central force network with natural length zero is determined by the geometrical connection. As long as there is a percolating cluster, the current always can flow from one side to the other. Similarly, there is always energy stored in the mapped elastic network through the backbone. This feature is different with the central force network studied by many other authors. The networks they used are such that every spring has its natural length in the absence of external stress.

Based on the above consideration, a new model --- the tennis racket model is formed naturally, which seems can fill the gap between conductivity percolation and rigidity percolation. The model is defined as follows. On a lattice background with space constant L, we stick at the place of each bond between nearest neighbors a Hooke's law spring with natural length L_0, which need not to be equal to L. The shape of the lattice is kept through a frame or periodic boundary conditions. In the equilibrium state, no net force exerting on each site, but the springs adjacent to this site might be stretched, which could be considered as internal strain. The physical behavior of such a system must be very interesting since it reflects the nature of a lot of real systems. For instance, the percolation threshold p^* is one of the interesting quantities. What we already know through constraint counting (Thorpe 1983) and the mean field theory as well as numerical simulations (Feng, Thorpe & Garboczi 1985) are two special cases: $L_0 = 0$, which mapped to the conductivity percolation and $L_0 = L$, which is the pure central force network. The effective medium theory gave the thresholds corresponding to these two cases:

$$p^* \; (L_0=0) = p_c = \frac{2}{z}$$

and

$$p^* \; (L_0=L) = p_{cen} = \frac{2d}{z}$$

where z is the coordination number and d is the dimensionality. These are very close to the numerical simulation results $p_c = 0.347$ and $p_{cen} = 0.65$. The question is how p^* changes when L_0 takes arbitrary value ?

It was noted that Feng & Sen (1984) observed a crossover in their numerical simulation by using the Born model. They found that when the contribution of the central force part is dominant, there is a strong crossover from isotropic-force like behavior near $p=p_c$ to central-force like behavior near $p=p_{cen}$. This crossover was used as strong evidence to classify the two universality percolation classes. As we will see in the next section, this case is corresponding to the case of, in our tennis racket model, that the natural length L_0 approaches from below to the lattice space L. However, it should be pointed out that Born model and the tennis racket model are different at least in two respects. First, Born model is actually the contribution to elastic energy in the second order of the displacement, where the isotropic term is not rotationaly invariant. While in the tennis racket model, we are considering the total central force potential in the system. It is rotationally invariant since only the distance r_{ij} involved there, of course we have to rotate the frame together with the lattice in the simulation which is done by keeping the periodic boundary conditions. Secondly, all the displacements in Born model are relative to the lattice points, while in tennis racket model, the displacement is defined relative to the new equilibrium position.

There is also an important conceptual advantage in the tennis racket model because the pressure enters in a natural way into the determination of internal stresses and therefore into the determination of elastic constants.

We believe that a careful research of the proposed tennis racket model would be very helpful to understand the macroscopic elastic theory through the microcopic structural modeling.

This chapter is organized as the following. Section 3.2 presents the elasticity analysis on a pure triangular network under tension. Section 3.3 describe a diluted tennis racket with internal stress and details of the simulation techniques. Numerical simulation results for the overall behavior of the diluted tennis racket are presented in section 3.4. Section 3.5 attempts to understand the results from the symmetry point of view and reduce the number of independent second order elastic constants. Section 3.6 presents an effective medium theory on the stretched network. Section 3.7 gives the conclusion for the current work and suggestion towards further research.

Section 3.2 Elasticity of Pure Triangular Net Under Stress

We start from an elastic network on a pure lattice where all bonds are the Hooke's law springs with force constant K. The natural length of the spring is L_0 and the lattice space is L. Except for the case $L_0=L$, the network is stretched ($0 \leq L_0/L < 1$). The elastic potential for this model is:

$$V = \frac{1}{2} K \sum_{\langle i,j \rangle} (r_{ij}-L_0)^2 \qquad (3.1)$$

where the sum is over all nearest neighbors and $r_{ij}=|\vec{R}_i-\vec{R}_j|$ is the distance in between which is just L. We introduce $\vec{u}_i$ to express the small displacement of site i relative to its equibrium position. It is noticed that in the pure lattice case, the equilibrium positions are exactly the corresponding lattice points, while in diluted case, these two might be far away from each other. The potential can be expanded about the equilibrium position in terms of $\vec{u}_{ij}=\vec{u}_i-\vec{u}_j$. To the second order of u_{ij}, we get:

$$V = \frac{1}{2} K \sum_{\langle i,j \rangle} (L - L_0)^2$$

$$+ K \sum_{\langle i,j \rangle} (L - L_0) (\vec{u}_{ij} \cdot \hat{r}_{ij})$$

$$+ \frac{1}{2} K \sum_{\langle i,j \rangle} \{ (1-\frac{L_0}{L}) u_{ij}^2 + \frac{L_0}{L} (\vec{u}_{ij} \cdot \hat{r}_{ij})^2 \} \qquad (3.2)$$

where $\hat{r}_{ij}$ is the unit vector between points i and j.

The first sum in (3.2) is the static energy of the stretched springs and can be written as

$$V_0 = \frac{1}{4} K N z (L-L_0)^2 \qquad (3.2a)$$

where N is the total number of sites in the system and z is the coordination number.

The second sum in (3.2) is the linear order contribution, which is written as:

$$V_1 = K (L - L_0) \sum_{\langle i,j \rangle} (\vec{u}_{ij} \cdot \hat{r}_{ij}) \qquad (3.2b)$$

The value of V_1 could be positive, negative or zero, depending on the details of the displacement $\vec{u}_{ij}$, or the strain in the network. We note that the equilibrium condition for the full potential is:

$$\frac{\partial V}{\partial \vec{r}_i} = 0$$

and for the expansion of the potential in terms of displacement, we have:

$$\frac{\partial V}{\partial \vec{u}_i} = 0$$

both of them lead to the same equation :

$$\sum_{\langle i,j\rangle} K_{ij}\,(r_{ij} - L_0)\,\hat{r}_{ij} = 0$$

The last sum in (3.2), i.e. the quadratic term in u_{ij} is:

$$V_2 = \frac{1}{2} K \left(1-\frac{L_0}{L}\right) \sum_{\langle i,j\rangle} u_{ij}^2$$

$$+ \frac{1}{2} K \frac{L_0}{L} \sum_{\langle i,j\rangle} (\vec{u}_{ij}\cdot\hat{r}_{ij})^2 \qquad (3.2c)$$

Comparing V_2 with the Born model potential:

$$V_{born} = \frac{1}{2}(\alpha-\beta) \sum_{\langle i,j\rangle} [\,(\vec{u}_i-\vec{u}_j)\cdot\hat{r}_{ij}]^2$$

$$+ \frac{1}{2}\beta \sum_{\langle i,j\rangle} (\vec{u}_i-\vec{u}_j)^2 \qquad (3.3)$$

We can see the correspondence between the Born model parameters α, β and the tennis racket parameters L_0/L and K:

$$K\left(1-\frac{L_0}{L}\right) = \beta \qquad (3.3a)$$

and $$K \frac{L_0}{L} = (\alpha - \beta) \qquad (3.3b)$$

which implies:

$$\alpha = K \qquad (3.3c)$$

Generally, the strain-energy is defined as: (Barron & Klein, 1965)

$$U = \sum_{\alpha\beta} S_{\alpha\beta}\, \varepsilon_{\alpha\beta} + \frac{1}{2} \sum_{\alpha\beta\gamma\tau} \varepsilon_{\alpha\beta} \varepsilon_{\gamma\tau}\, C_{\alpha\beta\gamma\tau} \qquad (3.4)$$

where $S_{\alpha\beta}$ is the stress tensor, $C_{\alpha\beta\gamma\tau}$ is the second order elastic constant and the strain is:

$$\varepsilon_{\alpha\beta} = \frac{\partial\, u_\alpha}{\partial\, x_\beta} \qquad (3.5)$$

For <u>isotropic external strain</u>, we have the expression for $S_{\alpha\beta}$ and $C_{\alpha\beta\gamma\tau}$ as the following:

$$A\, S_{\alpha\beta} = K\, (\, L - L_0\,) \sum_{\langle i,j \rangle} R_{ij}\, r_{ij}^{\alpha}\, r_{ij}^{\beta} \qquad (3.6)$$

and

$$A\, C_{\alpha\beta\gamma\tau} = K \frac{L_0}{L} \sum_{\langle i,j \rangle} R_{ij}^{2}\;\; r_{ij}^{\alpha}\, r_{ij}^{\beta}\, r_{ij}^{\gamma}\, r_{ij}^{\tau}$$

$$+ K \left(1 - \frac{L_0}{L} \right) \sum_{\langle i,j \rangle} R^2_{ij}\, r^{\alpha}_{ij}\, r^{\gamma}_{ij}\, \delta_{\beta\tau} \qquad (3.7)$$

where A is the area of the sample, R_{ij} is the nearest neighbor distance L and $\hat{r}_{ij}$ is the unit vectors.

For the triangular net, we have:

$$A = (\sqrt{3}\, L^2/2)\, N \qquad (3.8)$$

and

$$\begin{aligned} \hat{r}_{ij} = {} & (1,0), && (-1,0) \\ & (1/2, \sqrt{3}/2), && (1/2, -\sqrt{3}/2), \\ & (-1/2, \sqrt{3}/2), && (-1/2, -\sqrt{3}/2). \end{aligned} \qquad (3.9)$$

From which the moments of the $\hat{r}_{ij}$ can be worked out:

$$\begin{aligned} &\langle r^{\alpha}_{ij} \rangle = 0 \\ &\langle r^{\alpha}_{ij}\, r^{\beta}_{ij} \rangle = \frac{1}{2} \delta_{\alpha\beta} \qquad (3.10) \\ &\langle (r^{\alpha}_{ij})^2 (r^{\beta}_{ij})^2 \rangle = \frac{1}{8} + \frac{1}{4} \delta_{\alpha\beta} \end{aligned}$$

Substituting back to (3.6) and (3.7), we obtained the stress tensor and the elastic constants. The results are listed as the following where we used η to denote L_0/L:

<u>Stress tensor</u>:

$$S_{xx} = S_{yy} = \sqrt{3}\ K\ (1 - \eta) \qquad (3.11)$$

$$S_{xy} = S_{yx} = 0 \qquad (3.12)$$

where S_{xx} and S_{yy} are actually the external pressure.

Second order elastic constants:

$$C_{xxxx} = C_{11} = \frac{\sqrt{3}\ K}{4}\ (4 - \eta) \qquad (3.13)$$

$$C_{xxyy} = C_{12} = \frac{\sqrt{3}\ K}{4}\ \eta \qquad (3.14)$$

$$C_{xyxy} = C_{44} = \frac{\sqrt{3}\ K}{4}\ (4 - 3\eta) \qquad (3.15)$$

$$C_{xyyx} = C_{44}' = \frac{\sqrt{3}\ K}{4}\ \eta \qquad (3.16)$$

These results are plotted in Figure 3.1. As expected, these elastic constants include the known results for the pure scalar case and pure central force case.

For scalar case: ($\eta = 0$)

$$C_{11} = C_{44} = \sqrt{3}\ K$$

and for central force case: ($\eta = 1$)

$$C_{11} = 3\ \sqrt{3}\ K\ /\ 4$$

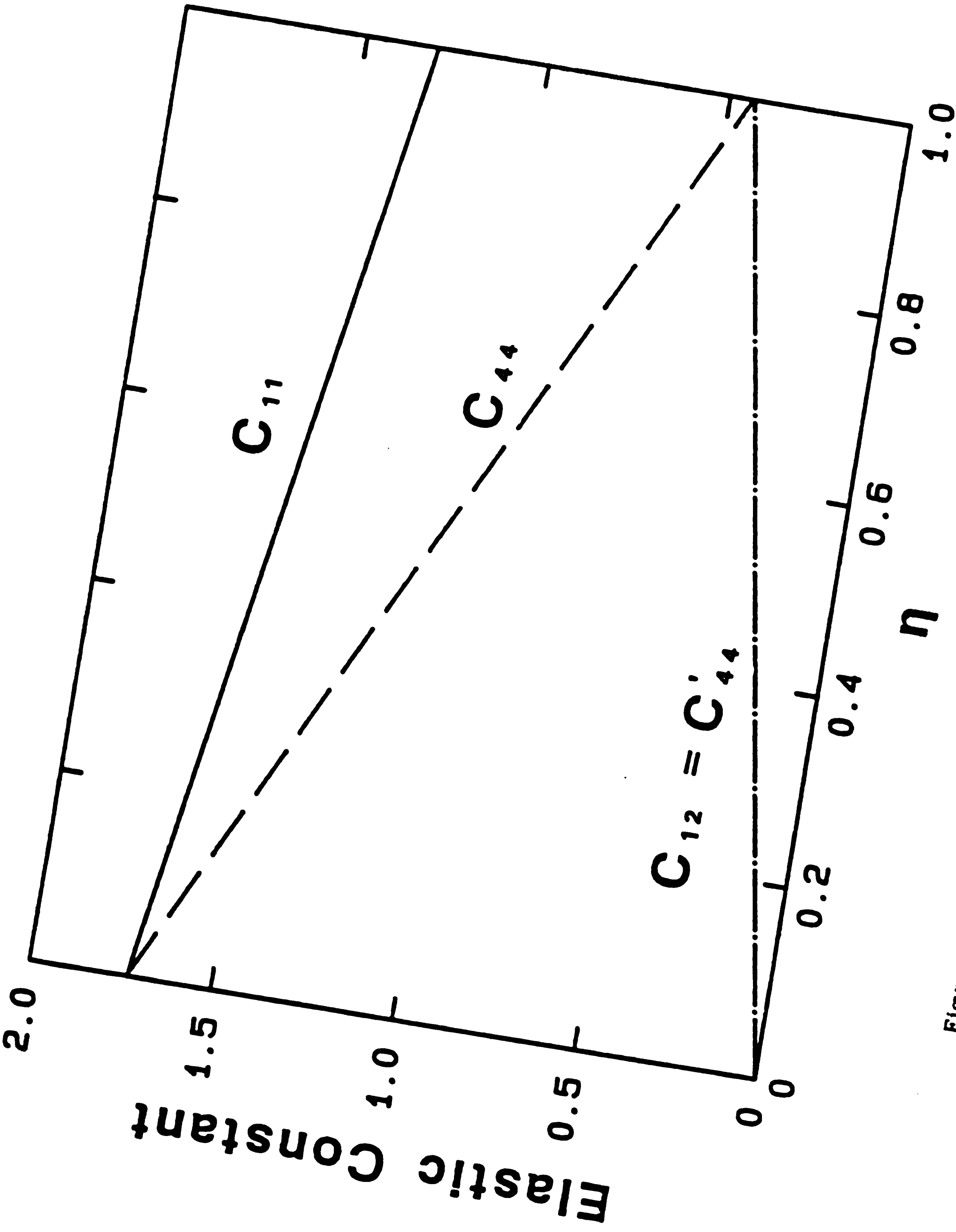

Figure 3.1 C_{11}, C_{44}, C_{12} and C_{44}' vs. $\eta = L_0/L$ for pure triangular lattice.

and $C_{44} = \sqrt{3}\ K / 4$

We checked these results through computer simulation, they all agree well. Since neither C_{44}' nor C_{12} comes out independently, we design other four cases of initial stress and combine their results to extract C_{44}' and C_{12}. The transformations corresponding to these four cases, in addition to those for computing C_{11} and C_{44}, are sketched in Figure 3.2. The corresponding second order elastic constant are respectively:

<u>Pure shear</u>: (Figure 3.2c)

$$\mu_s = \frac{1}{2} (C_{44} + C_{44}') = \frac{\sqrt{3}\ K}{4} (2 - \eta) \qquad (3.17)$$

<u>Pure rotation</u>: (Figure 3.2d)

$$\mu_r = \frac{1}{2} (C_{44} - C_{44}') = \frac{\sqrt{3}\ K}{4} (2 - 2\eta) \qquad (3.18)$$

<u>Bulk compression</u>: (Figure 3.2e)

$$B = \frac{1}{2} (C_{11} + C_{12}) = \frac{\sqrt{3}\ K}{2} \qquad (3.19)$$

<u>Compression/expansion</u>: (Figure 3.2f)

$$b = \frac{1}{2} (C_{11} - C_{12}) = \frac{\sqrt{3}\ K}{4} (2 - \eta) \qquad (3.20)$$

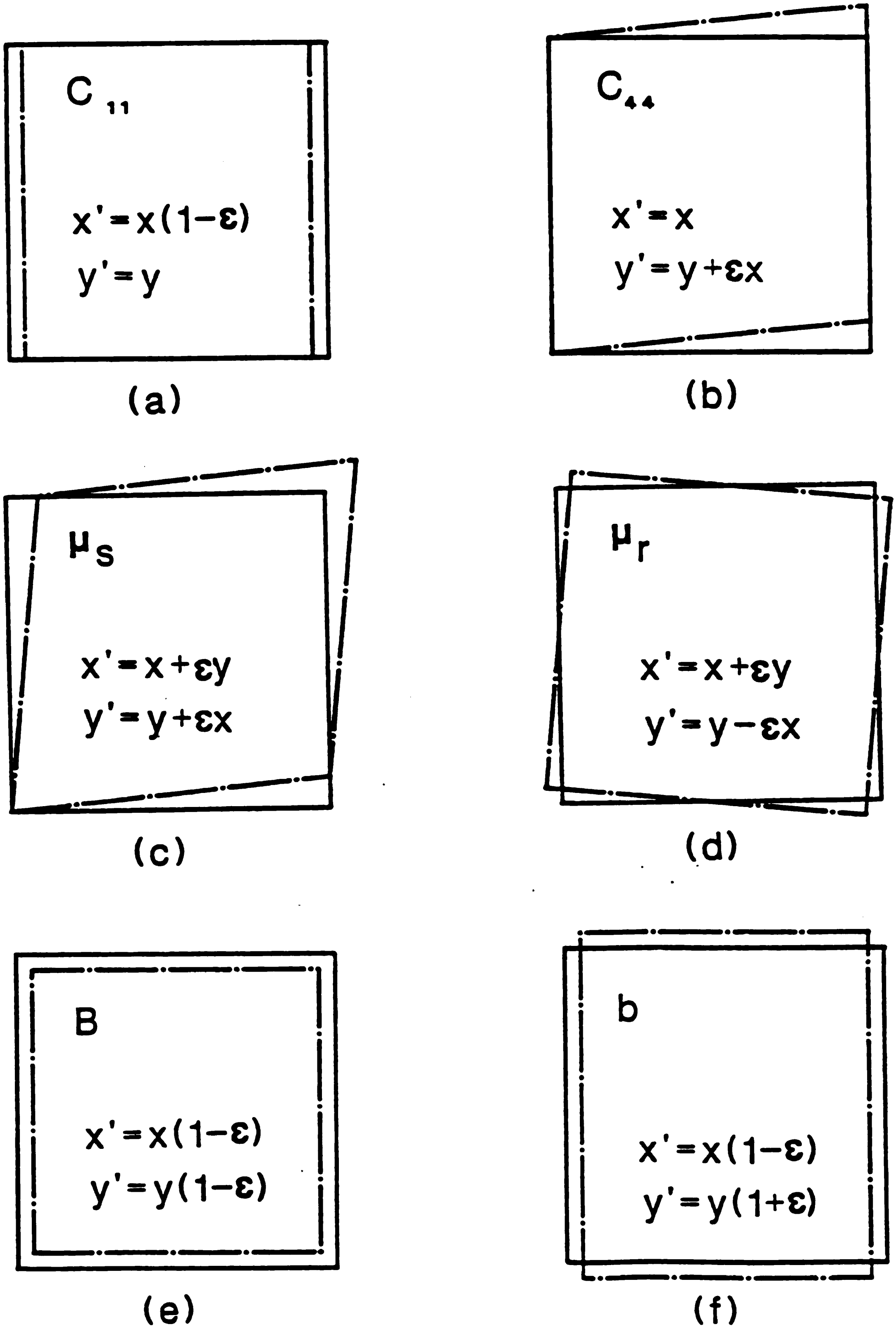

Figure 3.2 Transformations for uniform external strain.

Figure 3.3 plots these results.

From these combinational elastic moduli, we have:

$$C_{12} = B - b \tag{3.21a}$$

and

$$C_{44}' = \mu_s - \mu_r \tag{3.21b}$$

Note that C_{11} and C_{44} are also given by μ_s , μ_r , B and b.

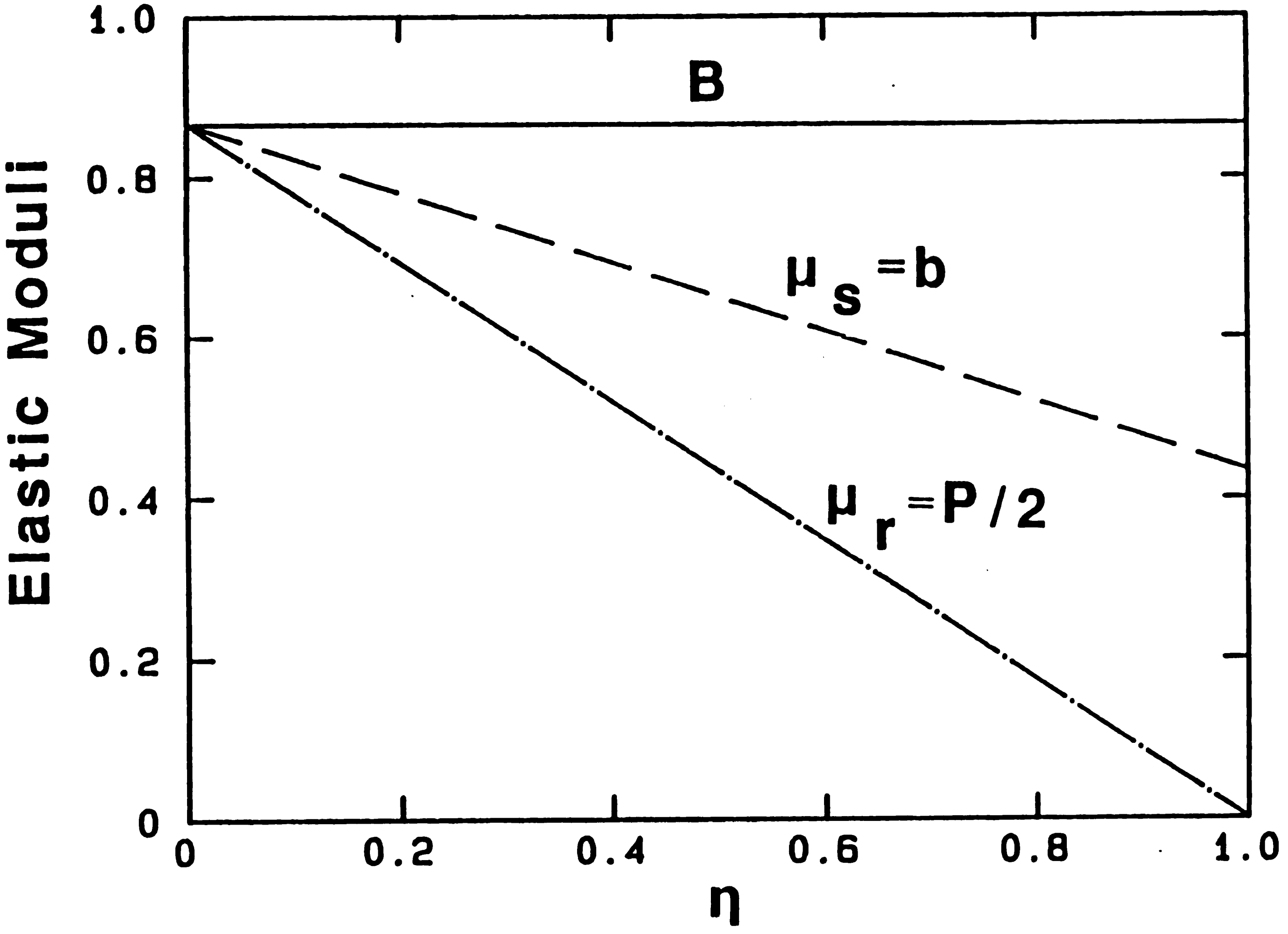

Figure 3.3 B, μ_r, μ_s and b vs. $\eta = L_0/L$ for pure triangular lattice.

Section 3.3 Diluted Triangular Net Under Stress ---- Simulation Technique

Special care is needed in studying the diluted network under stress. For a pure lattice where no bond is missing, the lattice node serves as the equilibrium position because the forces exerting on a site through adjacent stretched springs are balanced each other. However, as soon as the diluting process starts, this balance is destroyed and the network deforms around the missing springs. Related sites relaxed coherently to reach their new equilibrium position. It is around these new equilibrium positions, which might be far away from the corresponding original lattice nodes, that the sites in network are vibrating. The elastic constant and the stress tensor should be determined from the structure of this new equilibrium configuration.

The key point is that before applying any extra external stress, we have to obtain the relaxed configuration of the diluted network. Only internal stress plays the role in this relaxation. A certain amount of static energy is stored in this relaxed network.

The details of the numerical simulation are described as below.

(1) Generate a diluted triangular lattice by removing bonds randomly with probability (1-p) on a triangular lattice. Note that the resulted network is unrelaxed for the cases $L_0 = L$.

(2) Relax the network obtained from (1). The movement of site i is proportional to the force exerted on it. Specifically, during the procedure of iteration, the position of atom i is determined by the previous configuration through:

$$x_{\xi i}^{(n+1)} = x_{\xi i}^{(n)} + \alpha F_{\xi i}^{(n)} \qquad (3.22)$$

where $F_{\xi i}$ is the force component given by:

$$F_{\xi i} = \sum_{j} K_{ij} (r_{ij} - L_0) \hat{r}_{ij}^{\xi} \qquad (3.23)$$

and α is a number which could be adjusted to control the simulation. Principally, the iteration process should stop when the force on any site is zero. While practically, we choose an appropriate small number which is good enough to satisfy the requirement of the final result precision. For example, $F_{max} = 10^{-8}$ was used corresponding to $\varepsilon = 10^{-2}$ in our simulation. The energy of the relaxed network is calculated and written as $E_0(p, L_0/L)$.

(3) Now, depending on whether C_{11} or C_{44} or other elastic moduli is being computed, the coordinates of the sites are transformed corresponding to a certain external strain. Some uniform transformations are given in Figure 3.2.

(4) After exerting the extra strain, one then proceeds to relax the network again. To seperate the linear and

second order contribution, we reverse the sign of external strain ε and repeate the procedures (3) and (4). The energy of the relaxed configuration is:

$$E^{+} = E\ (p,\ L_0/L,\ \varepsilon>0) = E_0 + S\ |\varepsilon| + \frac{1}{2}\ C\ \varepsilon^2$$

$$E^{-} = E\ (p,\ L_0/L,\ \varepsilon<0) = E_0 - S\ |\varepsilon| + \frac{1}{2}\ C\ \varepsilon^2$$

$$(3.24)$$

where S and C stand for linear and second order coefficients respectively, given by:

$$S = \frac{(E^{+} - E_0) - (E^{-} - E_0)}{2\ |\varepsilon|} \qquad (3.25)$$

$$C = \frac{(E^{+} - E_0) + (E^{-} - E_0)}{\varepsilon^2} \qquad (3.26)$$

Section 3.4 Diluted Triangular Net Under Stress ------ Simulation Results

In this section, we present the results of the computer simulation described in the last section. All simulations were done on a 20x22 triangular net with periodic boundary conditions. Each network is specified by two parameters: L_0/L and p. We investigated the elastic behavior of the network in the plane of L_0/L -- p in the range of $0<L_0/L<1$ and $0<p<1$. Previous knowledge was on three lines as sketched in Figure 3.4. Two of them were along $L_0/L = 0$ and $L_0/L = 1$, representing conductivity percolation and rigidity percolation respectivity, and the other was along $p = 1$ with varing L_0/L which was studied in section 3.2.

At first, we present a survey for second order elastic constants for various p and L_0/L. Figure 3.5 shows the results of C_{11} and C_{44} versus p for different L_0/L. Other two elastic constants C_{12} and C_{44}' cannot be calculated from simulation directly. While, as illustrated in section 3.2, these elementary elastic constant C_{11}, C_{44}, C_{12} and C_{44}' can be determined completely from four combinational elastic moduli B, μ_s, μ_r and b, which can be calculated directly from simulation. Figure 3.6 plots the results for B, μ_s, μ_r, b. All the values at p=1 were actually predicted in section 3.2. For example, the bulk moduli for various L_0/L are starting from a single point at p=1 since in the elasticity analysis for pure triangular net, we have shown

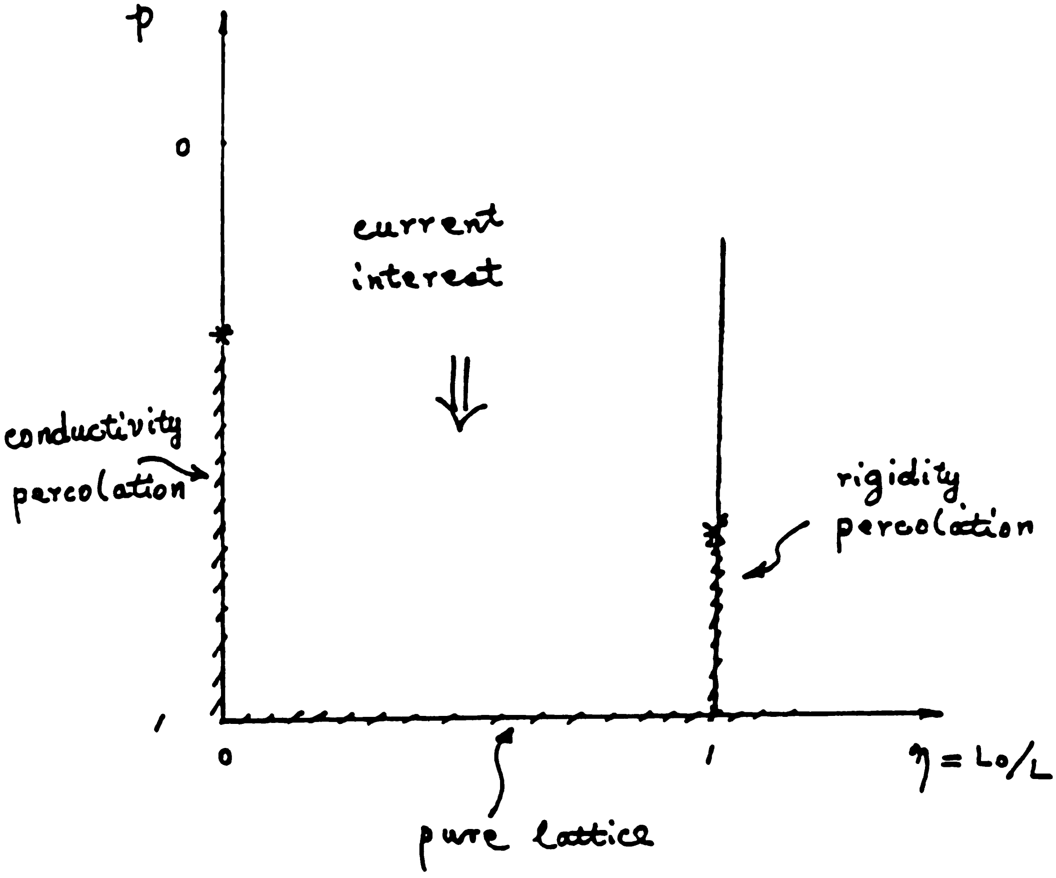

Figure 3.4 Relation between the percolation problem on tennis racket model and conductivity percolation and rigidity percolation.

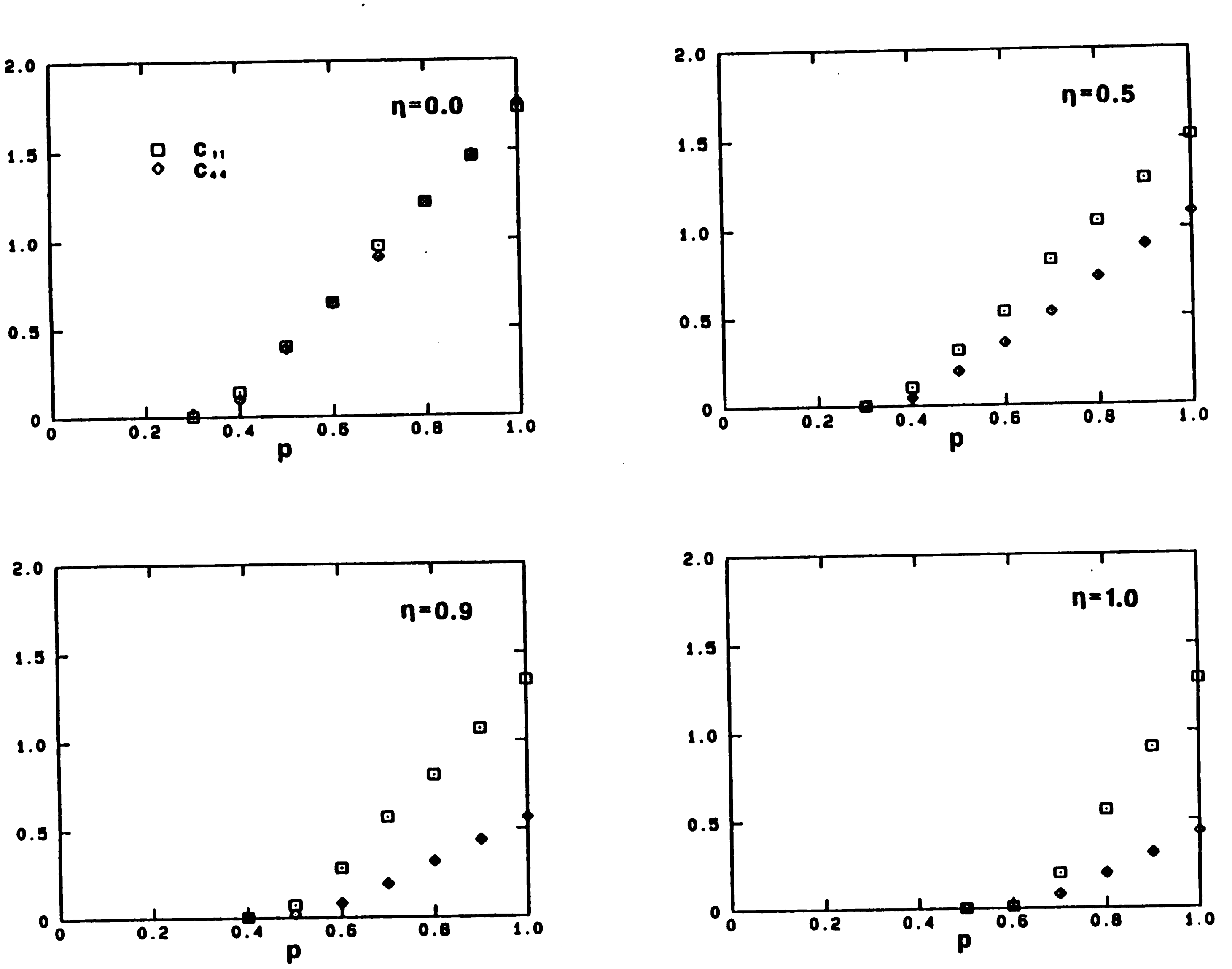

Figure 3.5 C_{11} and C_{44} for diluted triangular network.

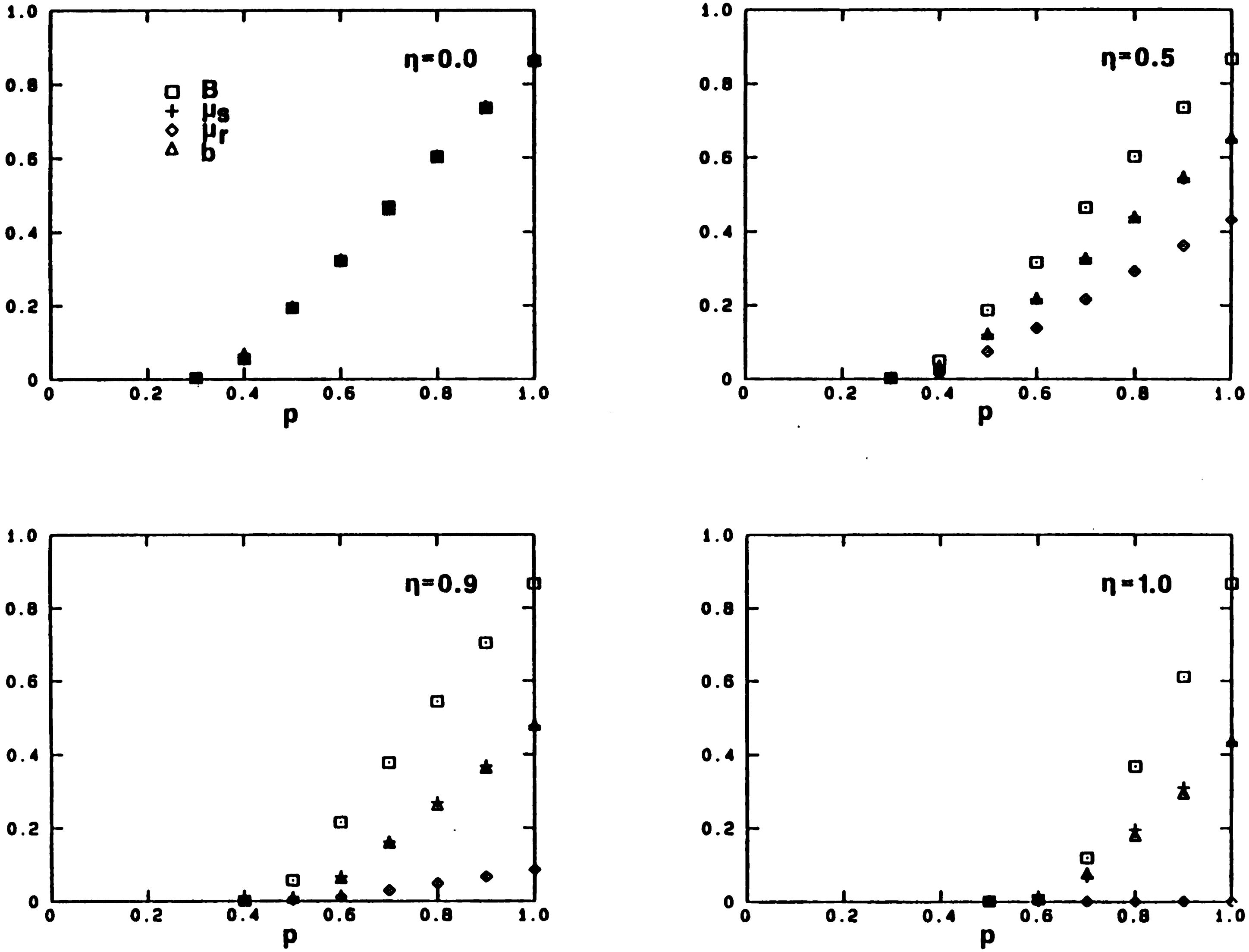

Figure 3.6 B, μ_s, μ_r and b for diluted triangular network

that B is just a constant for any L_0/L. In the intermediate region, i.e. p less than one but much greater than the threshold p^*, these elastic constants change linearly in a similar way, which strongly suggests an effective medium theory for the stretched network. It is crucial to observe that for the networks with different L_0/L, the thresholds p^* at which the elastic constant vanishes are different as revealed by our simulation. The smallest p^* is p_c, corresponding to the case of $L_0 = 0$, which is identical to the conductivity percolation. With the increasing of L_0/L, p^* is increasing very slowly at first. After passing through the point aroung $L_0/L = 0.5$, p^* experiences bigger and bigger jumps for the same amount of change in L_0/L. Finally p^* reaches p_{cen} when $L_0 = L$, which agrees with previous research on pure central force network.

This dependence of the threshold p^* on L_0/L is perhaps not so surprising. For example, one can envision a percolated cluster on lattice background (before relaxation) in which there existes a node i with coordination number two. As sketched in Figure 3.7, the two bonds adjacent to this particular site are connecting the other two parts of the cluster in a way that they are not aligned on a straight line. If the lattice space L is equal to the natural length of the spring, the current position of i is in equilibrium. Then because the bonds can pivot freely without costing any energy, this structure is not able to transmit any elastic forces. However, if $L_0/L < 0.5$, the equilibrium position

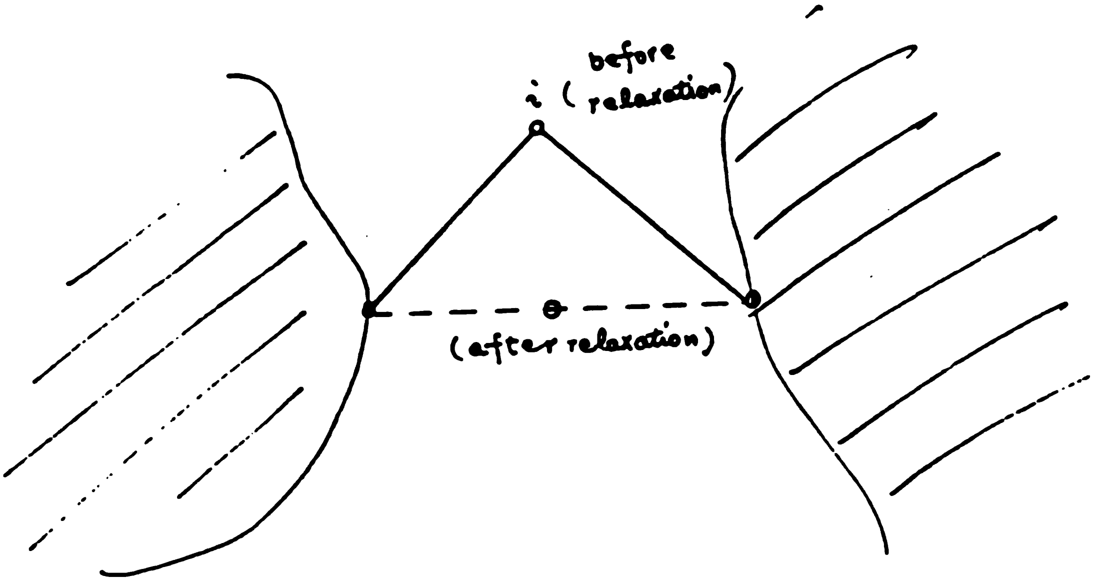

<u>Figure 3.7</u> Illustration of reduced "diode effect".

would be in the middle between two parts, while the spring is still stretched. Here we just ignore the relaxation of other part of the network without loosing the generality of the discussion. In other words, the elasticity would not vanish because of the existence of this diode hinge in the lattice background. Similarly, for other values of L_0/L, one could imagine many other structures, which would have "killed" the elasticity of the geometrically percolated cluster for a large value of L_0/L, now relaxed to a "good" effective elastic structure for smaller L_0/L. This explains why p^* is increasing with L_0/L.

Beside these second order elastic constants, there are two more quantities describe the property of the tennis racket. They are the first order coefficient which is the external pressure P and the zeroth order constant which is the static energy E. The simulation results of P and E are plotted in Figure 3.8 and Figure 3.9. Result is obtained by averaging over ten ramdom configurations. For the convenience of investigating the transition thresholds, both E and P are scaled such that their value are one for all LO/L at p=1, i.e. in the pure lattice case.

Obviously, for the networks with different LO/L, the threshold is different.

We end this section with a set of six quantities E, P, B, μ_s, μ_r, b to describe the diluted stretched networks. The next task is to find out the minimal set of independent quantities by exploring any possible relation between them.

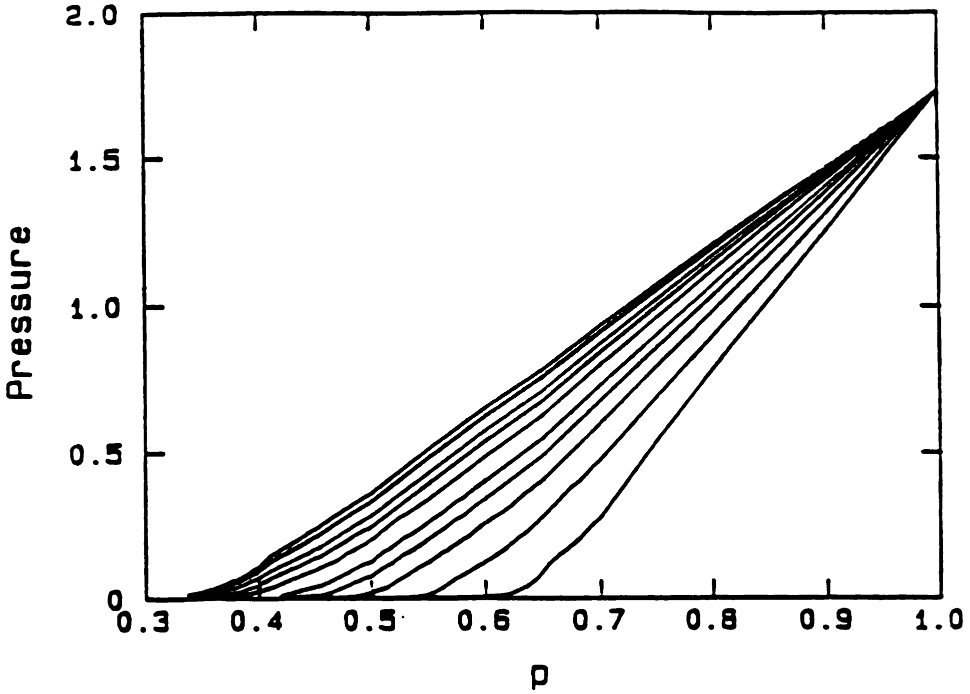

Figure 3.8 Pressure for relaxed diluted triangular net.

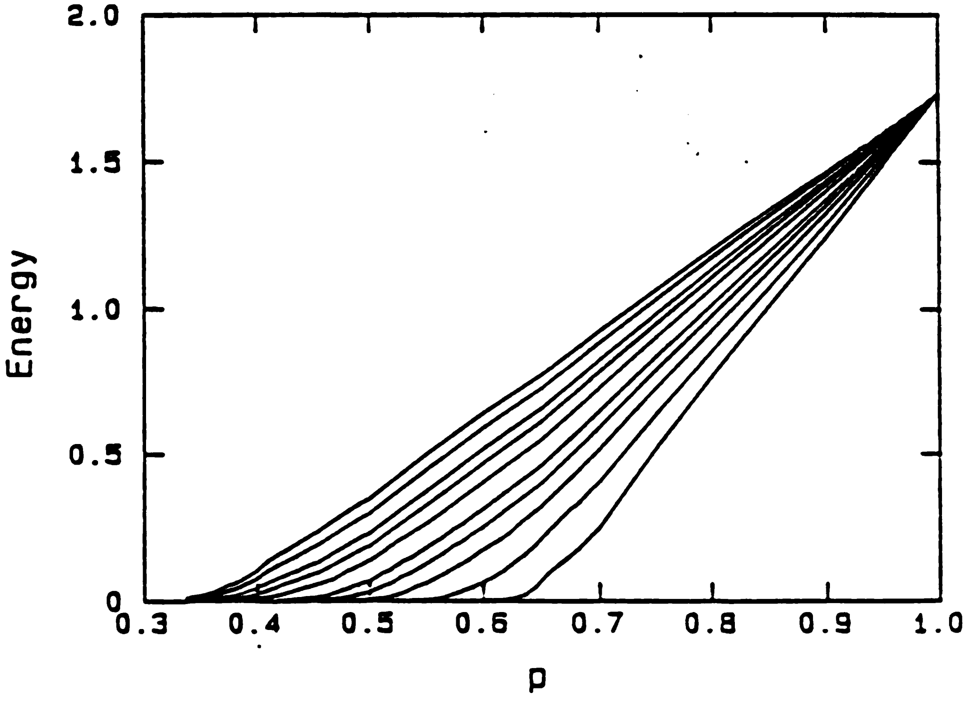

Figure 3.9 Static energy for relaxed diluted triangular net.

Section 3.5 Symmetry Analysis

In attempting to reduce the number of independent elastic constants describing the stretched network, we notice that in unstretched network the elastic constant $C_{\alpha\beta\gamma\tau}$ is invariant under the index exchange $(\alpha\beta \leftrightarrow \gamma\tau)$ and $(\alpha \leftrightarrow \beta)$, $(\gamma \leftrightarrow \tau)$. (see e.g. Love 1944) Because of the initial stress there are now first-order terms in $\varepsilon_{\alpha\beta}$ so that the symmetry relations needed to be changed. In section 3.2, we derived all of the elastic constants for the pure triangular lattice in terms of L_0/L. Recalling equations (3.13)-(3.20), we find three independent relations between the pressure and the second order elastic constants. These relations are:

$$C_{12} = C_{44}' \tag{3.27}$$

$$P = C_{44} - C_{44}' \qquad \text{i.e.} \quad P = 2\,\mu_r \tag{3.28}$$

$$C_{11} - C_{12} = C_{44} + C_{44}' \qquad \text{i.e.} \quad \mu_s = b \tag{3.29}$$

Thus the set of six constants E, P, B, μ_s, μ_r, b is reduced to three constants for pure lattice. We chose E, P and B as these three independent quantities, corresponding to the different order of the potential expansion.

For the diluted networks, one can anticipate that no more than three relations exist between E, P, B, μ_s, μ_r, b, since the symmetry broken induced by missing springs. In this section, we will study one by one the validity of equations (3.27)-(3.29) and the underlying physics on the diluted stretched network.

Rotational Invariance of the Strain-Energy

At first, we consider (3.28) which relates the pressure to the second order elastic constants C_{44} and C_{44}'. From the invariance of the strain-energy density (3.4) under an infinitesimal rigid rotation, Huang (1950) has shown macroscopically that

$$C_{\alpha\beta\gamma\tau} - C_{\beta\alpha\gamma\tau} = S_{\beta\tau}\delta_{\alpha\gamma} - S_{\alpha\tau}\delta_{\beta\gamma} \tag{3.30}$$

By substituting $\alpha\beta\gamma\tau$ with xyxy and yxyx in (3.30), we get:

$$C_{xyxy} - C_{yxxy} = S_{yy} \tag{3.31a}$$

$$C_{yxyx} - C_{xyyx} = S_{xx} \tag{3.31b}$$

These two equations are equivalent to each other since

$$S_{xx} = S_{yy} = P$$

and

$$C_{xyxy} = C_{yxyx} = C_{44}$$

$$C_{xyyx} = C_{yxxy} = C_{44}'.$$

so that both (3.31a) and (3.31b) lead to eq. (3.28).

We look at this relation from the microscopic point of view. Consider an infinitesimal rigid rotation:

$$\vec{u}_i = \vec{\omega} \times \vec{R}_i + \frac{1}{2} \vec{\omega} \times (\vec{\omega} \times \vec{R}_i) \qquad (3.32)$$

In our system, $\vec{\omega}$ is taken along the direction perpendicular to the network plane such that $\vec{u}_i$ can be written as:

$$\vec{u}_i = \vec{\omega} \times \vec{R}_i - \frac{\omega^2}{2} \vec{R}_i \qquad (3.33)$$

Replace $\vec{u}_i$ by (3.33) in the potential expansion (3.2) we get:

$$\begin{aligned} V = {} & \frac{1}{2} \sum_{\langle i,j \rangle} K_{ij} (R_{ij} - L_0)^2 \\ & - \frac{\omega^2}{2} \sum_{\langle i,j \rangle} K_{ij} (R_{ij} - L_0) R_{ij} \\ & + \frac{1}{2} \sum_{\langle i,j \rangle} K_{ij} (1 - L_0 / R_{ij}) \omega^2 R_{ij}^2 + O(\omega^3) \end{aligned} \qquad (3.34)$$

The second and third terms are cancelled so that V is invariant under a rigid rotation as it should be. We claim that these two terms are just the pressure and second order elastic constant $C_{44} - C_{44}'$. To prove that, we divide the $\vec{u}_i$ corresponding to the rigid rotation as two parts:

$$\vec{u}_i^{(p)} = - \frac{\omega^2}{2} \vec{R}_i = \varepsilon \vec{R}_i \tag{3.35}$$

where $\varepsilon = - \omega^2/2$, and

$$\vec{u}_i^{(r)} = \vec{\omega} \times \vec{R}_i \tag{3.36}$$

In the computer simulation, we actually investigate the effect of $\vec{u}_i^{(p)}$ and $\vec{u}_i^{(r)}$ seperately. For $\vec{u}_i^{(p)}$ the transformation is shown in Figure 3.2e, i.e.

$$\begin{aligned} x' &= x (1 - \varepsilon) \\ y' &= y (1 - \varepsilon) \end{aligned} \tag{3.37}$$

The pressure is obtained from the linear coefficient in energy:

$$P = \sum_{\langle i,j \rangle} K_{ij} (R_{ij} - L_0) R_{ij} \; / \; 2A \tag{3.38}$$

Note that the coefficient of the second order term is the bulk modulus. On the other hand, $\vec{u}^{(r)}$ is corresponding to the "pure rotation" transformation defined in Figure 3.2d:

$$x' = x + \omega y$$
$$y' = y - \omega x \qquad (3.39)$$

from which we get the second order elastic constant,

$$\mu_r = \frac{\sum_{\langle i,j\rangle} K_{ij} (1 - L_0 / R_{ij}) R_{ij}^2}{4 A} \qquad (3.40)$$

and the corresponding linear order term is always zero. Figure 3.10 presents a check for eq.(3.28) via the numerical simulation on the diluted network. We conclude that the rotational invariance is preserved in the diluted case.

Isotropy for the Sound Velocities

Now let us consider the eq.(3.29). With the given energy of deformation (3.4), the wave equation is:

$$\rho \ddot{u}_\alpha (\vec{x}) = \sum_\gamma \sum_{\beta\tau} C_{\alpha\beta\gamma\tau} \frac{\partial^2 u_\gamma (\vec{x})}{\partial x_\beta \partial x_\tau} \qquad (3.41)$$

For the plane wave solution:

$$\vec{u} \exp (i \vec{k} \cdot \vec{x} - i \omega t) \qquad (3.42)$$

we get

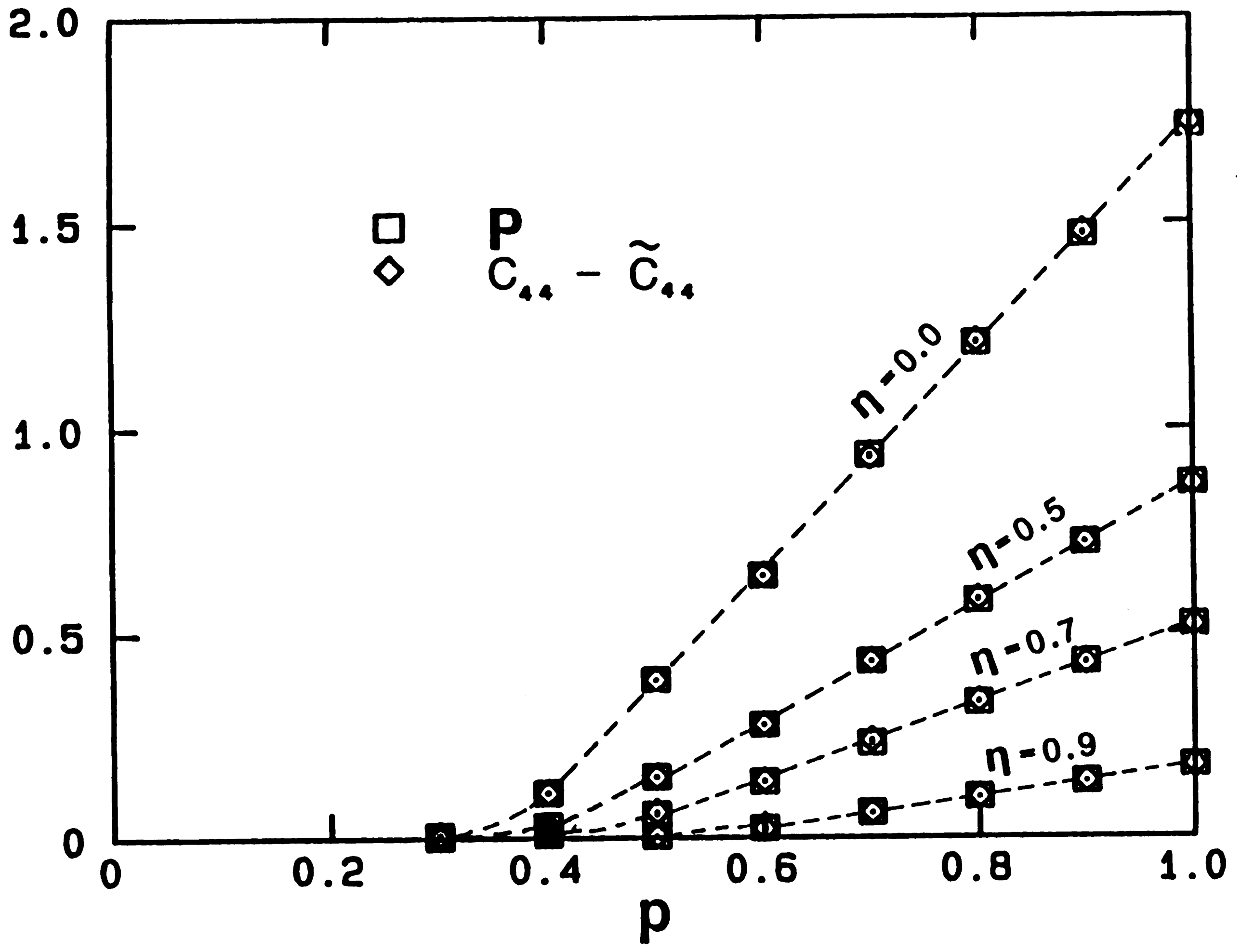

Figure 3.10 Simulation result of $C_{44} - C_{44}' = P$ for diluted networks.

$$\rho\,\omega^2\,u_\alpha = \sum_\gamma \left(\sum_{\beta\tau} C_{\alpha\beta\gamma\tau}\, k_\beta\, k_\tau \right) u_\gamma \qquad (3.43)$$

Specifically, for 2-D system, (3.43) is reduced to:

$$\rho\,\omega^2 \begin{vmatrix} u \\ v \end{vmatrix} = \begin{vmatrix} C_{11}\,k_x^2 + C_{44}\,k_y^2 & (C_{12} + C_{44}')k_x k_y \\ (C_{12} + C_{44}')k_x k_y & C_{44}\,k_x^2 + C_{11}\,k_y^2 \end{vmatrix} \begin{vmatrix} u \\ v \end{vmatrix}$$

(3.44)

In the (1,0) direction, we have two eigenvalues:

$$\rho\,\omega^2 / k^2 = \begin{matrix} C_{11} \\ C_{44} \end{matrix} \qquad (3.45)$$

Corresponding to the longitudinal and transverse wave respectively. In the (1,1) direction, i.e. $k_x = k_y = k/\sqrt{2}$, the two eigenvalues are

$$\rho\,\omega^2 / k^2 = \frac{C_{11} + C_{44} \pm (\, C_{12} + C_{44}')}{2} \qquad (3.46)$$

Since for isotropic system as the triangular net, the sound velocities are independent of directions, by equating (3.45) and (3.46), we have

$$C_{11} + C_{44} + (\, C_{12} + C_{44}'\,) = 2\,C_{11} \qquad (3.47)$$

$$C_{11} + C_{44} - (C_{12} + C_{44}') = 2 C_{44} \qquad (3.48)$$

both of them leads to equation (3.29). Figure 3.11 presents a numerical check for (3.29) on the diluted system. We conclude that eq.(3.29) based on the isotropy is valid in the diluted stretched system.

Cauchy's Relation

Finally, we study the validity of the Cauchy's relation on diluted network. From the numerical simulation results plotted in Figure 3.12, we can see that there is an obvious discrepancy between C_{12} and C_{44}' except for $L_0/L = 1$. This result may be not so disappointing since the hypothesis for the Cauchy's relation to be valid is totally destroyed in the diluted tennis racket. Assumptions for Cauchy's relation are (1) central force between pair of atoms, (2) inversional symmetry at each sites. (Love 1944) Garboczi (1985) claimed that the second assumption should be modified since that the numerical simulation suggested the existance of Cauchy's relation for the diluted central network, which is the case $L_0/L = 1$ in this work. As soon as the network is stretched, i.e. for L_0/L not equal to 1, we lost the Cauchy's relation. One explanation is for $L_0 /L = 1$, the equilibrium configuration still has the lattice background, while for $L_0/L = 1$ and $p<1$, the equilibrium positions are no longer at the lattice node.

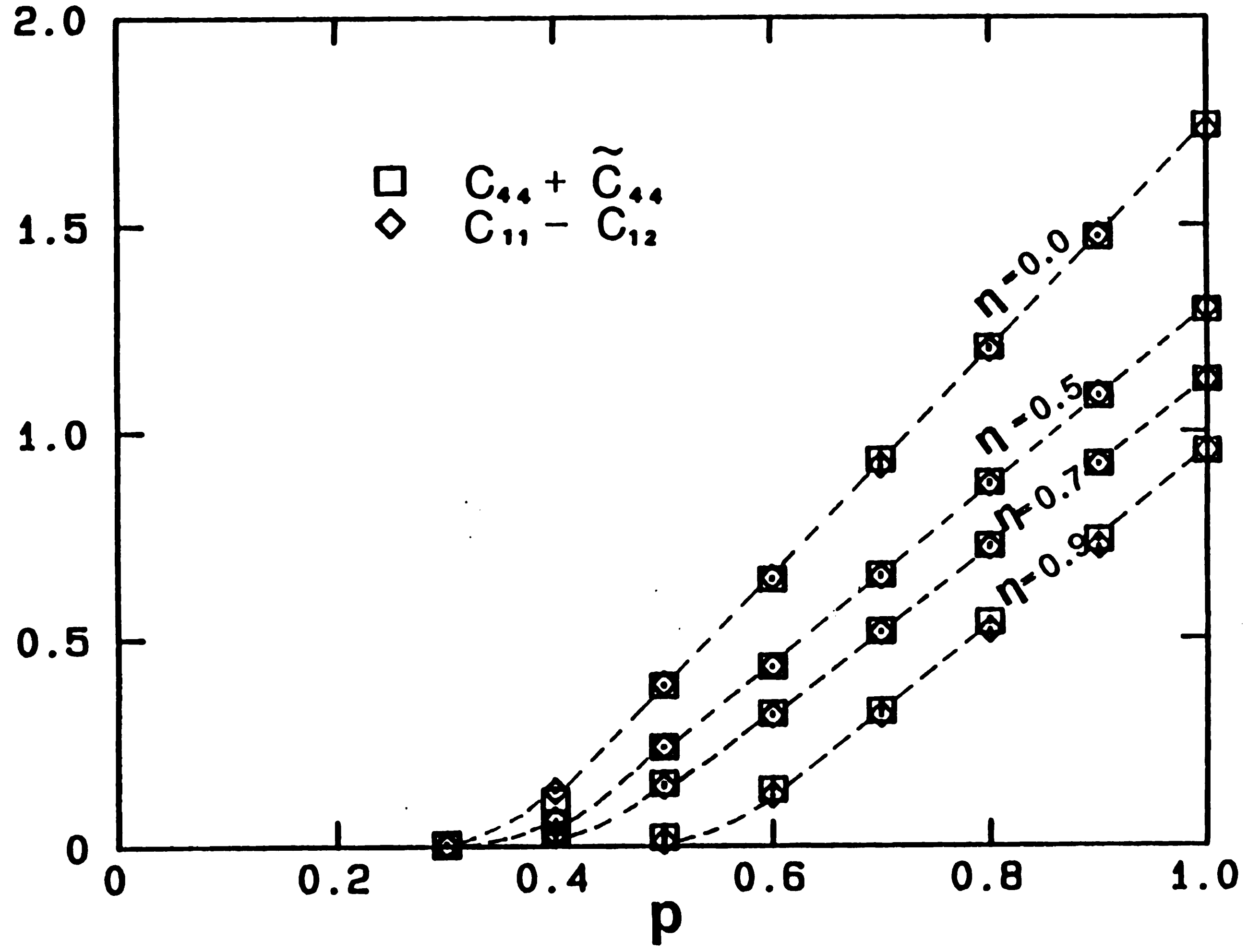

Figure 3.11 Simulation result of $C_{44} + C_{44}' = C_{11} - C_{12}$ for diluted networks.

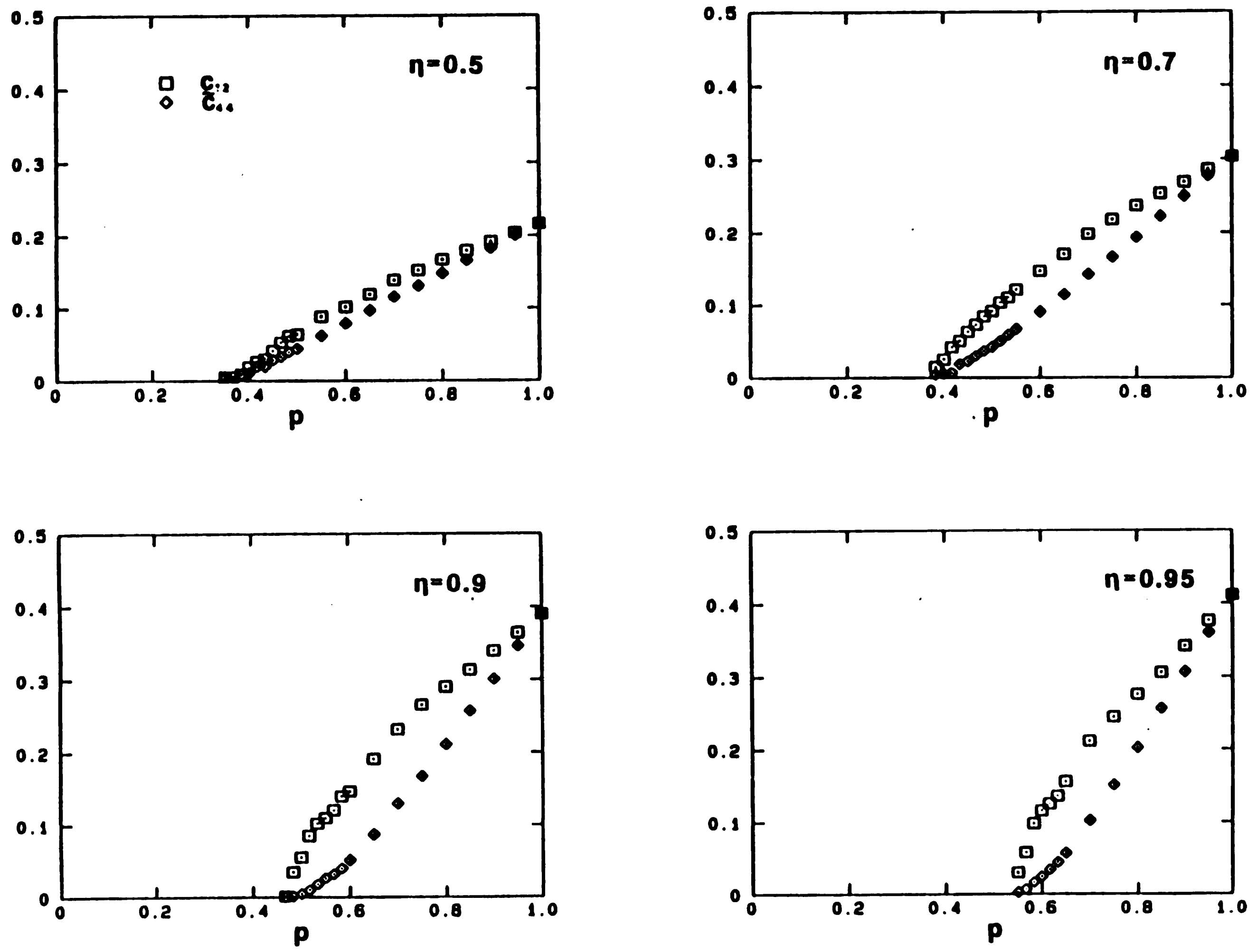

Figure 3.12 Simulation result for Cauchy's relation $C_{12} = C_{44}'$.

Through above analysis, we conclude that in the diluted tennis racket, eqs. (3.28) and (3.29) are still valid, but not the Cauchy's relation (3.27). This reduces the six quantities E, P, B, μ_s, μ_r, b to four independent ones.

Section 3.6 Effective Medium Theory

Now we have four independent quantities E (static energy), P (pressure), B (Bulk modulus) and μ_s(Shear modulus) to describe the elastic behavior of the tennis racket. Figure 3.8 and Figure 3.9 plot P and E vs. p for various η, where $\eta = L_0/L$. To see the transition effect clearly, both E and P are scaled by their corresponding value on pure lattice. Similarly, Figure 3.13 plots B and μ_s vs. p for several values of η, which are averaged over 5 samples. Note that for $\eta=0$, B and μ_s are exactly equal. Obviously, p^*, at which the elasticity vanishes depends on η. Figure 3.14 plots this phase boundary of p^* vs. η in the stretched region, i.e. $0 < \eta < 1$, where two extreme cases $\eta = 0$ and $\eta = 1$ were known before.

It can be seen from Figure 3.13 that B is almost a straight line for whole range of p down to p^*, while μ_s , as well as E and P which are shown in Figures 3.9 and 3.8, have more or less a tail near p^*. This tells us that the phase boundary in Figure 3.14 may be relative to the phase boundary determined by the initial slope of B. We introduce a single defect in a network, then let it relax. From the drop of the corresponding elastic quantities due to this defect , we extract their intercepts on the p-axis. Figure 3.15 presents the computer simulation results of the single defect case for p^*_E, p^*_P, p^*_B, $p^*_{\mu_r}$, $p^*_{\mu_s}$ and p^*_b. Again,

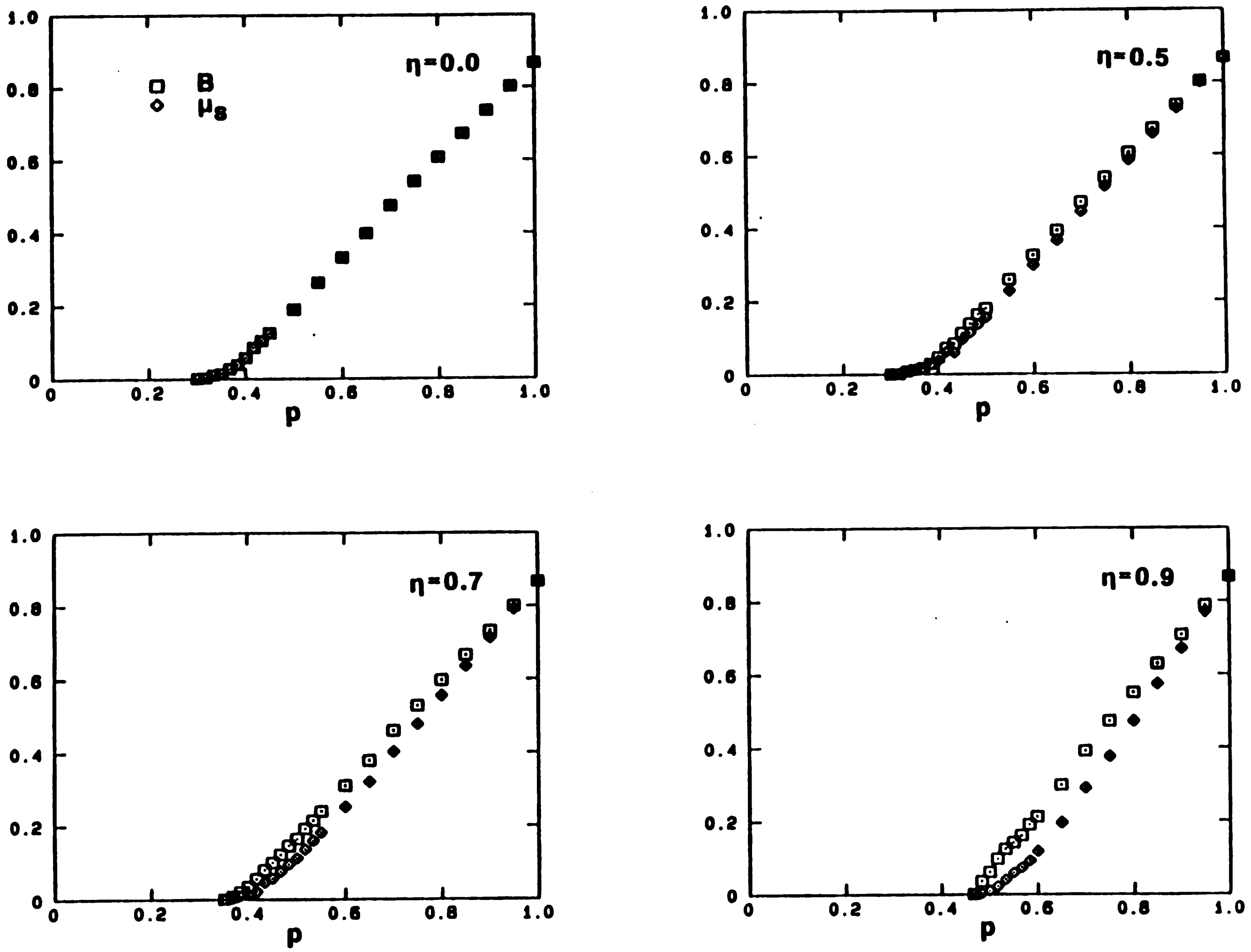

Figure 3.13 B (square) and μ_s (diamond) vs. p, averaged over 5 samples, where μ_s is scaled by the factor of $1/(1-\eta/2)$.

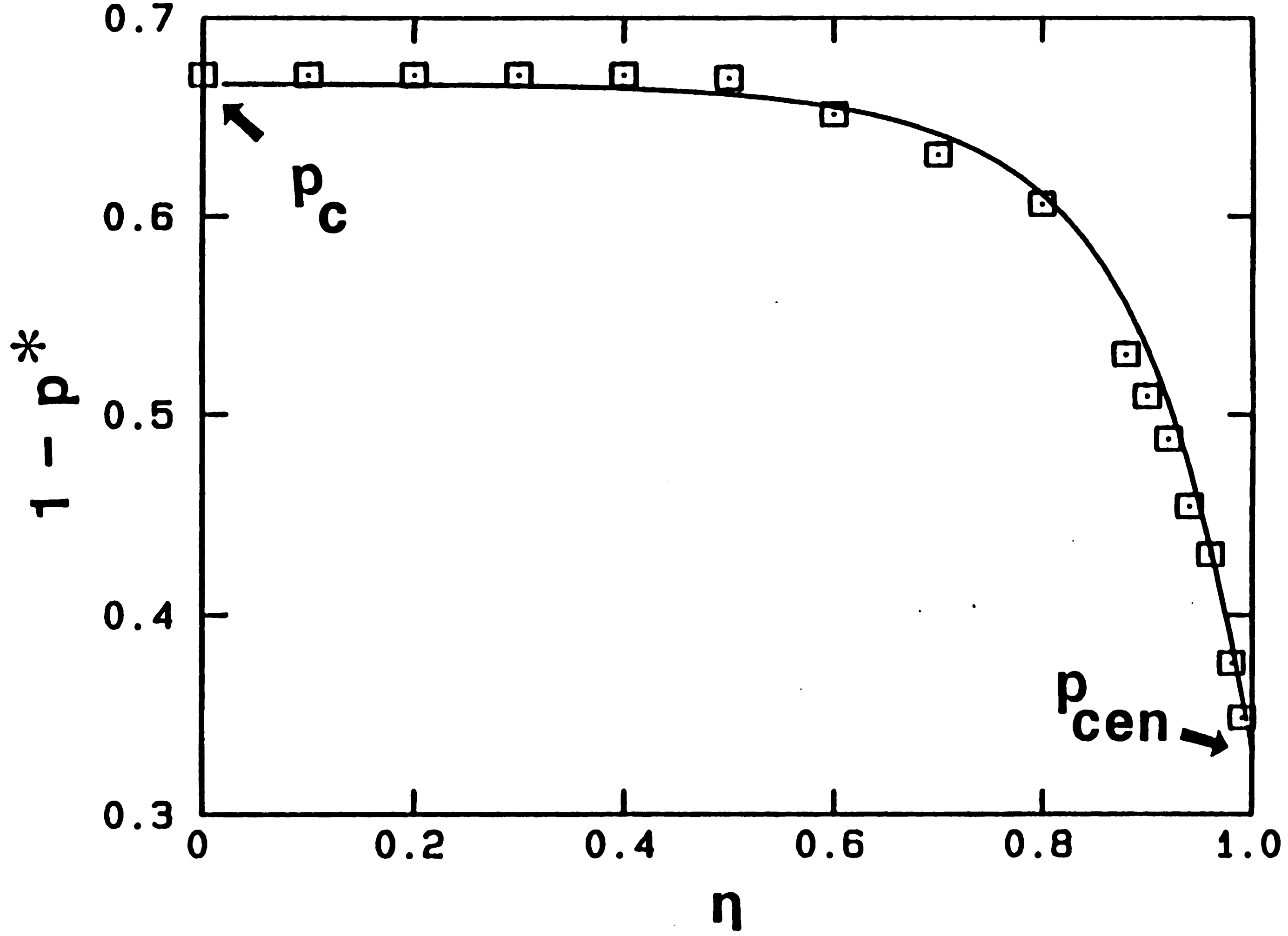

Figure 3.14 Phase boundary determined by vanishing of elastic constants.

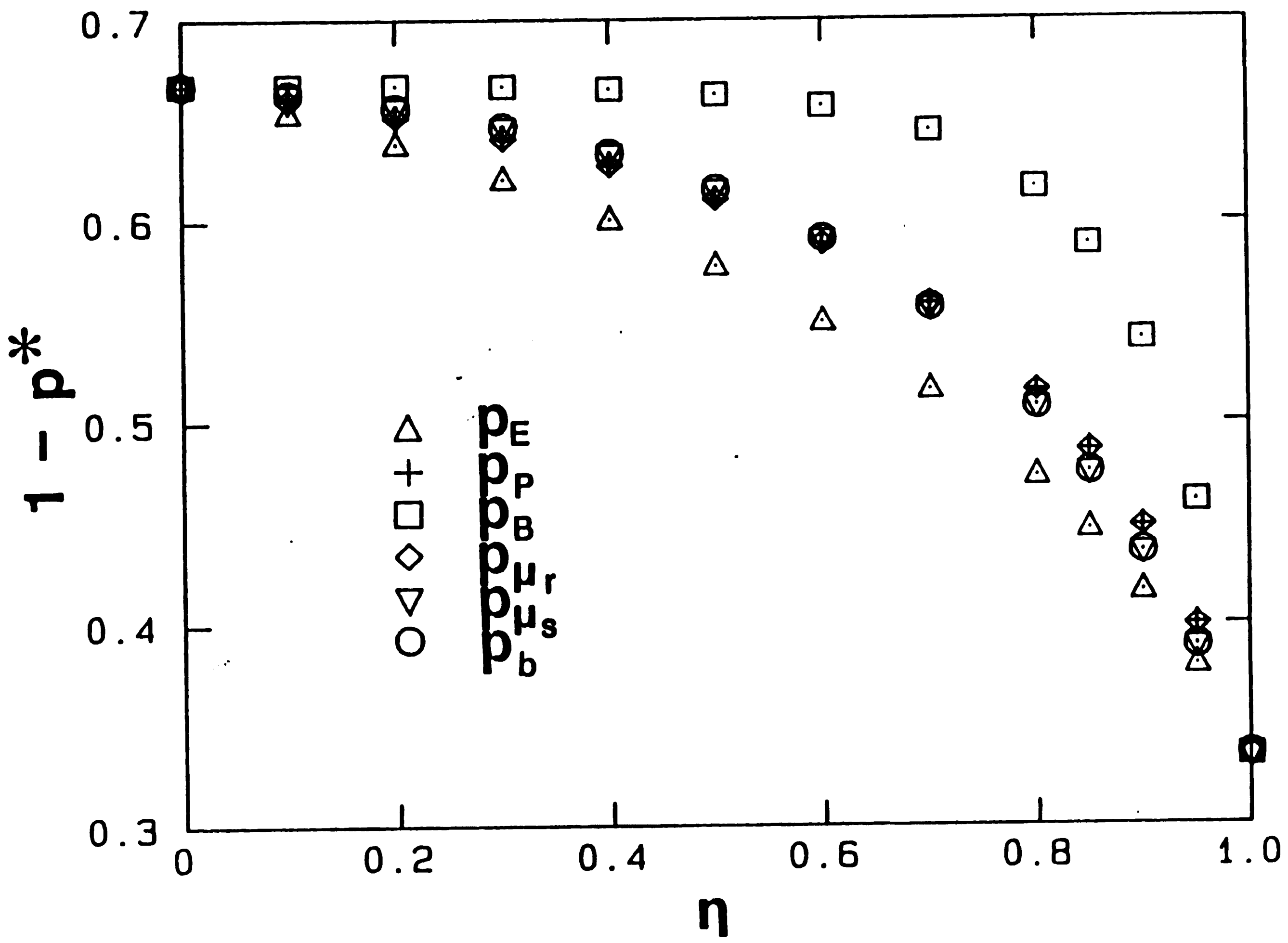

Figure 3.15 Computer simulation results for p^*_E, p^*_P, p^*_B, $p^*_{\mu_r}$, $p^*_{\mu_s}$, p^*_b.

there are two identical pairs, p^*_p and $p^*_{\mu_r}$, $p^*_{\mu_s}$ and p^*_b, as the results of the rotational invariance and isotropy which are proved in section 3.5. The differences between the four independent quantities are consistent with what shown in Figures 3.13, 3.8 and 3.9.

In the remain part of this section, we will present a theoretical analysis of the single defect case and predict the initial slopes via the effective medium theory.

Let us consider a tennis racket with one bond, for example, in between sites 1 and 2, removed as sketched in Figure 3.16. After relaxation, the distance between 1 and 2 changes from L to L_{eq}. The effective spring constant between site 1 and 2 are K/a^*, which includes the effects of both the direct spring and the lattice. We know that $0 < a^* < 1$, since the effect of the lattice background. Then after removing the spring between 1 and 2, the effective spring of the lattice background is

$$K_e = \frac{K}{a^*} - K \tag{3.49}$$

From Thorpe and Garboczi (1985), a^* can be calculated exactly from the dynamical matrix of the pure lattice,

$$a^* = \frac{2}{z}\frac{K}{N} \sum_{k} \mathrm{Tr} \{ \sum_{\delta} [1 - \exp (iL\vec{k}\cdot\hat{\delta})] (\hat{\delta}\hat{\delta}) \cdot \underline{D}^{-1}(\vec{k}) \} \tag{3.50}$$

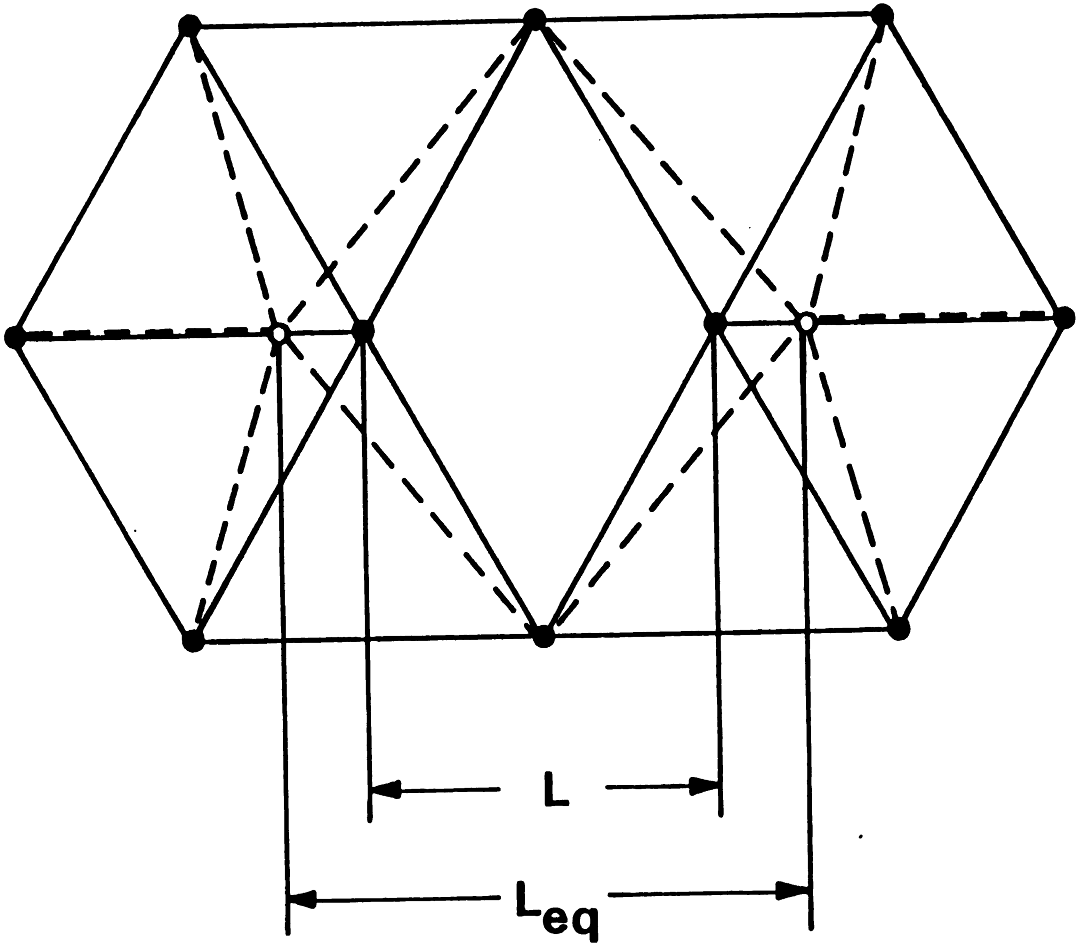

Figure 3.16 Sketch to explain the single defect configuration before and after relaxation.

where $\underline{D}(\vec{k})$ is the Fourier transform of the dynamical matrix:

$$\underline{D}(\vec{k}) = K \eta \sum_{\delta} [\ 1 - \exp(iL\vec{k}\bullet\hat{\delta})\ ]\ \hat{\delta}\hat{\delta}$$

$$+ K(1-\eta) \sum_{\delta} [\ 1 - \exp(iL\vec{k}\bullet\hat{\delta})\ ]\ \underline{I} \qquad (3.51)$$

where $\eta = L_0/L$ and $\underline{I}$ is the d×d unit matrix. The formula to calculate a^* of the tennis racket model on triangular net are shown in Appendix C.

If the potential about the equilibrium position of this effective spring is pure parabolic (checked by simulation for stretched network), we find L_{eq} is given by:

$$L_{eq} = \frac{L - L_0\, a^*}{1 - a^*} \qquad (3.52)$$

Substitute back to the expression of the energy, we find out the amount of energy that must be added to the one defect case to recover the no defect lattice energy is:

$$\Delta E = \frac{1}{2} K_e \left[\frac{L - L_0\, a^*}{1 - a^*} - L\ \right]^2 + \frac{1}{2} K\ (\ L - L_0)^2$$

$$= \frac{1}{2} K\ (\ L - L_0)^2 \left(\frac{1}{1 - a^*}\right) \qquad (3.53)$$

which determines the initial slope of the static energy

$$p^*_E = a^* \tag{3.54}$$

This result is plotted in Figure 3.17, where the solid curve is a^* and the symbols are p^*_E from computer simulation. The disagreement near $\eta = 1.2$ is due to the failure of the parabolic assumption in the strongly conpressed network. In this work, we will focus on the network with tension, i.e. $0<\eta<1$.

Now, we have the expression for the energy in the network with a few defects (fraction of 1-p):

$$E = \frac{Nz}{4} K L^2 (1 - \eta)^2 [\frac{p - a^*}{1 - a^*}] \tag{3.55}$$

For the initial slope for the pressure, we notice that P is proportional to $\frac{\partial E}{\partial L}$, we have

$$P = P_0 [1 - (1 - p) \Delta_1] \tag{3.56}$$

where

$$\Delta_1 = \frac{1}{1-a^*} [1 - \frac{1}{2} \eta (1-\eta) \frac{1}{1-a^*} \frac{\partial a^*}{\partial \eta}] \tag{3.57}$$

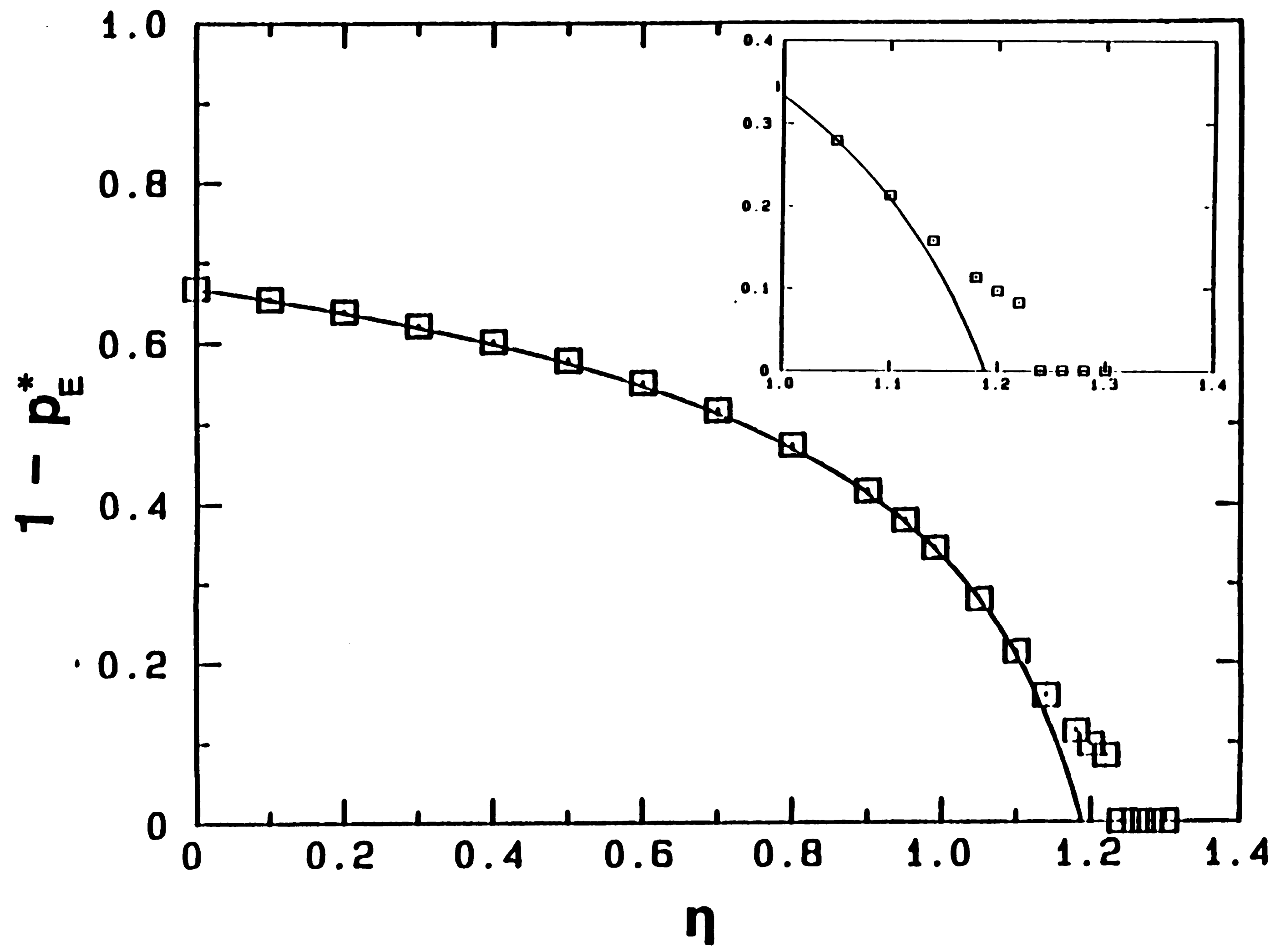

Figure 3.17 Effective medium theory result of a^*. The symbol is the initial slope intercepts on p-axis for static energy in the simulation.

and p^*_P is given by

$$p^*_P = 1 - 1/\Delta_1 \qquad (3.58)$$

For the Bulk modulus, we know

$$AB = \frac{L^2}{4A^2} \frac{\partial^2 E}{\partial L^2} \qquad (3.59)$$

where A is the area. We have

$$B = B_0 \; [\; 1 - (1-p) \; \Delta_2 \;] \qquad (3.60)$$

where

$$\Delta_2 = \frac{1}{1-a^*} \; \{ \; 1 - \eta \; (\; 1 - \eta^2) \; \frac{1}{1-a^*} \; \frac{\partial a^*}{\partial \eta}$$

$$+ \; [\; \eta \; (1-\eta) \; \frac{1}{1-a^*} \; \frac{\partial \; a^*}{\partial \; \eta} \;]^2$$

$$+ \; \frac{1}{2} \; \eta^2 \; (1-\eta)^2 \; \frac{1}{1-a^*} \; \frac{\partial^2 a^*}{\partial \; \eta^2} \; \} \qquad (3.61)$$

which gives

$$p^*_B = 1 - 1/\Delta_2 \qquad (3.62)$$

All of these results, p^*_E, p^*_P and p^*_B, as well as the corresponding simulation results are plotted in Figure 3.18.

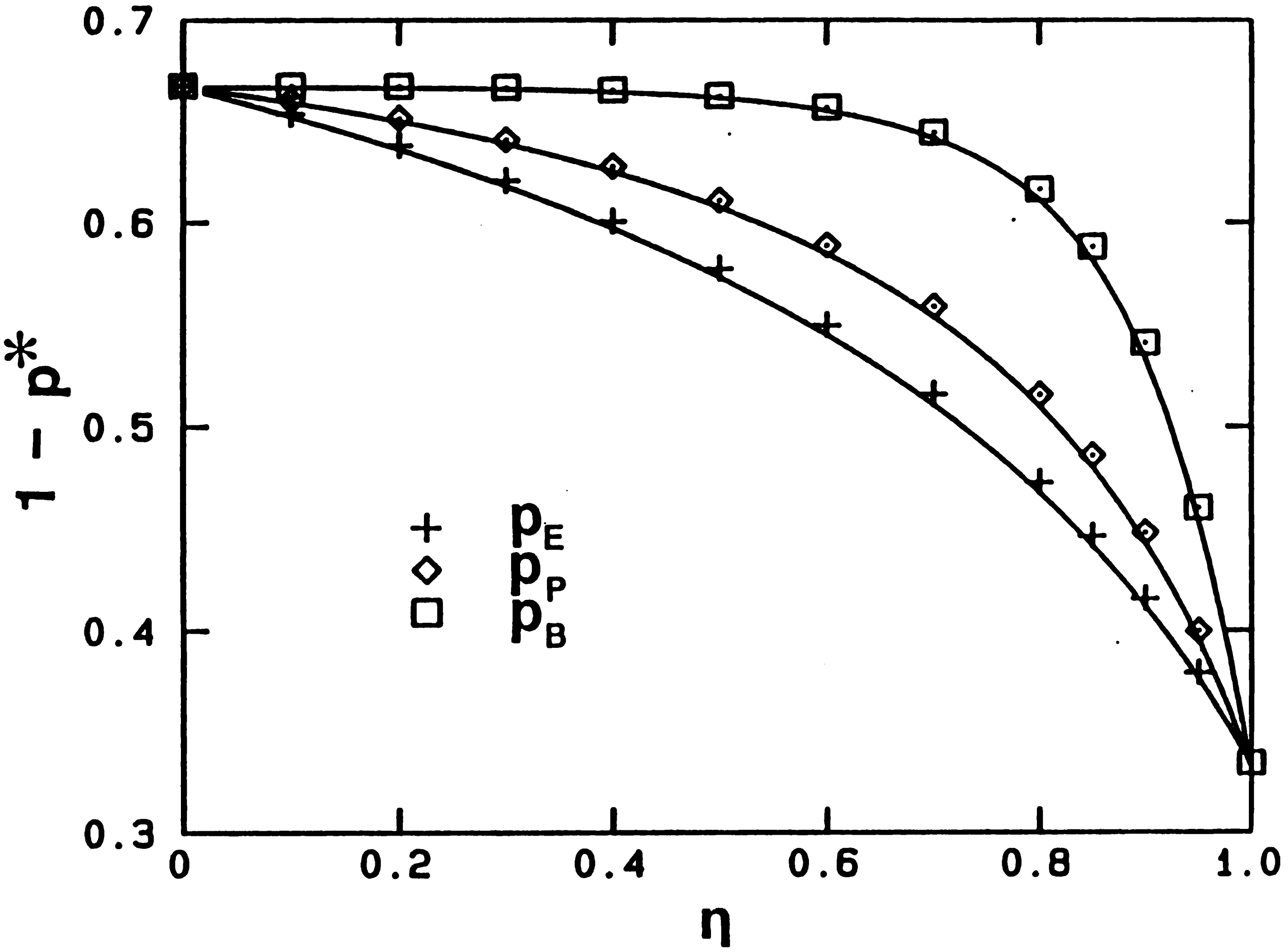

<u>Figure 3.18</u> Effective medium theory results for ρ^*_E, ρ^*_P and ρ^*_B.

Section 3.7 Conclusion and Future Research

We found that two kinds of percolation problem, conductivity percolation and rigidity percolation can be combined together in the stretched tennis racket model. Our main conclusion is that the threshold for the new model is not discontinuously changing from p_{cen} to p_c, as predicted by the simulation on the Born model. In the intermediate region, i.e. for $0<L_0/L<1$, we observed p^* between p_c and p_{cen}. An effective medium theory is derived for the single defect case.

Several suggestions can be made for future research. At first, study about the elastic behavior of compressed network ($L_0/L>1$) is certainly needed which is an important part in the complete phase diagram. Secondly, from the experimental point of view, a measurement of the longitudinal and transverse sound velocities in tennis racket must be very interesting. Of course, in a real system, there would be additional contributions to the elasticity which are not due to the network. Finally, determination of the standard exponents for the tennis racket model would be useful but also time consuming.

APPENDICES

Appendix A. Isolated defects in the static limit

Appendix A. Isolated defects in the static limit

Submitted to J. Phys. C

September 18, 1986

Isolated defects in the static limit

M. F. Thorpe and W. Tang
Department of Physics and Astronomy
Michigan State University
East Lansing, MI 48824

Abstract

We collect together the known results for the effect of a single defect, into a single compact form that can be used in any lattice in the static limit. The result is used to calculate the effect of single defects, either bonds or sites, on the diffusion constant and conductivity of various lattices. It is shown that the result of Izyumov for the spin wave stiffness can be simply generalized to any lattice.

PA Classification: 7155, 6350

1. Introduction

The effect of a single impurity on some desired response function is well understood (see e.g. Elliott et al 1974). Practical calculations are possible if the range over which the interactions are changed by the impurity, is very short. In general, the detailed symmetry around the defect site must be taken into account in order to complete the calculation. An exception is a mass defect, where a simple formula can be written down that is valid for any lattice. The lattice only comes in when the particular on-site Green function needed is calculated. Another similar situation is provided by a site diagonal impurity in a tight binding model (see e.g. Economu 1979).

In this paper, we look at two other cases that can also be carried through without worrying about the particular lattice until the pure lattice Green function has to be evaluated.

The first of these is the bond defect in a tight binding model; a result given by Kirkpatrick (1973). A more interesting and complex example is site defect when a site and all its bonds to its nearest neighbors are altered.

2. General Formalism

For convenience we consider a system described by a vibrational potential

$$U = \sum_{ij\alpha\beta} A_{ij}^{\alpha\beta} u_i^{\alpha} u_j^{\beta} \tag{1}$$

where all the atoms are mass points with mass m; i,j are sites and α,β are Cartesian components. The vector $\underline{u}_i$ is the displacement of the i^{th} site. The $A_{ij}^{\alpha\beta}$ are subject to various symmetry restrictions that we do not need to consider here. We will switch to tight binding language later. The dynamical matrix for this system is defined from the equation of motion.

$$m\omega^2 u_i^\alpha = \sum_{j\beta} A_{ij}^{\alpha\beta} u_j^\beta \tag{2}$$

or

$$m\omega^2 \underline{u} = \underline{\underline{D}}\ \underline{u} \tag{2a}$$

where $\underline{u}$ is considered to be a dN dimensional vector. The dimensionality of the system is d and there are N atoms. The dN by dN matrix $\underline{\underline{D}}$ is the usual dynamical matrix (see e.g. Born and Huang 1966).

If a force $\underline{f}_e$, also considered as a dN vector, is <u>externally</u> applied to the system, then

$$\underline{f}_e = - \underline{f} = \underline{\underline{D}}\ \underline{u}\ . \tag{3}$$

We will be considering only cases where $\underline{f}_e$ (and hence $\underline{f}$ the force produced by the system to oppose $\underline{f}_e$ in equilibrium) are non zero at the <u>surface</u>. Inverting equation (3) we find that

$$\underline{u} = \underline{\underline{G}}\ \underline{f}\ . \tag{4}$$

where $\underline{\underline{G}}$ is the zero frequency limit of the usual Green function $\underline{\underline{G}}(\omega^2)$ given by

$$\underline{\underline{G}}(\omega^2) = \left[m\omega^2 - \underline{\underline{D}}\right]^{-1} . \tag{5}$$

As we are only concerned with the static limit, the masses are irrelevant and so we will set them all equal to m. If the system described by (1) consists of a perfect crystal with a dynamical matrix $\underline{\underline{D}}_o$ plus a defect, where the defect has a (localized) potential $\underline{\underline{V}}$, then we have the usual Dyson equation

$$\underline{\underline{G}} = \underline{\underline{P}} + \underline{\underline{P}}\,\underline{\underline{V}}\,\underline{\underline{G}} . \tag{6}$$

where $\underline{\underline{D}} = \underline{\underline{D}}_o + \underline{\underline{V}}$. Here $\underline{\underline{P}}$ is the perfect crystal Green function and $\underline{\underline{G}}$ is the Green function of the system plus defect. Note that $\underline{\underline{D}}_o\,\underline{\underline{P}} = \underline{\underline{D}}\,\underline{\underline{G}} = -1$. We may solve (6) formally

$$\underline{\underline{G}} = (1 - \underline{\underline{P}}\underline{\underline{V}})^{-1}\underline{\underline{P}} . \tag{7}$$

The static energy E' of the system produced by the application of the external force $\underline{f}_e$ is

$$E' = \frac{1}{2}\,\underline{f}_e \bullet \underline{u} = -\frac{1}{2}\,\underline{f}\,\underline{\underline{G}}\,\underline{f} \quad . \tag{8}$$

We see from (6) and (7) that

$$\underline{\underline{G}} - \underline{\underline{P}} = \underline{\underline{P}}\underline{\underline{V}}\underline{\underline{G}} = \underline{\underline{P}}\underline{\underline{V}}(1-\underline{\underline{P}}\underline{\underline{V}})^{-1}\underline{\underline{P}} .$$

The <u>change</u> in the energy $\Delta E = E' - E$ due to the presence of the defect is therefore

$$\Delta E = -\frac{1}{2}\,\underline{f}(\underline{\underline{G}} - \underline{\underline{P}})\underline{f}$$

$$= -\frac{1}{2}\,\underline{f}\,\underline{\underline{P}}\,\underline{\underline{V}}\,(1 - \underline{\underline{P}}\,\underline{\underline{V}})^{-1}\underline{\underline{P}}\,\underline{f}\;. \qquad (9)$$

This form is quite convenient as usually $\underline{f}$ is only nonzero at the surface of the sample. However a better form for our purposes is obtained by writing the equation similar to (4) but for the perfect system

$$\underline{u}_o = \underline{\underline{P}}\,\underline{f} \qquad (10)$$

where $\underline{u}_o$ are the displacements produced by the force $\underline{f}$ *before* the defect was introduced and using this we can write

$$\Delta E = -\frac{1}{2}\,\underline{u}_o\,\underline{\underline{V}}(1 - \underline{\underline{P}}\underline{\underline{V}})^{-1}\underline{u}_o. \qquad (9a)$$

This result can be rewritten using the $\underline{\underline{T}}$ matrix

$$\underline{\underline{T}} = \underline{\underline{V}}(1 - \underline{\underline{P}}\underline{\underline{V}})^{-1} \qquad (11)$$

as

$$\Delta E = -\frac{1}{2}\,\underline{u}_o\,\underline{\underline{T}}\,\underline{u}_o\;. \qquad (12)$$

This is a very convenient form for developing effective medium theories of many defects as well as the single defect problem we are considering here. Equation (12) is simple because the range of $\underline{\underline{T}}$ is the same as $\underline{\underline{V}}$ and so is localized around the defect. In order to calculate ΔE, it is therefore only necessary to know $\underline{u}_o$ around the defect. Remember that the $\underline{u}_o$ are the displacements produced by the external force $\underline{f}_e$ in the absence of the defect. When the defect is introduced, the force $\underline{f}$ is held constant and the strain changes. The situation is particularly simple in a Bravais lattice if $\underline{f}_e$ is a uniform external stress (e.g. shear, compression). Then the lattice distortion is homogeneous and the $\underline{u}_o$ is very easy to write down. This is the only case we shall be considering here.

3. Isotropic Born Model

We apply the work of the preceding section to the isotropic Born model (Born 1914), where the perfect lattice is described by the potential

$$U = \frac{\alpha}{4} \sum_{i,j} (\underline{u}_i - \underline{u}_j)^2 . \tag{13}$$

and the sum is restricted to nearest neighbors. This model decouples in the d orthogonal Cartesian directions into d separate tight binding Hamiltonians

$$H = \alpha \sum_{i,j} (a_i^\dagger a_i - a_j^\dagger a_i) \tag{14}$$

where the sums in (13) and (14) go over j which are nearest neighbors of i, which is also summed over. We will work in the language of the isotropic Born model and "translate" into tight binding language later. This is convenient as stresses and homogeneous strains are easier to visualize than the equivalent in the tight binding model.

Let us consider a uniform strain ($\underline{u}_o$) in which the i th atom has a displacement.

$$\underline{u}_i = \epsilon \underline{R}_i \tag{15}$$

where ϵ is the magnitude of the strain. This homogeneous strain (15) is appropriate for any Bravais lattice. Because all homogeneous strains (i.e. shear, compression, etc.) for the potential (13) are trivially related, we use the simple form (15) where ϵ is a scalar. The methods outlined here become a little more complex for lattices with a basis where the strain is not usually homogeneous. Inserting (15) into (13), we find that the strain energy E is given by

$$E = \frac{1}{4}\alpha\epsilon^2 Nza^2 \tag{16}$$

where the a is the separation of the z nearest neighbors. Note that the origin used for the external strain (15) is irrelevant as only differences in displacements contribute toward the strain energy (16).

4. Bond Defect

We now consider a very simple defect. A single bond is changed from $\alpha \rightarrow \alpha_0$. We will number the atoms 1,2 as in figure 1. In general the strain (15) will produce displacements $\underline{u}_1 = -\underline{u}_2 = \frac{1}{2}\epsilon\underline{R}_{12}$ where $\underline{R}_{12} = \underline{R}_1 - \underline{R}_2$ is a nearest neighbor vector. Because the defect is localized, no other displacements need be used as basis functions in (9a). It is convenient to choose the center of the bond 1,2 as the origin for the strain. This excludes any uniform motion of the defect bond, which may be included, but does not contribute to (9a). In this basis (Feng, Garboczi and Thorpe 1985), the $\underline{\underline{V}}$ matrix may be written

$$\underline{\underline{V}} = (\alpha_o - \alpha) \begin{pmatrix} 1 & -1 \\ -1 & 1 \end{pmatrix} \tag{17}$$

and

$$\underline{u}_o = \varepsilon a \begin{pmatrix} \frac{1}{2} \\ -\frac{1}{2} \end{pmatrix} \tag{18}$$

$$\underline{u}_o = \frac{\varepsilon a}{\sqrt{2}} \, |s\rangle \tag{19}$$

where

$$|s\rangle = \begin{pmatrix} \frac{1}{\sqrt{2}} \\ -\frac{1}{\sqrt{2}} \end{pmatrix}$$

so that the state vector $|s\rangle$ is properly normalized. Note that

$$\underline{\underline{V}} \, |s\rangle = 2(\alpha_o - \alpha) \, |s\rangle \tag{20}$$

so that

$$\Delta E = -\frac{1}{4}\varepsilon^2 a^2 \left[\frac{2(\alpha_o - \alpha)}{1 - 2(\alpha_o - \alpha)\langle s|\underline{\underline{P}}|s\rangle}\right] \tag{21}$$

where we have also used the fact that $|s\rangle$ is an eigenvector of $\underline{\underline{P}}$. This happens because the two states on the atoms 1,2 transform as a symmetric and an antisymmetric vector under the symmetry group of the bond. Because there is a single representation of each kind, there is no mixing so that the antisymmetric vector $|s\rangle$ must be eigenstate of $\underline{\underline{P}}$. The symmetric representation corresponds to the uniform translation and so is irrelevant.

This kind of argument becomes much more powerful in the site defect case to be considered later.

Therefore

$$\langle s|\underline{\underline{P}}|s\rangle = \frac{1}{2}[P_{11} + P_{22} - P_{12} - P_{21}] \tag{22}$$

$$= P_{11} - P_{12} \qquad \text{by symmetry,}$$

where

$$P_{ij} = \frac{1}{N}\sum_{\underline{k}} \frac{\exp(i\underline{k}\bullet\underline{R}_{ij})}{m(\omega^2 - \omega_{\underline{k}}^2)} \tag{23}$$

and

$$m\omega_{\underline{k}}^2 = \alpha z(1 - \gamma_{\underline{k}}) \tag{24}$$

where

$$\gamma_{\underline{k}} = \frac{1}{z}\sum_{\underline{\delta}} e^{i\underline{k}\bullet\underline{\delta}} \tag{25}$$

and $\underline{\delta}$ are the z nearest neighbor vectors. The excitations (24) are just those of the pure isotropic Born model. In general the P_{ij} must be be evaluated numerically, but in the present case we can make a shortcut that by using the equation of motion for P_{11}

$$m\omega^2 P_{11} = 1 + z\alpha(P_{11} - P_{12}) \tag{26}$$

so that as $\omega^2 \to 0$, $(P_{11} - P_{12}) = -(z\alpha)^{-1}$ and hence

$$\Delta E = -\frac{1}{2}\varepsilon^2 a^2 \left[\frac{(\alpha_o - \alpha)}{1 + 2(\alpha_o - \alpha)/z\alpha} \right] \tag{27}$$

Remembering that when the defect is introduced, the <u>stress</u> is held constant, it is the quantity $1/\alpha$ that is renormalized as the energy $\sim f^2/\alpha$. Hence we may write

$$\frac{\alpha}{\alpha_e} = \frac{E'}{E} = 1 + \frac{\Delta E}{E} = 1 + \frac{\underline{f}\,\underline{\underline{P}}\,\underline{\underline{T}}\,\underline{\underline{P}}\,\underline{f}}{\underline{f}\,\underline{\underline{P}}\,\underline{f}} \qquad (28)$$

using equations (9) and (11). This can be rewritten in terms of the $\underline{u}_o$ produced by the $\underline{f}$,

$$\frac{\alpha}{\alpha_e} = 1 - \frac{\underline{u}_o\,\underline{\underline{T}}\,\underline{u}_o}{\underline{u}_o\,\underline{\underline{D}}\,\underline{u}_o} \qquad (29)$$

This result is quite general. We find that in the present case

$$\frac{\alpha}{\alpha_e} = 1 - \frac{\frac{1}{2} N_o \varepsilon^2 a^2 \dfrac{\alpha_o - \alpha}{1 + 2(\alpha_o - \alpha)/zd}}{\frac{1}{4} N \varepsilon^2 z a^2 \alpha} \qquad (30)$$

$$= 1 - \frac{c(\alpha_o - \alpha)}{\alpha + 2(\alpha_o - \alpha)/z}$$

where $N_o = \frac{1}{2} Ncz$ is the (small) number of noninteracting defects. It is more usual to invert (30) to give

$$\alpha_e = \alpha + \frac{c(\alpha_o - \alpha)}{1 - 2(\alpha_o - \alpha)\langle s|\underline{\underline{P}}|s\rangle} \qquad (30a)$$

$$= \alpha + \frac{c(\alpha_o - \alpha)}{\alpha + 2(\alpha_o - \alpha)/z}$$

to first order in the concentration of defects c. This has been obtained previously by Kirkpatrick (1973) but serves to illustrate the method.

A particularly interesting case occurs for a missing bond ($\alpha_o = 0$) when

$$\alpha_e = \alpha - c\alpha/(1 - 2/z) \qquad (31)$$

which extrapolates to zero at

$$c_I = 1 - \frac{2}{z}$$

or

$$p_I = 1 - c_I = \frac{2}{z} \qquad (32)$$

This is the intercept in a plot of α against p when the initial slope is extrapolated to where it crosses the horizontal axis. This is discussed in more detail in the next section. Going back to (21), an alternative expression for p_I is given by

$$p_I = -2\alpha\langle s|\underline{\underline{P}}|s\rangle \qquad (32a)$$

where $|s\rangle$ is the state vector characterizing the local strain around the defect, but in the absence of the defect, and $\underline{\underline{P}}$ is the perfect crystal Green function. This form is useful as a similar but different form holds for a site vacancy. The place where α_e actually goes to zero is of course the percolation concentration p_c. Kirkpatrick (1973) has shown that the conductance of a network of wires behaves as α_e if we identify the tight binding parameter (or in our case the spring constant) α with the conductance of a wire joining adjacent sites. Kirkpatrick has also shown that the diffusion constant D can be obtained from G via

$$G = P_s D \tag{33}$$

where P_s is the probability that a site is connected into the infinite cluster. Throughout this paper we will use units such that G and D are normalized to unity at $p = 1$. This saves having to write G/G_o and D/D_o everywhere. It is easy to calculate P_s for small c in the present case. To isolate a site, it must have all z bonds cut, therefore

$$P_s = 1 - c^z + O\left(c^{2z-1}\right) \tag{34}$$

and so makes no contribution to O(c). Therefore the initial slope of the diffusion constant D is the same as that of the conductance G and the extrapolated intercept p_I' is just given by

$$p_I' = p_I \tag{35}$$

In table 1, we show p_c, p_I and p_I' for some common Bravais lattices. The quantities G, D, P_s all go to zero at p_c. If $G \sim (p - p_c)^t$, $D \sim (p - p_c)^{t'}$ and $P_s \sim (p - p_c)^{\beta}$, then $t' = t - \beta$. In 2D, $t = 1.3$ and $\beta = 0.14$ whereas in 3D, $t = 1.9$ and $\beta = 0.4$ from Stauffer (1985). These indices depend only upon dimensionality and are the same for both site and bond percolation.

Finally in this section we note that the relation $G = P_s D$ is the analogue of

$$E = \rho v_s^2 \tag{36}$$

where E is an elastic modulus, ρ is the mass density and v_s is the sound velocity. It is clear that such a mapping exists because of the equivalence of the tight binding model and the isotropic Born model.

4. Site Defect

Using the general ideas of the previous section, we can obtain an expression for a general site defect. It is convenient to use a uniaxial, rather than a hydrostatic strain as in the previous section, so that the i^{th} atom has a displacement

$$\underline{u}_i = \epsilon(\underline{R}_i \bullet \hat{x})\hat{y} \tag{37}$$

where $\hat{x}$, $\hat{y}$ are any directions; these need not be orthogonal and they can be the same. Also $\hat{y}$ may be perpendicular to the lattice(e.g. the z direction for a 2D network in the x,y plane). In that case the isotropic Born potential (13) must also contain terms in the z direction. All this arbitrariness is because of the isotropy which leads to a single diffusion constant or elastic stiffness. This formalism can also be used with anisotropic interactions, like central forces, in which case careful track must be kept of directions (Thorpe and Garboczi 1986).

The strain energy of the system, using (13) and (37) is

$$E = \frac{1}{4} \alpha\varepsilon^2 Nza^2/d \tag{38}$$

The vector $\underline{u}_o$ is formed from the homogeneous strain (37). All the z bonds around the defect site have force constants α_o, while all the other bonds have the original force constants α. It is convenient to choose the origin at the center of the defect (see figure 2). As in the bond case, this does not affect the result but simplifies the algebra. The nearest neighbors of the central site have displacements

$$\underline{u}_{\underline{\delta}} = \varepsilon(\underline{\delta}\cdot\hat{x})\hat{y} \tag{39}$$

where $\underline{\delta}$ goes over the z nearest neighbor vectors each of length a. The normalization is given by

$$\sum_\delta u_\delta^2 = \varepsilon^2 \sum_\delta (\underline{\delta}\cdot\hat{x})^2 = \varepsilon za^2/d \tag{40}$$

if all d directions are equivalent. This is true for all the cases to be considered here and listed in table 2. Thus we are restricted to <u>Bravais lattices in which a second rank tensor is a constant times the unit matrix</u>. The formalism becomes a little more complex in other situations but can still be used. We may write the state vector |s> as

$$\underline{u}_o = \varepsilon a \sqrt{\frac{z}{d}}\ |s\rangle \tag{41}$$

which is a little different from (19). The vector $|s\rangle$ varies depending on the defect and the direction of the strain. For the strain in the triangular net, shown in figure 2.

$$|s\rangle = \sqrt{\frac{1}{3}} \begin{pmatrix} 1 \\ \frac{1}{2} \\ -\frac{1}{2} \\ -1 \\ -\frac{1}{2} \\ \frac{1}{2} \end{pmatrix} \tag{42}$$

Fortunately we will not need to write $|s\rangle$ down in detail. A little thought will convince the reader that for <u>any</u> $|s\rangle$ derived from (39),

$$\underline{\underline{V}}\,|s\rangle = (\alpha_o - \alpha)\,|s\rangle \tag{43}$$

which differs from (20) by a factor 2, because each atom in the shell connects only to the stationary center in this case. Hence

$$\Delta E = -\frac{z}{2d}\,\varepsilon^2 a^2 \left[\frac{\alpha_o - \alpha}{1 - (\alpha_o - \alpha)\langle s|\underline{\underline{P}}|s\rangle}\right] \tag{44}$$

where we again use the fact that $|s\rangle$ is an eigenstate of $\underline{\underline{P}}$. The argument in this case is a little more subtle. The state vector $|s\rangle$ transforms as a vector on the shell of the defect. As $\underline{\underline{P}}$ is a scalar, and there is only single vector representation on the shell, the result follows.

Combining (38) and (44), we see that

$$E + \Delta E = \frac{1}{4}\,\epsilon^2 N z a^2/d\,\left[\alpha - \frac{2c(\alpha_o - \alpha)}{1 - (\alpha_o - \alpha)\langle s|\underline{\underline{P}}|s\rangle}\right] \tag{45}$$

The factor 2 in the numerator occurs because of the counting, and comes about because a bond is removed if either of the two sites at its end are removed. From (28) we can define α_e as

$$\frac{\alpha}{\alpha_e} = 1 - \frac{2c(\alpha_o - \alpha)}{1 - (\alpha_o - \alpha)\langle s|\underline{\underline{P}}|s\rangle} \tag{46}$$

Inverting to first order in c, we have

$$\alpha_e = \alpha + \frac{2c(\alpha_o - \alpha)}{1 - (\alpha_o - \alpha)\,\langle s|\,\underline{\underline{P}}\,|s\rangle}\quad . \tag{46a}$$

Notice how the factors 2 occur differently in (30a) and (46). The problem is now reduced to evaluating $\langle s|\underline{\underline{P}}|s\rangle$. The components of $|s\rangle$ are just proportional to $\underline{\delta}_i \cdot \hat{x}$ as seen for example in (42). If normalized properly to 1, they become $\sqrt{\frac{d}{z}}(\delta_i \cdot \hat{x})/a$.

Therefore

$$\langle s|\underline{\underline{P}}|s\rangle = \frac{-d}{Nza^2} \sum_{k} \frac{(\underline{\delta}_i \bullet \hat{x})e^{i\underline{k}\bullet\underline{\delta}_i}(\underline{\delta}_j \bullet \hat{x})e^{-i\underline{k}\bullet\underline{\delta}_j}}{m\omega_k^2} = -\frac{1}{\alpha N}\sum_{\underline{k}} \frac{(\underline{\nabla}\gamma_{\underline{k}})^2}{1-\gamma_{\underline{k}}} \tag{47}$$

where $$\underline{\nabla} = \left(\frac{\partial}{\partial(k_x a)}, \frac{\partial}{\partial(k_y a)} \cdots\right) \tag{48}$$

and it is convenient to include the nearest neighbor distance a in the definition of the ∇ operator. For the special case of a missing site, $\alpha_o = 0$ and α_e extrapolates to zero at

$$p_I = \frac{1}{2} - \frac{\alpha}{2}\langle s|\underline{\underline{P}}|s\rangle \tag{49}$$

$$= \frac{1}{2} + \frac{1}{2N}\sum_{\underline{k}} \frac{(\nabla\gamma_{\underline{k}})^2}{1-\gamma_{\underline{k}}} \tag{49a}$$

These integrals for p_I have to be computed numerically in most cases. They are listed for a number of lattices in table 2. The square net has

$$\gamma_k = \frac{1}{2}\left[\cos k_x a + \cos k_y a\right]$$

and so $$p_I = \frac{1}{2} + \frac{1}{8N}\sum_{k} \frac{2 - \cos 2k_x a - \cos 2k_y a}{2 - \cos k_x a - \cos k_y a}$$

$$= \frac{1}{2} + \frac{1}{8}\int_{0}\int^{\pi} \frac{[2 - \cos 2x - \cos 2y]dxdy}{2 - \cos x - \cos y}$$

$$= 1 - 1/\pi$$

as previously found by Watson and Leath (1974). The result for the simple cubic lattice was first obtained by Izyumov (1966) in the slightly more complex situation involving spins. His result agrees with ours.

Equation (33) still holds for the site vacancy of course where now

$$P_s = 1 - c + O(c^2) \tag{50}$$

as removing a single site, reduces the number of sites in the infinite cluster. Hence G has a different initial slope from D. Using (33)

$$\left(1 - \frac{c}{1 - p_I}\right) = \left(1 - c\right)\left(1 - \frac{c}{1 - p_I'}\right)$$

and hence

$$p_I' = 2 - 1/p_I \tag{51}$$

These values are also listed in table 2. The results of computer simulations for G and P_s (and hence D) for site percolation on the triangular net are shown in figure 3 (Tang, 1986). The dashed lines corresponding to the intercepts p_I and p_I' from table 2 are shown. The diffusion constant D was obtained in figure 3 using (33).

5. Comments

We have shown how a number of known results can be put together. Although we have concentrated on bond and site vacancies, knowledge of p_I allows α_e to be found for any defect that has strength α_o in a host α. For a bond, using (30a) and (32a)

$$\alpha_e = \alpha + \frac{c\alpha(\alpha_o - \alpha)}{\alpha(1 - p_I) + \alpha_o p_I} \tag{52}$$

while using (46a) and (49) for a <u>site</u> defect

$$\alpha_e = \alpha + \frac{2c\alpha(\alpha_o - \alpha)}{2\alpha(1 - p_I) + \alpha_o(2p_I - 1)} \tag{53}$$

where in both cases p_I can be looked up in tables 1 or 2. For example these can be used in the "<u>superconducting limit</u>" (see Straley 1983) when $\alpha_o \to \infty$, to give

$$\alpha_e = \alpha + c\alpha/p_I \tag{52a}$$

in the bond case and

$$\alpha_e = \alpha + 2c\alpha/(2p_I - 1) \tag{53a}$$

in the site case. It is more usual to write these results in terms of the inverses, which to first order in c are:

$$\frac{1}{\alpha_e} = \frac{1}{\alpha}(1 - c/p_I) \tag{52b}$$

and

$$\frac{1}{\alpha_e} = \frac{1}{\alpha}\left(1 - \frac{2c}{2p_I - 1}\right) \tag{53b}$$

From (52b) and (53b), we can determine a new quantity p_I^s for the superconducting limit where the initial slope crosses the abscissa. This is clearly simply related to p_I for the dilute resistor network on the same lattice. It is more usual to introduce of a fraction (P) of superconducting links so that both problems have a common p_c as sketched in figure 4. This can be imagined as follows. Take a resistor network with a fraction p of bonds having resistence R_1 and a fraction 1-p having R_2 with $R_2 >> R_1$. The dilute resistor limit is reached as $R_2 \to \infty$, whilst the superconducting limit is reached when $R_1 \to 0$. A similar situation holds for site percolation. Therefore using (52b) and (53b) and remembering to put $p \to 1-p$ for the superconducting case we find that for <u>bonds</u>

$$p_I^s = p_I \tag{54}$$

whilst for <u>sites</u>

$$p_I^s = p_I - \frac{1}{2} \ . \tag{55}$$

Again like equations (35) and (51), relating p_I' to p_I, equations (54) and (55) do not depend upon the lattice or the dimensionality. Note that p_I^s for <u>sites</u> is given from (49a) and (55) as

$$p_I^s = \frac{1}{2N} \sum_{\underline{k}} \frac{(\underline{\nabla}\gamma_{\underline{k}})^2}{1 - \gamma_{\underline{k}}} \ . \tag{55a}$$

We note that <u>if</u> the defects are sufficiently far apart, it is $1/\alpha_e$ (or the resistance) that is linear in c the concentration of defects and contains <u>no</u> c^2 terms. The c^2 terms therefore would represent <u>interactions</u> between defects. On the other hand α_e (or the conductivity) is also linear c but contains terms in c^2 even if the defects are sufficiently far apart that they do not interact. These come purely from the expansion of the denominator i.e.

$$[1 + c/(1 - p_I)]^{-1} = 1 - c/(1 - p_I) + O(c^2). \qquad (55b)$$

This is rather obvious but we have not been aware of it before.

Finally we comment on the spin wave stiffness. Consider a Heisenberg ferromagnet with spins S coupled by nearest neighbor exchange J and introduce a few isolated site impurities S' that are be coupled to their neighbors with exchange J'. Izyumov (1966) calculated the spin wave stiffness D_s by looking at long wavelengths when the excitation energies E_k are given by $E_k = D_s k^2$. This is a dynamic calculation which is technically quite a bit harder than the static strain calculations done in this paper. Izyumov's result for D_s (again in units where $D_s = 1$, when p=1) is

$$D_s = 1 - c[\sigma - 1 - \frac{2\rho}{1 + \Lambda\rho}] \qquad (56)$$

where

$$\sigma = S'/S$$

$$(57)$$

$$\rho = \frac{J'S'}{JS} - 1$$

and Λ is a number that is given as a lattice integral over the cubic Brillouin zone. Using (33) we can identify

$$G = 1 + \frac{2c\rho}{1 + \Lambda\rho} \qquad (58)$$

$$\text{and } P_s = 1 + c(\sigma - 1) \qquad (59)$$

The quantity (58) reduces to our G or α_e in equation (46) if we put S = S' (to get to the usual tight binding model) and identify $\rho = J'/J-1 = \alpha_o/\alpha - 1$ and also use in (49)

$$p_I = \frac{1 + \Lambda}{2} \qquad (60)$$

We have checked equation (60) for the simple cubic lattice using our expression for p_I and the expression given by Izyumov for Λ and shown that the two lattice integrals are identically the same.

We therefore conclude that the spin wave stiffness (56) of Izyumov can be used for <u>any</u> of the lattices in table 2, if $\Lambda = 2p_I - 1$ is used. This may surprise the reader familiar with the intricacies of Izyumov's paper which seem to be very dependent upon the simple cubic lattice. The work here shows that is not so and the result (56) only depends on the lattice through Λ.

The inertia term (59) reduces to the usual P_s given in (49) if S' = 0, when the central spin plays no role in the dynamics. For a <u>mass</u> defect m' in a host with masses m

$$P_s = 1 + c\left(\frac{m'}{m} - 1\right) \qquad (61)$$

which is proportional to the total mass of the system. As long as the impurity mass m is coupled into the lattice (61) is the correct expression. As soon as $\alpha_o = 0$, however m' is irrelevant in the propogation of sound waves and therefore should be set equal to zero, hence recovering (50). This is also the case in the spin wave result (56) where S' should be set equal to zero (i.e. $\sigma = S'/S = 0$) if $J' = 0$, as the central spin is decoupled from the rest of the lattice and so should not contribute to the inertia term (59) for the propogation of spin waves.

If we return to the original isotropic Born model, we may combine (53) and (61) using (36) to give the sound velocity v_s for a small concentration of <u>site</u> defects as from

$$mv_s^2 = \frac{za^2}{2d}\left[\alpha + \frac{2c\alpha(\alpha_o - \alpha)}{2\alpha(1 - p_I) + \alpha_o(2p_I - 1)}\right] \Big/ \left[1 + c(m'/m - 1)\right] \qquad (62)$$

where the p_I are given in table 2.

6. Acknowledgments

We would like to thank A. R. Day for useful comments and the National Science Foundation for support under grant DMR 8317610.

Table Captions

Table 1. Showing the percolation concentration p_c, the intercept p_I of the extrapolated initial slope for the conductance G; the intercept p_I' of the extrapolated initial slope for the diffusion constant D and the intercept p_I^s of the extrapolated initial slope in the superconducting limit. It will be helpful to glance at figures 3 and 4 to see what these are. All values are for bond percolation. The values of p_c are from Zallen (1983).

Table 2. Same as table 1 except for site percolation.

Table 1

Lattice	p_c	p_I	p_I'	p_I^s
linear chain	1	1	1	1
square net	.5	.5	.5	.5
triangular net	.347	.333	.333	.333
s.c.	.247	.333	.333	.333
b.c.c.	.179	.25	.25	.25
f.c.c.	.119	.167	.167	.167
d = 4 hypercube	.160	.25	.25	.25
d = ∞ hypercube	0	0	0	0

Table 2

Lattice	p_c	p_I	p_I'	p_I^s
linear chain	1	1	1	.5
square net	.593	.682	.534	.182
triangular net	.5	.641	.440	.141
s.c.	.311	.605	.347	.105
b.c.c.	.245	.579	.273	.079
f.c.c.	.198	.561	.217	.061
d = 4 hypercube	.197	.573	.255	.073
d = ∞ hypercube	0	.5	0	0

Figure Captions

Figure 1. Showing the two displacements $\underline{u}_1$ and $\underline{u}_2$ produced by a uniform external stress around a single altered *bond*. These comprise the components of the vector $|s\rangle$.

Figure 2. Showing the displacements produced by a uniform uniaxial external stress in a triangular lattice around a single altered *site*. These comprise the components of the vector $|s\rangle$.

Figure 3. The symbols show the quantities D, P_s and G for site percolation on the triangular net obtained numerically using methods similar to those described in Kirkpatrick (1973). Each sample contained 1600 atoms and the results were averaged over 20 samples. The quantities p_I and p_I' where the initial slopes cross the abscissa are indicated.

Figure 4. A *sketch* of the conductance G versus p showing the intercept p_I of the initial slope. This network has a fraction p of missing units (sites or bonds). Also shown is a sketch of the resistance R versus p superconducting limit showing the intercept of the initial slope p_I^s. This network has a fraction $1-p$ of superconducting bonds. Both G and R are normalized to the same quantity in the respective pure system.

Figure A1.
Showing the two displacements $\underline{u}_1$ and $\underline{u}_2$ produced by a uniform external stress around a single altered bond. These comprise the components of the vector |s>.

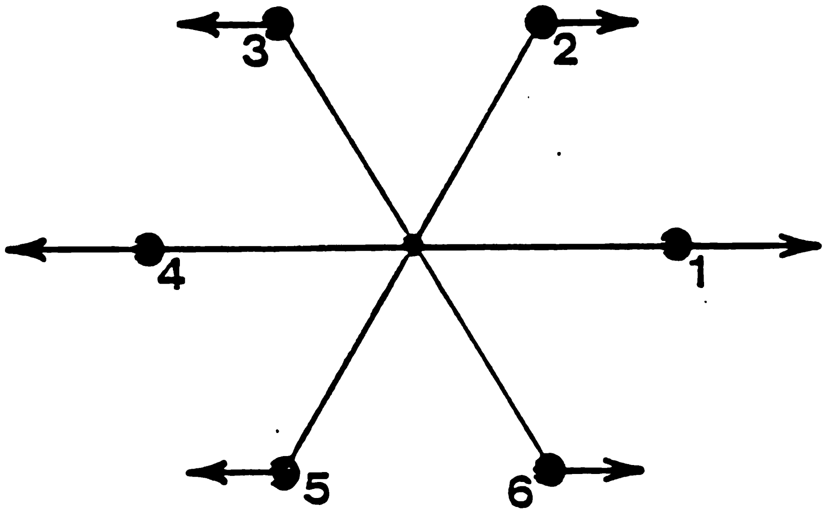

Figure A2.
Showing the displacements produced by a uniform uniaxial external stress in a triangular lattice around a single altered site. These comprise the components of the vector |s>.

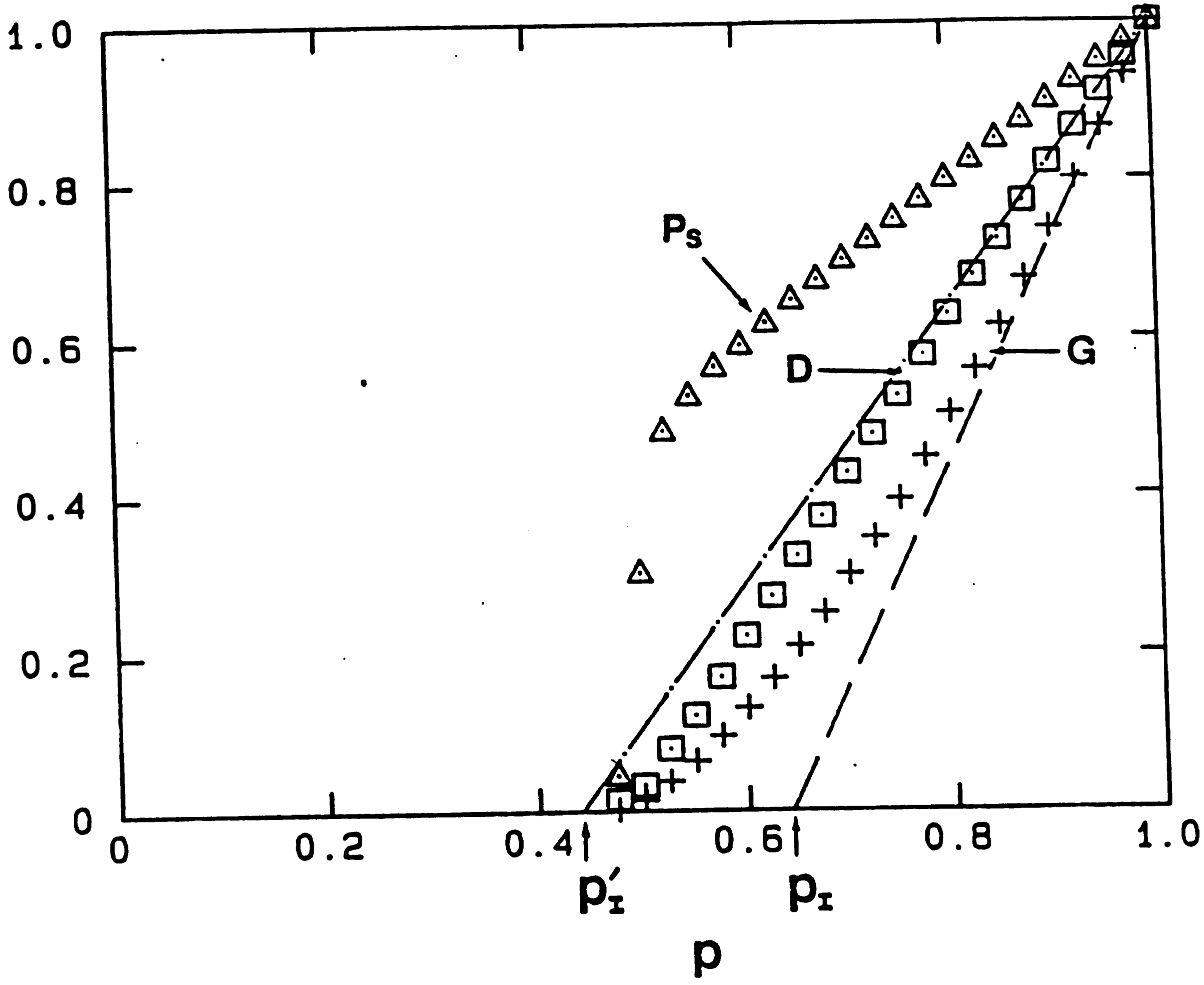

Figure A3.
The symbols show the quantities D, P_s and G for site percolation on the triangular net obtained numerically using methods similar to those described in Kirkpatrick (1973). Each sample contained 1600 atoms and the results were averaged over 20 samples. The quantities p_I and p_I' where the initial slopes cross the abscissa are indicated.

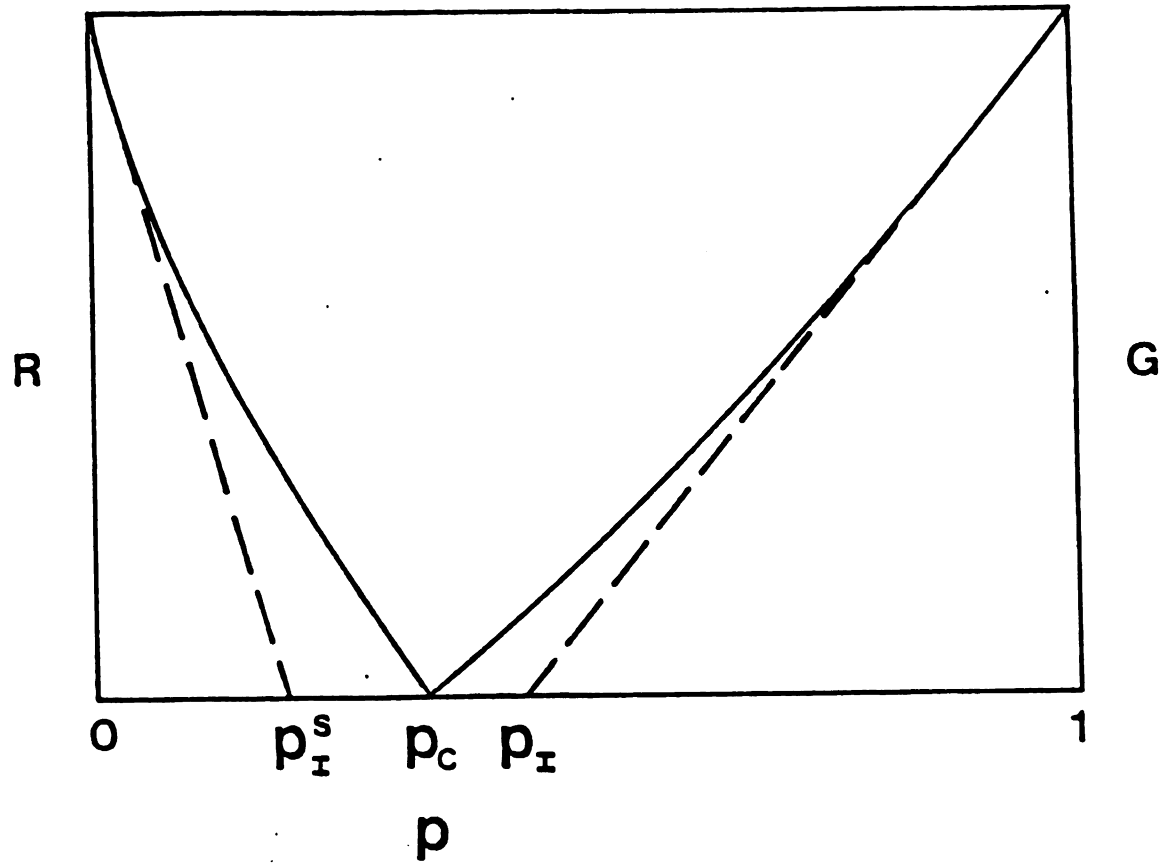

Figure A4.

A sketch of the conductance G versus p showing the intercept p_I of the initial slope. This network has a fraction p of missing units (sites or bonds). Also shown is a sketch of the resistance R_s versus p superconducting limit showing the intercept of the initial slope p_I^s. This network has a fraction 1-p of superconducting bonds. Both G and R are normalized to the same quantity in the respective pure system.

References

Born M 1914, Ann. Phys. Lpz 44, 605

Born M and Huang K 1966 Dynamical Theory of Crystal Lattices (Clarendon, Oxford)

Elliott R J, Krumhansl J A, Leath P L 1974 Rev. Mod. Phys. 46, 465

Economu E N 1979 Green's Functions in Quantum Physics (Springer-Verlag, Berlin)

Feng S, Thorpe M F, and Garboczi E J 1985 Phys. Rev. B 31, 276

Izyumov, Yu 1966 Proc. Phys. Soc 87, 505

Kirkpatrick S 1973 Rev. Mod. Phys. 45, 574

Stauffer D 1985 Introduction to Percolation Theory (Taylor and Francis, London) and references contained therein

Straley J P 1983 in Percolation Structures and Processes. Eds. Deutscher G, Zallen R, and Adler J Ann. Israel Phys. Soc. V5, ch. 15

Tang W 1986 unpublished

Thorpe M F and Garboczi E J 1986 to be published

Watson B P and Leath P L 1974 Phys. Rev. B 9, 4893

Zallen R 1983 The Physics of Amorphous Solids (Wiley & Sons, New York)

Appendix

The general result for the effective α_e, due to the presence of a defect is

$$\frac{\alpha}{\alpha_e} = 1 - \frac{\underline{u}_o \, \underline{\underline{T}} \, \underline{u}_o}{\underline{u}_o \, \underline{\underline{D}}_o \, \underline{u}_o} \tag{29}$$

where $\underline{u}_o$ is the strain in the system before the defect is added. Although (29) was derived with a local defect in mind, it is quite generally true for <u>any</u> change $\underline{\underline{V}}$ in the dynamical matrix. We give two simple illustrations of the use of (29).

In the first we suppose that <u>all</u> the bonds in a system described by (13) have their force constants changed from α to α_o. This is not a localized defect, but (29) is general for any $\underline{\underline{V}}$. In this case

$$\underline{\underline{V}} = \left(\frac{\alpha_o - a}{\alpha}\right) \underline{\underline{D}}_o \tag{A1}$$

and hence

$$\begin{aligned} \underline{\underline{T}} &= \underline{\underline{V}} \left[1 - \underline{\underline{P}} \left(\frac{\alpha_o - \alpha}{\alpha}\right) \underline{\underline{D}}_o\right]^{-1} \\ &= \underline{\underline{V}} \left[1 + \frac{\alpha_o - \alpha}{\alpha}\right]^{-1} \\ &= \frac{\alpha}{\alpha_o} \; \underline{\underline{V}} \end{aligned} \tag{A2}$$

where we have used $\underline{\underline{P}} \, \underline{\underline{D}}_o = -1$. Therefore we have

$$\frac{\alpha}{\alpha_e} = 1 - \frac{\underline{u}_o \left(\frac{\alpha}{\alpha_o} \underline{\underline{V}}\right) \underline{u}_o}{\underline{u}_o \underline{\underline{D}}_o u_o} = 1 - \frac{\alpha}{\alpha_o} \left(\frac{\alpha_o - \alpha}{\alpha}\right) = \frac{\alpha}{\alpha_o} \qquad \text{(A3)}$$

which gives the expected result $\alpha_e = \alpha_o$.

In the second example, we consider a 1D chain described by (13) in which a single bond is changed from α to α_o.

Equation (30) becomes (with $c = 1/N$ and $z = 2$)

$$\frac{\alpha}{\alpha_e} = 1 - \frac{1}{N} \frac{(\alpha_o - \alpha)}{1 + (\alpha_o - \alpha)/\alpha}$$

$$= 1 - \frac{1}{N} \frac{\alpha_o - \alpha}{\alpha_o} \qquad \text{(A4)}$$

which can be rewritten as

$$\frac{N}{\alpha_e} = \frac{N - 1}{\alpha} + \frac{1}{\alpha_o} \qquad \text{(A5)}$$

which is the expected result for $(N - 1)$ springs α and one spring α_o in series.

Appendix B. Absorbing rate in continuum media

Appendix B. Absorbing rate in continuum media

In this Appendix, we study the absorbing boundary problem in continuum media.

We start from the general diffusion equation:

$$D \nabla^2 P(\vec{r},t) = - \frac{\partial^2 P(\vec{r},t)}{\partial t^2} \qquad (B1)$$

where D is the diffusion constant. Assuming $\psi(r,t)$ can be seperated into the form:

$$P(r,t) = R(r)\ T(t) \qquad (B2)$$

Then we have the differential equation for R and T respectively:

$$\frac{dT}{dt} = - k^2 D\ T \qquad (B3)$$

and

$$(\nabla^2 + k^2)\ R = 0 \qquad (B4)$$

where (B3) has the solution:

$$T(t) = e^{-k^2 Dt} \qquad (B5)$$

The complete set of eigenfunction of eq.(B1) has the following form:

$$P(r,t) = \sum_k A_k \; R_k(r) \; T_k(t) \qquad \text{(B6)}$$

where the $T_k(r)$ and $R_k(t)$ are the solutions of (B3) and (B4), and k is indicating the discrete eigenvalue for the corresponding boundary condition.

If we have the initial probability distribution given by P(r,t=0), by substituting into eq.(B6), we get:

$$P(r,0) = \sum_k A_k R_k(r) \qquad \text{(B7)}$$

and assuming the orthoganality of the eigenfunction:

$$\int R_k(r) \; R_{k'}(r) \; \underline{dr} = B_k \; \delta_{kk'} \qquad \text{(B8)}$$

Then we have:

$$\int P(r,0) \; R_k(r) \; \underline{dr} = A_k B_k \qquad \text{(B9)}$$

Substituting (B9) into (B6), we write P(r,t) as:

$$P(r,t) = \sum_k \frac{\int_{V_0} P(r',0) \; R_k(r') \; \underline{dr}'}{B_k} \; R_k(r) \; T_k(t) \qquad \text{(B10)}$$

We define the following quantities:

$I_1(t)$ --- Total number of the particles in the media at any time t:

$$I_1(t) = \int_{v_0} P(r,t)\, \underline{dr} \qquad \text{(B11)}$$

where v_0 is the volume of the media.

$I_2(t)$ --- Number of particles leaving at time t:

$$\begin{aligned} I_2(t) &= -\frac{\partial\, I_1(t)}{\partial\, t}\, dt \\ &= \int_{v_0} -\frac{\partial\, P(r,t)}{\partial\, r}\, \underline{dr}\, dt \\ &= -\int_{v_0} \nabla^2\, P(r,t)\, \underline{dr} \qquad \text{(B12)} \\ &= -\int_s [\nabla\, P(r,t)] \bullet d\vec{r} \end{aligned}$$

where s is the surface of v_0.

$\langle t \rangle$ --- Average time for a particla reach the boundary:

$$\langle t \rangle = \frac{\int_0^\infty t\, I_2(t)\, dt}{\int_0^\infty I_2(t)\, dt} = \int_0^\infty I_1(t)\, dt \qquad \text{(B13)}$$

and substituting (B7) and (B8) into (B12) and (B13) we got:

$$\langle t\rangle = \sum_k \frac{\int_{v_0} P(r,0)\, R_k(r)\, \underline{dr}}{D\, k^2 \int_{v_0} R_k^2\,(r)\, \underline{dr}} \int_{v_0} R_K(r)\, \underline{dr} \qquad (B14)$$

Actually, the recipracal of <t> is the deposit rate of particle on the absorbing wall. For any given initial distribution P(r,0), boundary condition as well as geometrical structure of the system which determines the set of eigenfunction $R_k(r)$, eq. (B14) gives the deposit rate or absorbing rate. We summarize several cases corresponding to the uniform initial distribution as the following:

<u>case 1)</u>. Initial distribution is a δ-function at center:

$$P(r,0) = \delta(\underline{r}) \qquad (B15)$$

then

$$D\,\langle t\rangle = \sum_k \frac{\int_{v_0} R_k(r)\, \underline{dr}}{k^2 \int_{v_0} R_k^2(r)\underline{dr}}\, R_k(0) \qquad (B16)$$

<u>case 2)</u>. Uniform initial distribution in the whole region.

$$\begin{aligned} P(r,0) &= 1/v_0 \qquad \text{if } r<r_0 \\ &= 0 \qquad \text{otherwise} \end{aligned} \qquad (B17)$$

then

$$D\langle t\rangle = \sum_k \frac{\{\int_{v_0} R_k(r)\,\underline{dr}\}^2}{k^2\int_{v_0} R_k^2(r)\,\underline{dr}}\left(\frac{1}{v_0}\right) \qquad (B18)$$

case 3). Uniform initial distribution in partial region.

$$\begin{aligned} P(r,0) &= 1/v' && \text{if } r<r' \\ &= 0 && \text{otherwise} \end{aligned} \qquad (B19)$$

then

$$D\langle t\rangle = \sum_k \frac{\{\int_{v_0} R_k(r)\underline{dr}\}\,\{\int_{v'} R_k(r)\underline{dr}\}}{k^2\int_{v_0} R_k^2(r)\,\underline{dr}}\left(\frac{1}{v'}\right)$$

(B20)

Actually, case (2) is included in case (3) for $v'=v_0$. All of the formula derived above are suitable to any dimension. Let us consider a circular piece in two dimension , i.e., $r\leq r_0$. The Bessel function gives the complete set of the eigenfunction:

$$R_k(r) = J_0(kr) \qquad (B21)$$

where $J_0(x)$ is the zero-th order of the Spherical Bessel Function and eigenvalues are given by:

$$k=x_n^{(0)}/r_0 \qquad (B22)$$

where $J_0(x_n^{(0)}) = 0$

We found out that the diffusion constant is given by:

$$D = \frac{r_0^2}{\langle t \rangle} \qquad \text{for case (1)} \qquad \text{(B23)}$$

and

$$D = \frac{1}{2}\,\frac{r_0^2}{\langle t \rangle} \qquad \text{for case (2)} \qquad \text{(B24)}$$

case (3) is more complicated.

Appendix C. Formulation of Effective Medium on Triangle Net

Appendix C. Formulation of Effective Medium on Triangle Net

The value of a^* can be calculated exactly through the formula Thorpe & Garboczi 1985):

$$a^* = \frac{2\ K_m}{z\ N} \sum_k \ \mathrm{Tr}\ \{ \sum_\delta [\ 1 - \exp(iL\vec{k}\cdot\hat{\delta})\ ]\ (\hat{\delta}\hat{\delta}) \cdot \underline{D}^{-1}(\ \vec{k}\ )\ \} \qquad \text{(C1)}$$

where $\underline{D}\ (\vec{k})$ is the Fourier transform of the dynamical matrix:

$$\begin{aligned} \underline{D}\ (\vec{k}) &= K_m\ \eta \sum_\delta [\ 1 - \exp(iL\vec{k}\cdot\hat{\delta})\ ]\ \hat{\delta}\hat{\delta} \\ &+ K_m\ (1-\eta) \sum_\delta [\ 1 - \exp(iL\vec{k}\cdot\hat{\delta})\ \underline{I} \qquad \text{(C2)} \end{aligned}$$

where $\eta = L_0/L$ and $\underline{I}$ is the d×d unit matrix.

Through some matrix algebra, we get the result:

$$a^* = \frac{2d}{z} \eta^{-1} - \frac{2}{z} (\ \eta^{-1} - 1\ )\ S \qquad \text{(C3)}$$

where S is the sum in $\vec{k}$ space:

$$S = \frac{K_m}{N} \sum_\kappa \{ \sum_\delta [\ 1 - \exp(iL\vec{k}\cdot\hat{\delta})\ ]\ \mathrm{Tr}\ [\underline{D}^{-1}\ (\vec{k})\ ]\ \} \qquad \text{(C4)}$$

For the triangular lattice, we have

$$a^* = \frac{2}{3}\eta^{-1} - \frac{1}{3}(\eta^{-1} - 1) S \qquad \text{(C5)}$$

and

$$S = \frac{1}{N}\sum_k X \frac{D_{xx} + D_{yy}}{D_{xx}D_{yy} - D_{xy}D_{yx}} \qquad \text{(C6)}$$

where

$$\begin{aligned} D_{xx} &= (1-\eta)(6 - 2\cos 2x - 4\cos x \cos y) \\ &\quad + \eta(3 - 2\cos 2x - \cos x \cos y) \qquad \text{(C7a)} \end{aligned}$$

$$\begin{aligned} D_{yy} &= (1-\eta)(6 - 2\cos 2x - 4\cos x \cos y) \\ &\quad + \eta(3 - 3\cos x \cos y) \qquad \text{(C7b)} \end{aligned}$$

$$D_{xy} = D_{yx} = \surd 3\, \eta \sin x \sin y \qquad \text{(C7c)}$$

and

$$X = 6 - 2\cos 2x - 4\cos x \cos y \qquad \text{(C7d)}$$

where $x = \frac{1}{2} k_x L$

$y = \frac{\surd 3}{2} k_y L$

LIST OF REFERENCES

LIST OF REFERENCES

R. Alben, S. Goldstein, M. F. Thorpe and D. Weaire, Phys. Stat. Solid (b) 53, 545 (1972).

R. Alben, S.Kirkpatrick, D.Beeman, Phys. Rev. B 15, 346 (1977).

Broadbent, S.R., and J.M.Hammersley, Proc. Camb. Phillos. Soc. 53, 629 (1957).

T.H.K.Barron and M.L.Klein, Proc. Phys. Soc. 85, 523 (1965).

R.J.Elliott, J.A.Krumhansl and P.L.Leath, Rev. Mod. Phys. 46, 465 (1974).

J. W. Essam in Phase Transitions and Critical Phenomena, Ed. by C. Bomb and M. S. Green (Academic Press, New York, 1972) Vol. 2, p.197.

S. Feng, M. F. Thorpe, E. Garboczi, Phys. Rev. B 31, 276 (1985).

S. Feng and P. N. Sen, Phys. Rev. Lett. 52, 216 (1984).

P. G. de Gennes, J. Phys. (Paris) 37, L-1 (1976).

W. A. Harrison, Electronic Structure and the Properties of Solids (W. H. Freeman and Co., San Francisco, 1980).

H.He, Ph.D. Thesis, Michigan State University (1985).

H. He and M. F. Thorpe, Phys. Rev. Lett. 54, 2107 (1985).

C.L.Henley, submitted to Comm. in Cond. Mat. Phys. (1986).

K.Huang, Proc. Roy. Soc. A, 203, 178 (1950).

J. B. Keller, J. Math. Phys. 5, 548 (1964).

A. Khurana, Phys. Today, 40, No. 4, 23 (1987).

S. Kirkpatrick, Rev. Mod. Phys. 45, 574 (1973).

P. M. Kognt and J. P. Straley, J. Phys. C 14, 909 (1981).

D. Levine and P.J.Steinhardt, Phys. Rev. B 34, 596 (1986).

A.E.H. Love, A Treatise on the Mathematical Theory of Elasticity, Dover, New York (1944).

K. S. Mendelson, J. Appl. Phys. 46, 917 (1975); 46, 4740 (1975).

D.Shechtman, J.Blech, D.Gratias and J.W.Cahn, Phys. Rev. Lett. 53, 1951 (1984).

J.E.S.Socolar and P.J.Steinhardt, Phys. Rev. B 34, 617 (1986).

D. Stauffer, Introduction to Percolation Theory (Taylor and Francis, London, 1985).

J. P. Straley in Introduction to Percolation Processes, Eds. G. Deutscher, R. Zallen and J. Adler, Isreal Phys. Soc. V5, Ch.15 (1983).

J. P. Straley, J. Phys. C 9, 783 (1978).

J. P. Straley, Phys. Rev. B 15, 5733 (1977).

M.F.Thorpe, J. Non-Crys. Sol. 57, 355 (1983).

B. P. Waston and P. L. Leath, Phys. Rev. B 9, 4893 (1974).

R. Zallen, The Physics of Amorphous Solids (Wiley and Sons, New York, 1983).